# INTEGRATED RESERVOIR CHARACTERIZATION

# AND SIMULATION STUDIES IN STRIPPER OIL AND GAS FIELDS

A Dissertation

by

JIANWEI WANG

Submitted to the Office of Graduate Studies of
Texas A&M University
in partial fulfillment of the requirements for the degree of

DOCTOR OF PHILOSOPHY

December 2008

Major Subject: Petroleum Engineering

# INTEGRATED RESERVOIR CHARACTERIZATION

# AND SIMULATION STUDIES IN STRIPPER OIL AND GAS FIELDS

A Dissertation

by

JIANWEI WANG

Submitted to the Office of Graduate Studies of
Texas A&M University
in partial fulfillment of the requirements for the degree of

DOCTOR OF PHILOSOPHY

Approved by:

| | |
|---|---|
| Co-Chairs of Committee, | Walter B. Ayers |
| | Duane A. McVay |
| Committee Members, | J. Bryan Maggard |
| | Yuefeng Sun |
| Head of Department, | Stephen A. Holditch |

December 2008

Major Subject: Petroleum Engineering

# ABSTRACT

Integrated Reservoir Characterization and Simulation

Studies in Stripper Oil and Gas Fields. (December 2008)

Jianwei Wang, B.S., Petroleum Institute of Xinjiang;

M.S., China University of Petroleum (Beijing)

Co-Chairs of Advisory Committee: Dr. Walter B. Ayers
Dr. Duane A. McVay

The demand for oil and gas is increasing yearly, whereas proven oil and gas reserves are being depleted. The potential of stripper oil and gas fields to supplement the national energy supply is large. In 2006, stripper wells accounted for 15% and 8% of US oil and gas production, respectively. With increasing energy demand and current high oil and gas prices, integrated reservoir studies, secondary and tertiary recovery methods, and infill drilling are becoming more common as operators strive to increase recovery from stripper oil and gas fields. The primary objective of this research was to support optimized production of oil and gas from stripper well fields by evaluating one stripper gas field and one stripper oil field.

For the stripper gas field, I integrated geologic and engineering data to build a detailed reservoir characterization model of the Second White Specks (SSPK) reservoir in Garden Plains field, Alberta, Canada. The objectives of this model were to provide insights to controls on gas production and to validate a simulation-based method of in-fill drilling assessment. SSPK was subdivided into Units A – D using well-log facies.

Units A and B are the main producing units. Unit A has better reservoir quality and lateral continuity than Unit B. Gas production is related primarily to porosity-net-thickness product and permeability and secondarily to structural position, minor structural features, and initial reservoir pressure.

For the stripper oil field, I evaluated the Green River formation in the Wells Draw area of Monument Butte field, Utah, to determine interwell connectivity and to assess optimal recovery strategies. A 3D geostatistical model was built, and geological realizations were ranked using production history matching with streamline simulation. Interwell connectivity was demonstrated for only major sands and it increases as well spacing decreases. Overall connectivity is low for the 22 reservoir zones in the study area. A water-flood-only strategy provides more oil recovery than a primary-then-water-flood strategy over the life of the field. For new development areas, water flooding or converting producers to injectors should start within 6 months of initial production. Infill drilling may effectively produce unswept oil and double oil recovery. $CO_2$ injection is much more efficient than $N_2$ and $CH_4$ injection. Water-alternating-$CO_2$ injection is superior to continuous $CO_2$ injection in oil recovery.

The results of this study can be used to optimize production from Garden Plains and Monument Butte fields. Moreover, these results should be applicable to similar stripper gas and oil field fields. Together, the two studies demonstrate the utility of integrated reservoir studies (from geology to engineering) for improving oil and gas recovery.

# DEDICATION

I dedicate this work to my parents, Hefa Wang and Niu Yang, for their love and support throughout my entire life and my wife, Fengli, and my son, Kevin, for their love, patience, and understanding.

# ACKNOWLEDGEMENTS

I would like to express my sincere gratitude to my committee co-chairs, Dr. Walter B. Ayers and Dr. Duane A. McVay, for their valuable advice and academic guidance.

I would like to thank my committee members, Dr. Yuefeng Sun, Dr. Bryan Maggard, and Dr. Jerry Jensen, for serving as my advisory committee members and their advice and guidance throughout the course of this research.

I would also like to thank my research colleague, Joseph Abiazie, and friends Jesus Salazar, Rasheed Bello, Xianlin Ma, and Mark Dickins, for their valuable discussion, time, effort, and friendship during the course of this research.

Thanks also go to the department faculty and staff for making my time at Texas A&M University a great experience. I also want to extend my gratitude to Quicksilver and Newfield Exploration Company for providing the data and support for this study.

# TABLE OF CONTENTS

Page

Page

# LIST OF FIGURES

FIGURE Page

FIGURE Page

FIGURE Page

FIGURE Page

FIGURE Page

# LIST OF TABLES

# 1. INTRODUCTION

The demand for oil and gas is increasing yearly, whereas proven oil and gas reserves are being depleted. It is increasingly important to use current technologies to improve hydrocarbon recovery from existing oil and gas reservoirs, especially from stripper oil and gas fields. Stripper fields are those in which the average well produces less than 10 barrels of oil or less than 60 thousand cubic feet of gas daily. According to the Interstate Oil and Gas Compact Commission (IOGCC, 2006), there were 393,463 stripper oil wells and 260,563 stripper gas wells in the U.S., as of January 1, 2004. These totals are approximately 77% and 63% of the country's total oil and gas well populations, respectively. Stripper well oil production was 313,748,001 barrels in 2003, accounting for 15% of total domestic oil production. Stripper gas production totaled 1.478 trillion cubic feet (Tcf) of natural gas in 2003, when it accounted for 8 percent of the U.S. gas supply (IOGCC, 2006).

The large number of wells, variability of reservoir quality, well spacing and well completion practices, and marginal economics complicate the challenging problem of optimizing production from stripper oil and gas fields. The most accurate method for characterizing reservoirs and optimizing production is an integrated reservoir study. Such a study requires detailed databases, development of geological models, reservoir property determination (e.g., porosity and permeability), simulation model construction and calibration, and finally, simulation of various operational scenarios to optimize oil or

---

This dissertation follows the style of the *SPE Reservoir Engineering*.

gas recovery. Integrated reservoir studies can greatly decrease the uncertainty associated with reservoir management, but they are time-consuming and expensive, relative to the value of stripper oil and gas fields. Moreover, most stripper well fields are operated by independent companies that lack the manpower, expertise, and economic resources for such studies. However, the nation's depleting energy supply, increasing energy demand, current high oil and gas prices, and new technologies have improved economics of marginal or stripper oil and gas fields. Integrated reservoir studies, secondary and tertiary recovery methods, and infill drilling are becoming more common as operators strive to increase recovery from stripper oil and gas fields.

The primary objective of this research was to support optimized production of oil and gas from stripper well fields. To accomplish this objective, I evaluated one stripper gas field and one stripper oil field. Both fields are low-permeability, unconventional reservoirs, with an average permeability of 0.45 md for the stripper gas field and 5 md for the stripper oil field. Results of both studies should be applicable to other low-permeability, unconventional stripper gas and oil fields. Together, the two studies demonstrate how integrated reservoir studies (from geology to engineering) can be used to characterize low-permeability unconventional reservoirs and optimize oil and gas recovery.

For the stripper gas field, I integrated geologic and engineering data to build a detailed reservoir characterization model of the Second White Specks (SSPK) reservoir in Garden Plains field, Alberta, Canada. The objective of this model was to provide insights to controls on gas production. Additionally, it was used to assess viability of a

companion study in which a rapid, low-cost method for assessing infill drilling potential was being tested in this stripper gas fields (Cheng et al., 2008).

For the stripper oil field, I conducted history matching and simulation to evaluate the Green River formation in Monument Butte field, Utah. Monument Butte field produces oil from low-permeability, lacustrine, fluvial-deltaic sandstones of the Green River formation. Reservoir sands are heterogeneous, lenticular, and have limited aerial extent and vertical communication, resulting in poor inter-well connectivity. Total (primary and secondary) recovery is less than 5% of the OOIP. The objectives of this research were to (1) assess reservoir connectivity via geological modeling and reservoir simulation history matching and (2) determine optimal oil recovery strategies and well spacing for future developing areas in Monument Butte field. To accomplish these objectives, detailed reservoir characterization and simulation studies in a pilot area of Monument Butte field were conducted to determine interwell connectivity and to identify methods to improve oil recover. I built a 3D geostatistical model and ranked geological realizations using production history matching with streamline simulation. Detailed petrophysical and geological modeling were used to quantify interwell connectivity of sands as a function of well spacing. A combination of manual and assisted history matching methods was used to calibrate the reservoir model. Infill drilling potential was evaluated by simulating downspacing from the original 40-ac to 20-ac well spacing. Primary, secondary, and tertiary development strategies were then evaluated for future optimization of oil recovery in the field.

# 2. RESERVOIR CHARACTERIZATION OF THE SECOND WHITE SPECKS FORMATION (UPPER CRETACEOUS), GARDEN PLAINS FIELD, WESTERN CANADA SEDIMENTARY BASIN

## 2.1 INTRODUCTION

### Background and Literature Review

Stripper gas wells are defined as those wells that produce less than 60 Mcf (<1,700 $m^3$) gas daily. Despite their low production rates, stripper gas wells are important to the U.S. and North American gas supply. In 2003, 260,563 stripper wells produced 1.478 trillion cubic feet (Tcf) of natural gas and accounted for 8% of the U.S. gas supply (IOGCC, 2006). Full-scale reservoir simulation studies of stripper well fields are rarely performed, owing to marginal economics, and commonly, these fields are operated by independent companies that lack the staff for such studies.

This study was funded primarily by the U.S. DOE Stripper Well Consortium, which is managed by Pennsylvania State University. Several stripper gas well fields were reviewed initially. Garden Plains stripper field was selected for this study because it is a large field with the necessary types of data, and the operator, MGV Energy, provided additional support in the form of production, well logs and core data. Also, in Garden Plains field, a high percentage (75.4%) of wells are stripper wells, and production is not heavily commingled. The geology was reported to be simple, and SSPK reservoir sands were said to have good lateral continuity. Approximately 800

wells have been drilled in the field in the last 8 to 9 years, which provided a modern database.

The upper Cretaceous (Cenomanian to Turonian) SSPK formation is present across much of the Western Canada Sedimentary Basin (WCSB) (Bloch et al., 1993; Leckie et al., 1994). SSPK is composed of calcareous, very fine-grained, shaly sandstone with sandy shale interbeds. SSPK reservoirs are shallow, low permeability sands that are charged with biogenic methane (O'Connell, 2005). Although the SSPK formation reportedly contains 2 to 3 Tcf of natural gas in southern Alberta and southwest Saskatchewan, gas is produced from the formation is produced only locally in Garden Plains and 17 other fields in Alberta and Saskatchewan (Snowdon, 1995; O'Connell, 2005).

Garden Plains field is the northern-most gas field that produces from the SSPK. There are few published studies of the SSPK formation. Three reasons for this neglect are that: (1) significant gas occurs only in local sand lenses encased in extensive, fine-grained marine sediments; (2) limited extent and subtle variation of SSPK sandstone facies requires detailed stratigraphic analysis for reservoir delineation; and (3) owing to low production rates, the gas wells are marginally economic.

New technologies are needed to develop SSPK and other low-permeability sands. In another phase of the SSPK study, I refined and validated a simulation-based inversion approach for rapidly, and cost-efficiently assessing infill drilling potential in stripper gas fields (Cheng et al., 2008). This study, which is the first publicly available,

comprehensive reservoir characterization for this field, provided insights into reservoir performance and was used to assess infill drilling potential in this stripper gas field.

**Objectives**

The objectives of this study were to integrate geologic and engineering data and to build a detailed reservoir characterization model. The goal of this model was to provide insights to controls on gas production performance and to assess the validity of a rapid method to assess infill drilling potential in stripper gas field, in another part of this study.

**Research Approach**

To characterize SSPK reservoirs in Garden Plains field, I used well logs, core reports, and production data to make structural, isopach, net sandstone thickness, porosity, permeability, and production maps. Production data from 920 wells in Garden Plains field were available for this study. However, of these 920 wells, only 772 wells produce solely from the SSPK; in the remaining 148 wells, SSPK production is commingled with that from other formations.

Digital log curves were provided for 173 wells that were located primarily in the middle and northeast parts of Garden Plains field. Raster image log curves were provided for 901 wells, including many of those for which I had digital logs. The geophysical log suite varied among wells but generally included combinations of gamma ray, neutron porosity, caliper, and other curves, including resistivity and density

porosity. Although core analysis data were provided for 25 cored wells, only 5 wells had both core analysis data and digital logs. The core analysis data include porosity, permeability, grain density, water saturation, and lithologic descriptions.

To accomplish the objectives of this study, I:

1. correlated the SSPK formation in well logs;
2. conducted a petrophysical analysis by integrating well log and core analyses;
3. mapped depositional systems, thickness and reservoir properties using well log data;
4. built a static reservoir model; and
5. evaluated production data and assessed geologic controls on reservoir performance.

## 2.2 GEOLOGICAL SETTING

### Regional Geology

Garden Plains field is located on the east flank of the WCSB (**Fig. 2.1**). It extends from Township 30N to 34N and from Range 11W4 to Range 16W4 and is approximately 40 mi long and 20 mi wide (64 X 32 km). In Garden Plains field, SSPK is shallow (2,478 – 3,423 ft; 760-1050 m deep). Dip of the SSPK formation is less than 1° westward. Structural relief across the field is 350 ft (107 m). A gas/water contact was not identified.

The SSPK formation occurs in the lower part of the Upper Colorado Group, which was deposited in Late Cretaceous (Turonian) time **(Fig. 2.2)**, when sea level was globally high (Schroder-Adams et al., 1996). SSPK reservoirs rocks are low-permeability, clay-rich sandstones that are interbedded with sandy shale beds. The formation is named for the abundant calcareous nannofossils that are typically concentrated in white, fine- to very fine-grained, sand-sized fecal pellets. The SSPK formation overlies the Belle Fourche formation and is overlain by clastic sediments of the upper part of the Upper Colorado Group. According to Glass (1990) and Bloch et al. (1993), SSPK sands in southern Alberta and Saskatchewan occur in the uppermost part of the newly defined Belle Fourche formation, and the term Second White Specks formation refers only to the speckled, coccolithic shales that overlie the sandy interval of the SSPK formation. However, the name “Bell Fourche formation” has not been adopted for this interval by the oil industry, and the Energy and Utilities Board, Alberta, Canada

(EUB) continues to use the designation "Second White Specks formation." Thus, I will use the SSPK terminology of the EUB and industry.

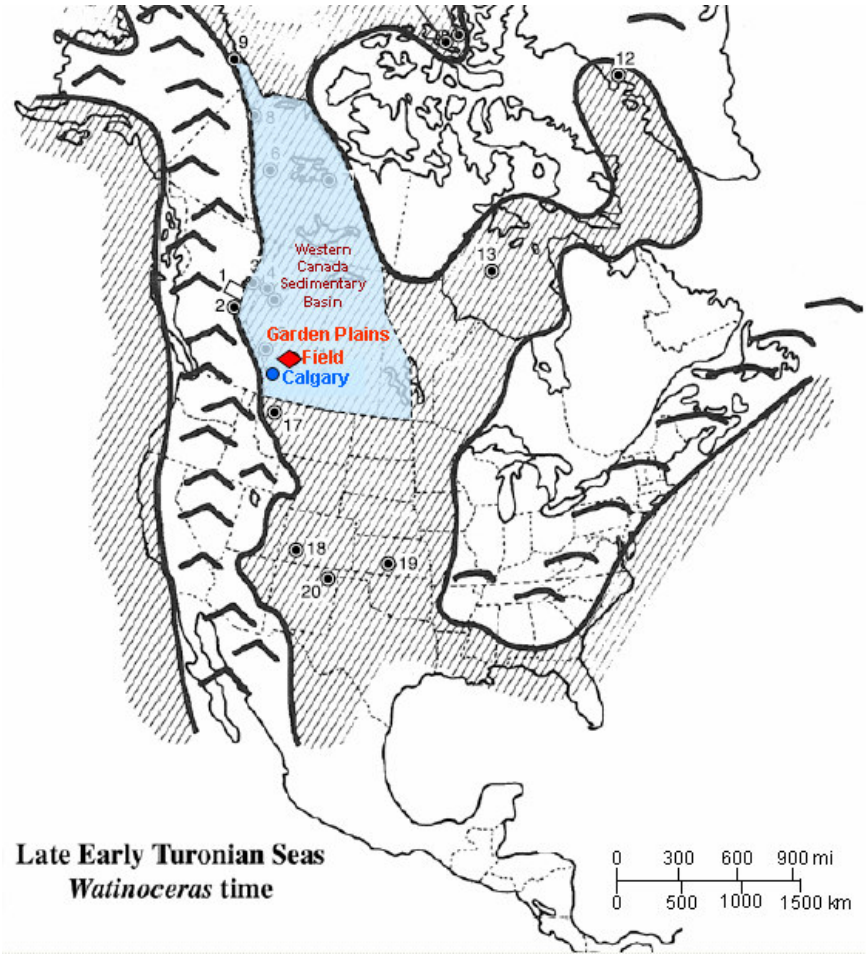


**Fig. 2.1—Location of Garden Plains field in the Western Canada Sedimentary Basin. Base map is a Turonian paleogeographic map of North America (modified from Stelck et al., 2002, after Williams and Stelck, 1975).**

## Depositional Systems

The depositional systems of SSPK formation (SSPK sands and shales) are unclear. O'Connell (2005) proposed that SSPK sands were deposited in a lowstand shoreface or an upper offshore environment. According to O'Connell, the east-trending SSPK reservoirs in southern Alberta (Bow Island Arch area) and southwestern

Saskatchewan (Bowdoin Dome) were deposited in progradational and transgressive shoreface environments. In Garden Plains field, SSPK reservoir sandbodies trend northeastward, discordant to sandbodies in other SSPK fields.

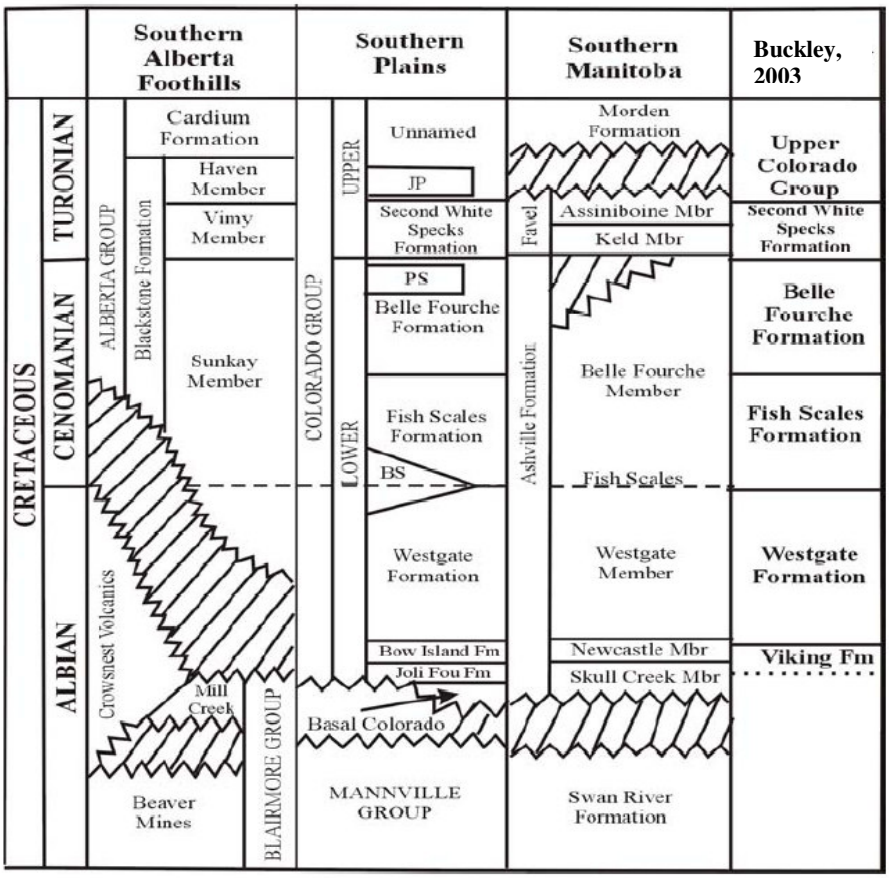


**Fig. 2.2—Stratigraphic nomenclature of the Colorado Group in the Western Canada Sedimentary Basin (from Buckley and Tyson, 2003; after Bloch et al., 1993). PS= Phillips sandstone.**

Rice (1984) proposed that the SSPK sands are equivalent to the shallow, gas-bearing Phillips sandstone in north-central Montana and the Mosby sandstones of late Cenomanian age in Alberta, southwestern Saskatchewan, and Montana. Phillips and Mosby sandstones were deposited as marine bars. According to Rice, SSPK sediments

were derived from the Dunvegan delta in northeastern British Columbia and northwestern Alberta. Sediments were transported as much as 1100 km southeastward by the interaction of waves and southward-flowing, geostrophic currents enhanced by wind forcing. The sandstones were deposited in the shallow, flat, western shelf of a north-trending epicontinental seaway in Alberta, southwestern Saskatchewan, and central Montana (**Fig. 2.3**). Most SSPK shelf sandstones form upward-coarsening sequences indicative of shoaling and/or upward increase of energy level. SSPK reservoir sandstones are elongate bodies that have directional features (primary sedimentary structures) that indicate southward storm transport (Rice, 1984). SSPK sandstones are overlain by calcareous SSPK shales. SSPK shales represent a change in depositional pattern, from fine-grained sandstone to calcareous mudstones. The calcareous mudstones may indicate deposition during a major transgression and worldwide rise in sea level during late Cenomanian time.

In the Bow Island and Arch Bowdoin Dome areas (Fig. 2.3), SSPK sandstone is inferred to have been deposited as a series of northwest-trending, offshore bar complexes that generally are 55 km wide and 80 km long (Rice, 1984). Axes of the reworked sand bars may be oblique to the shoreline (Galloway, 2002).

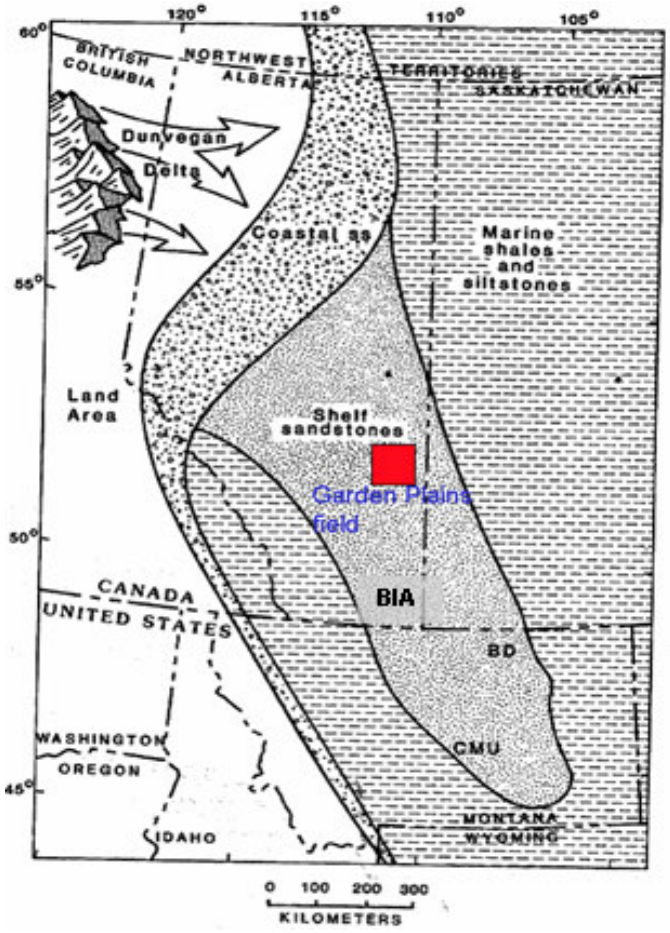


**Fig. 2.3—Paleogeographic map of northwestern United States and southwestern Canada during deposition of Mosby Sandstone Member. BIA – Bow Island Arch; BD – Bowdoin Dome; CMU – Central Montana Uplift (From Rice, 1999).**

## Source Rock and Thermal Maturity

Reportedly, the SSPK formation serves as both a petroleum source rock (Creaney and Allan, 1990) and as a reservoir (Portigal et al., 1989). However, the SSPK formation and adjacent shales are thermally immature, and the methane is locally generated, biogenic gas in parts of Alberta and southwestern Saskatchewan (Shurr and Ridgley, 2002; Buckley, 2003). Total organic content (TOC) of the upper Belle Fourche (SSPK interval in the southern part of the WCSB) averages 1.7%; organic matter is dominantly

type III kerogen with relative low hydrogen index (HI) (approximately 104 mgHC/gOC). In the northern part of the WCSB, SSPK organic matter is dominantly type II kerogen (Schroder-Adams et al., 1996), and TOC is as high as 12 wt %). HI exceeds 300 mgHC/gOC), indicating high marine organic productivity.

The onset of oil generation is generally considered to begin when $T_{max}$ values reach 435 °C, and gas generation and thermal cracking of oil begin at approximately $T_{max}$ of 450 °C. Therefore, the SSPK formation is thermal maturation for oil west of 115° W longitude, and SSPK is thermally immature for oil and gas in Garden Plains field (longitude 112° W, **Fig. 2.4**). However, Bloch et al., 1999 proposed that the thermal maturation of the SSPK formation may begin before the 435 °C $T_{max}$ threshold, owing to "suppression" (lower $T_{max}$ values at equivalent depth) related to high sulfur content of the SSPK organic matter, or the absence of refractory type III or IV organic matter. If SSPK oil generation occurs at lower temperatures, then a much larger volume of SSPK sediment is in the oil window (Fig. 4). Bloch also indicated that the SSPK formation east of 114° longitude is a potential source rock and is the source of biogenic gas produced in some parts of southern Saskatchewan. Other potential source rocks for SSPK gas are the Westgate, Bell Fourche, and Fish Scales formations. The abundance of type III organic matter in these formations indicates that they are gas prone.

Considering the low porosity and poor permeability of SSPK fine-grained sediments, natural fracture systems may be a critical component of liquid hydrocarbon migration and production from the SSPK formation.

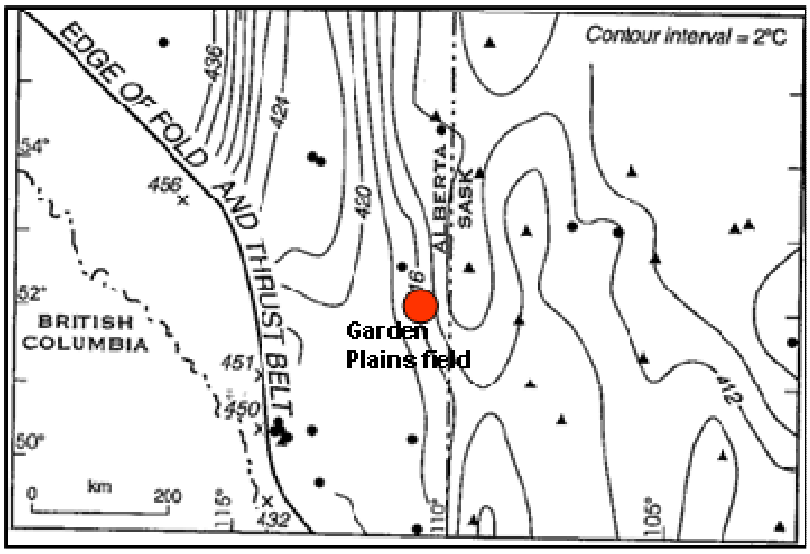


**Fig. 2.4—$T_{max}$ contour map of the SSPK formation (Bloch, 1999). Thermal maturation of SSPK formation occurs at about 115° longitude and farther to the west. If oil generation is occurring at lower temperatures, then a much larger volume of SSPK sediment is in the oil window.**

## 2.3 STRATIGRAPHIC AND FACIES ANALYSIS

### SSPK Stratigraphy

The Second White Specks formation is composed of very fine-grained sandstone and non-bioturbated, calcareous, organic-rich, siltstones that are distinctive due to the abundance and diversity of marine bioclasts, the foraminiferal assemblage, the predominance of type II organic matter, and the high total organic content (as great as 12 wt%) (Bloch et al., 1993). Historically, the SSPK formation has been divided into upper and lower Second White Specks stratigraphic units (O'Connell, 2003). The main reservoir facies is the lower SSPK, which consists of very fine-grained, muddy sandstones that are 18 to 29 ft (5.5 to 9 m) thick.

To assess the SSPK formation stratigraphy and reservoir characteristics, I divided the SSPK into four stratigraphic units (**Fig. 2.5,** Units A-D), which I correlated throughout Garden Plains field using interlocked strike and dip cross sections. Next, I correlated the SSPK in all other well logs in the field to those picks made in the cross sections, and I made structure and isopach maps.

The base of the SSPK formation is placed at the base of an upward coarsening sequence, SSPK Unit A, which occurs above the Belle Fourche formation shale (Fig. 2.5). Unit A is capped by a thin (~2 ft; 60 cm thick), low-porosity (high density), high-resistivity zone. This low-porosity zone is inferred to be sandstone that is tightly cemented with carbonate cement. Typically, Unit B is shaly, upward-fining sandstone that commonly is separated from Unit A by a very thin shale unit (Fig. 2.5). Units A is

further differentiated from Unit B on the basis that Unit A has higher resistivity and lower gamma ray and neutron porosity values (Fig. 2.5). SSPK formation Units A and B are the main gas producing zones in Garden Plains field, as is indicated by high resistivity, low gamma ray, and low neutron porosity (gas effect) values, and by perforation data (Fig. 2.5).

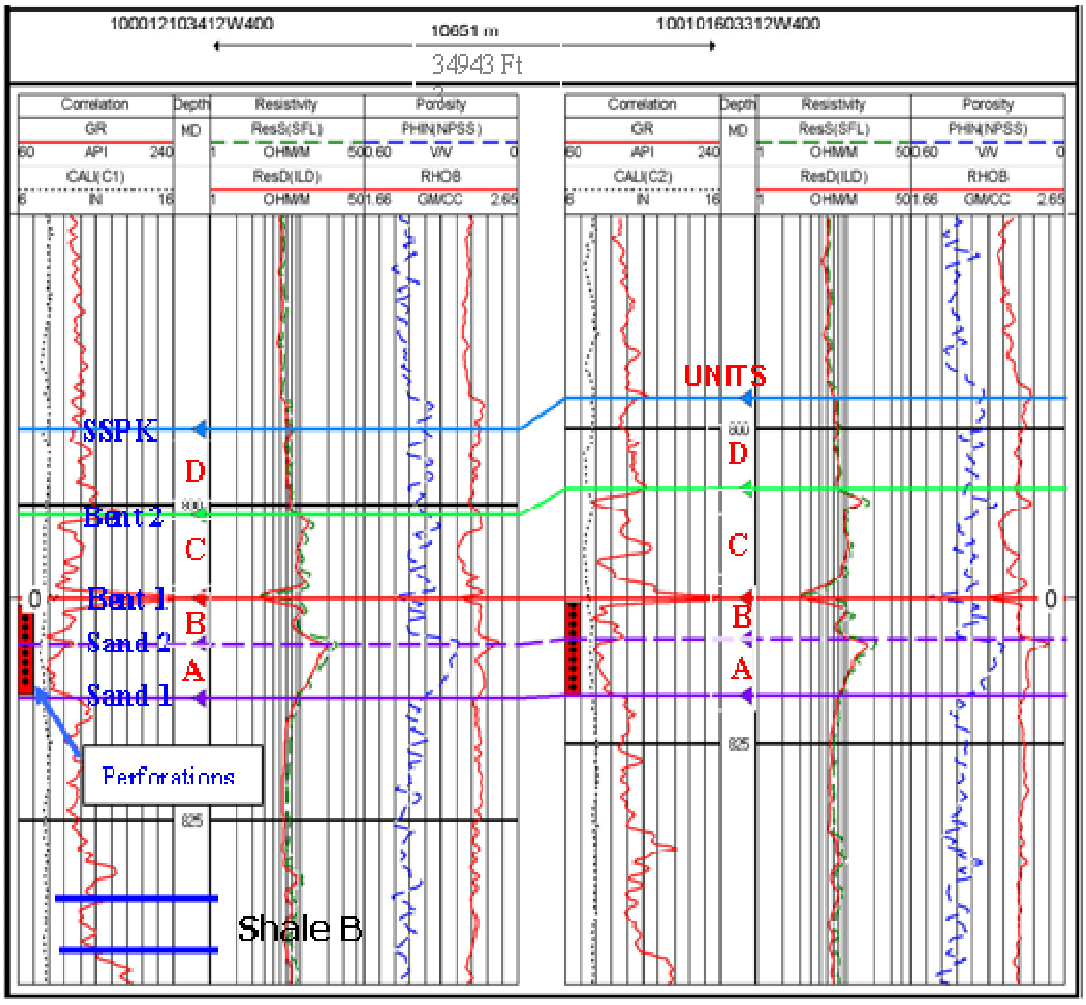


**Fig. 2.5—Log curve responses and marker beds for 2 wells in Garden Plains Field. Datum is Bentonite 1 marker bed. Sand 1 = Unit A base; Sand 2 = Unit B base; Bent 1 = Bentonite 1 and Unit C base; Bent 2 = Bentonite 2 and Unit D base; SSPK = Unit D top. Gas production is primarily from Units A and B. SSPK is the top of the SSPK Sandstone.**

Bentonite 1 occurs between the lower, gas productive SSPK and upper, shalier SSPK, which has few perforations (Fig. 2.5). In well logs, Bentonite 1 is approximately 1 ft (30 cm) thick and is recognized by (1) very high gamma ray API values, (2) high neutron porosity, and (3) low formation resistivity. Because of its distinctive appearance in well logs, field-wide occurrence, and significance as a time horizon, Bentonite 1 is a good correlation and structural marker.

Unit C includes at least 2 shaly sands that are interbedded with shales and have relatively high gamma ray response, high neutron porosity (shale effect), and low resistivity. Bentonite 2 (Fig. 2.5) separates Units C and D in the southwest and central parts of the field, but it thins northward and is absent in the northeast area. Unit D is a sandy shale interval in the upper SSPK formation. In well logs, the top of SSPK formation is placed at the small natural gamma spike at the transition from SSPK shaly sands to a dominantly shale interval at the base of the Colorado Shale Group (Fig. 2.5).

In Garden Plains field, the SSPK formation dips approximately 0.1 degree westward (**Fig. 2.6,** Bentonite 1 structure map). A west-plunging syncline crosses the west-central part of the field. Structural relief on the syncline is approximately 147 ft (45 m). Because the field strikes northeastward, oblique to structural dip, the highest elevation of the SSPK is at the northeast margin of the field (Figs. 2.6 and **2.7**). Structural relief across the field is 355 ft (109 m). There is no structural closure in Garden Plains field. A gas/water contact was not identified.

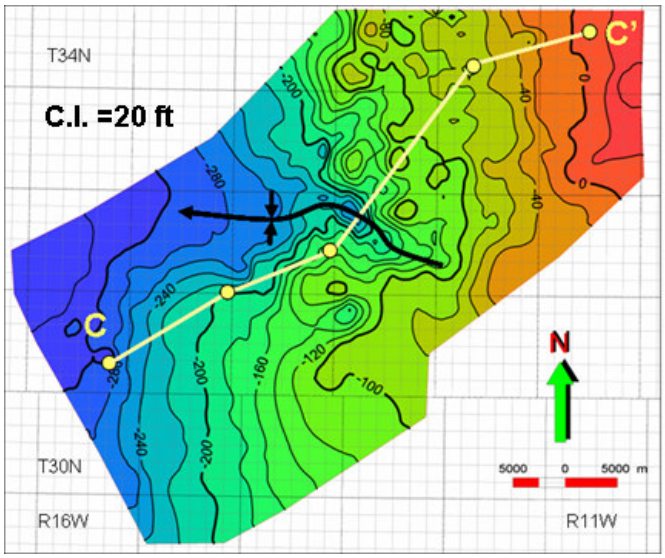


**Fig. 2.6—Structure map of Bentonite 1, Garden Plains field, Sea Level datum. Regional dip is approximately 0.1° westward. Structural relief of the west-plunging syncline is approximately 45 m. See Fig. 2.5 for the stratigraphic occurrence of Bentonite 1 and Fig. 2.7 for cross section C-C.'**

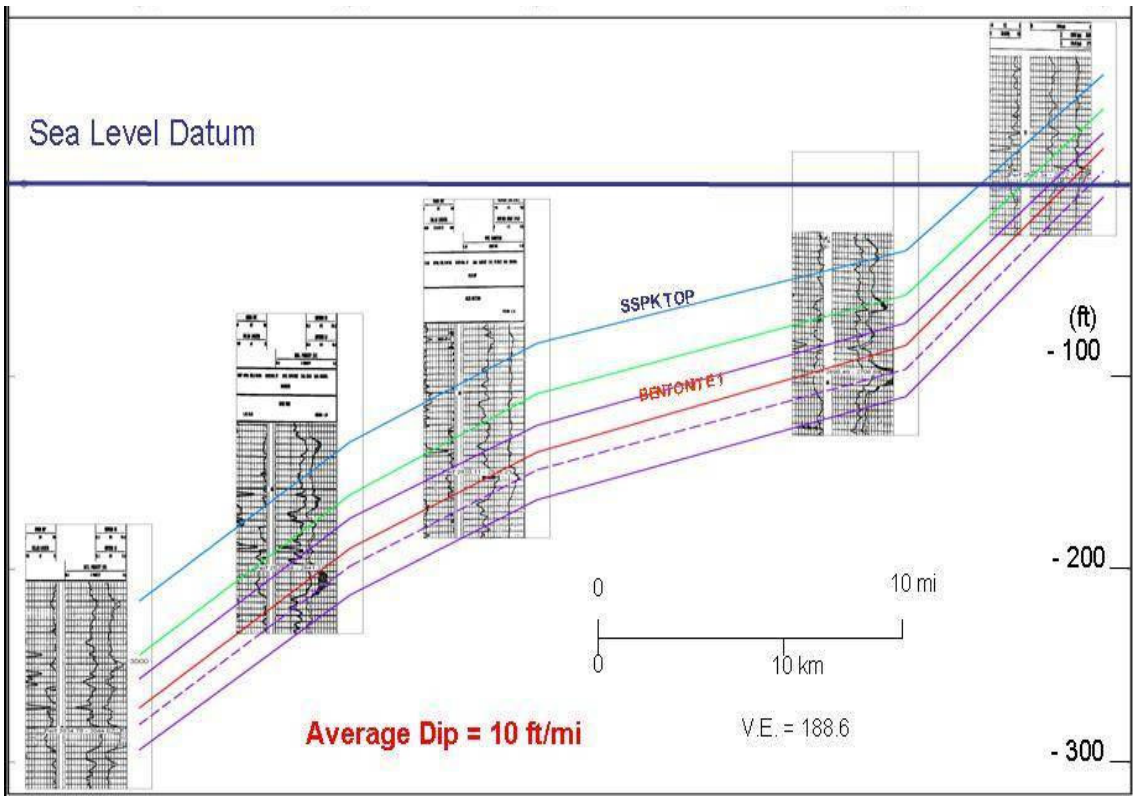


**Fig. 2.7—Northeast-trending structural cross section C—C.' See Fig. 2.6 for location. Gas/water contact was not identified.**

**SSPK Reservoir Architecture**

Unit A is an upward coarsening, northeast-trending, lensoid sand body that ranges between 7 and 17 ft (2-5 m) thick and averages 15 ft (4.6 m) thick (Fig. 2.5 and **Fig. 2.8a**). Lateral extent of the unit is 32 x 10 mi (51.5 x 16 km). Unit B is dominantly upward-fining sand interbedded with shale (Fig. 2.5). It also trends northeastward, but instead of a lensoid geometry in Garden Plains field, it is a north-trending sedimentary wedge that thickens from approximately 7 ft (2.2 m) thick on the southeast to 13 ft (4 m) thick on the northwest side of the field (**Fig. 2.8b**). Its average thickness is approximately 10.5 ft (3.2 m).

Unit C is 18 to 42 ft (5.5 to 13 m) thick (**Fig. 2.8c**). The unit is thickest (as much as 33% thicker) coincident with the west-plunging syncline, indicating that the syncline was forming during deposition of Unit C (compare Figs. 2.6 and 2.8c), whereas isopach maps of Units A and B (Fig. 2.8a and Fig. 2.8b) indicate that the syncline was not actively forming as they were deposited. Unit D strikes northeastward and generally thickens northwestward (**Fig. 2.8d**). It ranges between 20 and 32 ft (6 and 10 m) thick in Garden Plains field. The syncline had minor effect on thickness of Unit D (compare Fig. 2.6 and Fig. 2.8d). Although combined thickness of Units C and D is twice the combined thickness of Units A and B, Units C and D have poor reservoir quality, and thus, they are rarely perforated and are less important in understanding performance of SSPK gas wells.

I favor an offshore bar or shelf ridge origin of the SSPK sands. The SSPK sands in Garden Plains field trend northeastward, oblique to SSPK shoreline. The sand

complexes are approximately 35 mi (60 km) long, 18 mi (30 km) wide, and 16 ft (5 m) thick, typical dimensions for a shelf sand ridge or offshore bar complex. In contrast, shoreface sands commonly are thick 30-45 ft (10-15 m), narrow and linear, extending tens of kilometers along the ancient coastline. SSPK sands are upward-coarsening, and heterogeneous. They have low to moderate porosities and very low permeabilities because primary bedding structures have been obliterated by bioturbation. These are typical characters of shelf sands. Shoreface sands are usually well sorted, upward-coarsening, and very clean fine- to very fine-grained sands. They usually are relatively thick and homogeneous with relatively high porosities and permeabilities. In SSPK sands, strong bioturbation or the reworking of sediment by benthic organism is common (O'Connell, 2005). While this is common in shelf deposition environments, shoreface sands have little or no bioturbation. SSPK sands mainly have upward coarsening well log patterns (typical off-shore bar log pattern), and some upward fining and compound patterns that indicate stacking and amalgamation of storm beds. Shoreface sands usually exhibit upward coarsening log patterns. Core from well 0070102919W4, which is near Garden Plains field, is highly bioturbated in SSPK sands with large zoophycus (typical of marine mud or muddy sand), planolites (characteristic of middle-lower shoreface or offshore shallow marine), and skolithos (common in high energy shallow marine settings) burrows.

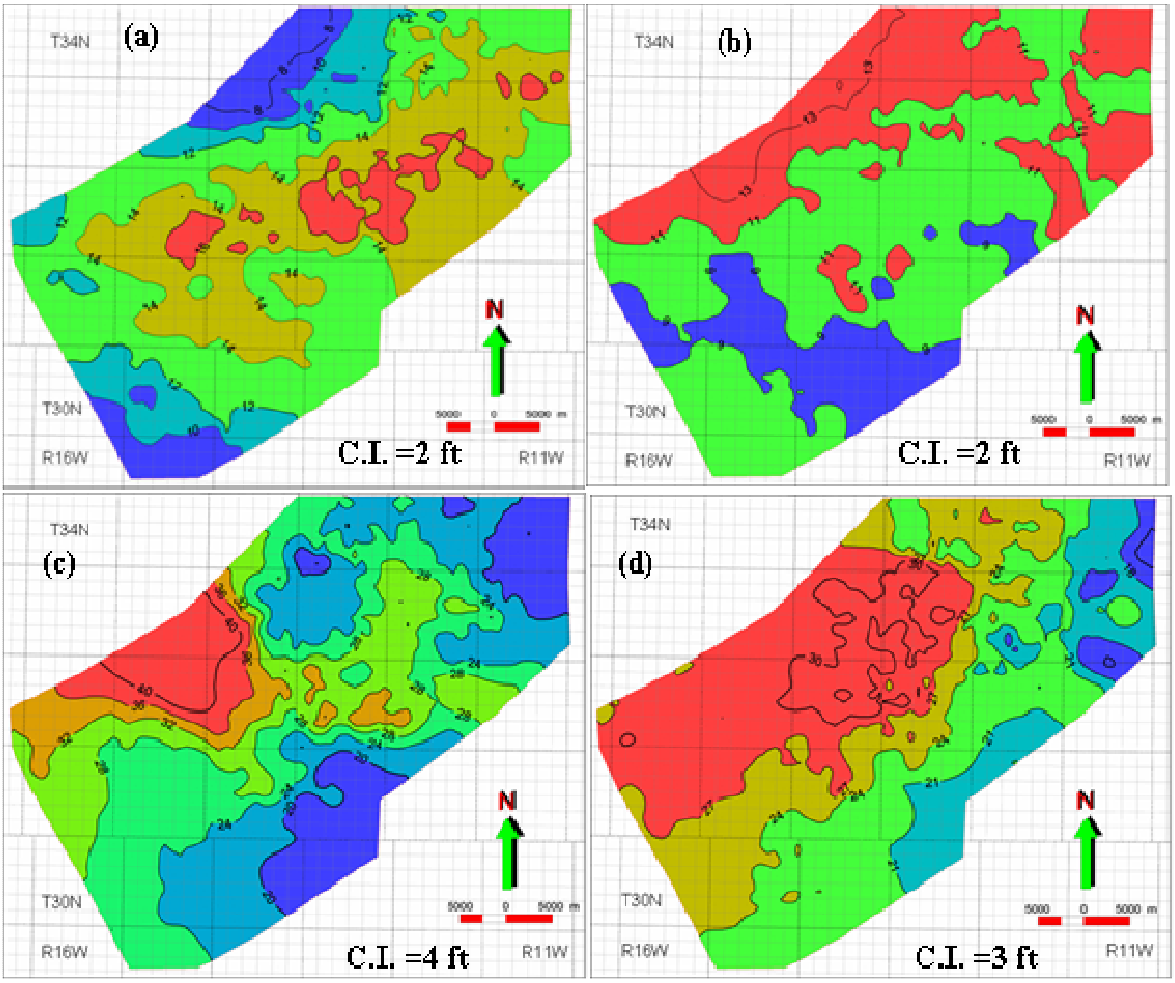


**Fig. 2.8—Gross thickness maps for SSPK Units A- D, Garden Plains field. (a) Unit A is an upward-coarsening interval (Fig. 2.5) that trends east-northeastward. (b) Unit B is an upward-fining interval (Fig. 2.5) that trends northeastward and thickens to the northwest. (c) Unit C is thickest in a west-trending area that coincides with the minor west-plunging anticline (Fig. 2.6). (d) Unit D trends northeastward and thickens to the northwest.**

## 2.4 PETROPHYSICAL ANALYSIS

### Well Log Normalization

Commonly, well log response within a stratigraphic unit varies across a field, owing to instrument calibration error, acquisition error, differences in borehole environments, and differences in various service company instruments. Therefore, reservoir characterization requires that well logs be normalized. Stratigraphic analysis and reviews of well logs revealed significant variation in quality of log response in Garden Plains field. In Shale B (Fig. 5), a marine unit that immediately overlies the SSPK formation, gamma ray (GR) values are highly variable, ranging from 75 to 150 API units among closely-spaced wells (**Fig. 9a**). It was necessary to normalize GR curves to (1) accurately calculate petrophysical properties, such as shale volume, (2) correct the shale effect on neutron porosity response, and (3) determine net-sandstone cutoffs.

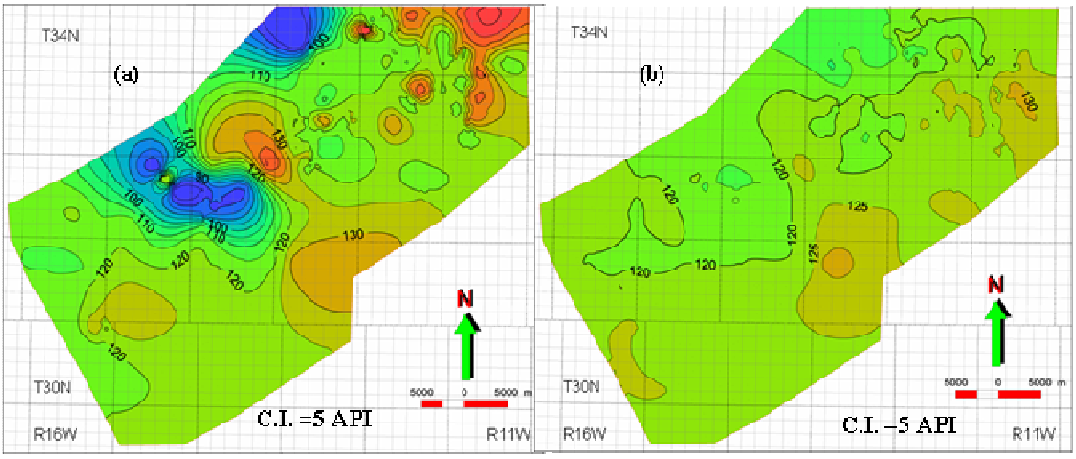


**Fig. 2.9—(a) Average gamma ray response (API units) of Shale B before log normalization. Great variability and range of values GR values in this marine shale suggest the need for log normalization. (b) Average GR response of Shale B after normalization.**

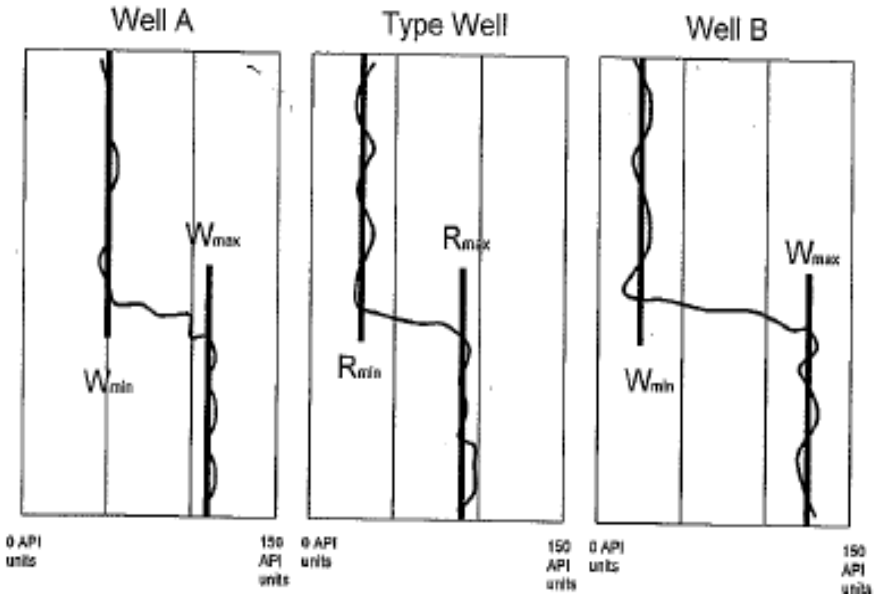


**Fig. 2.10—Normalization parameters for GR curve (from Shier, 2004).**

Preliminary petrophysical analysis showed no relationship between porosity of SSPK sandstone Units A and B determined from core samples and porosity determined from neutron logs, owing to the lack of normalization and neutron calibration. To normalize logs in Garden Plains field, I used Shier's method (Shier, 2004), which is given in **Eq. 2.1**,

$$GR_{norm} = R_{\min} + \frac{(R_{\max} - R_{\min})}{(W_{\max} - W_{\min})} * (GR_{\log} - W_{\min}) \quad \ldots\ldots\ldots\ldots (2.1)$$

where $GR_{norm}$ is the normalized value, $GR_{log}$ is original GR log value, $R_{min}$ and $R_{max}$ are the regional best estimates of the minimum and maximum values of the GR curve in the studied interval, and $W_{min}$ and $W_{max}$ are the corresponding values for each well (**Fig. 2.10**).

After normalization, log values of closely-spaced wells should be similar in the same stratigraphic interval, such as a shale or clean sandstone with consistent fluid

composition. After normalizing the SSPK interval in Garden Plains field, the GR response of Shale B ranges between 110 and 130 API units, whereas before normalization the range was 75 to 150 API units (Fig. 2.9).

**Calculation of Shale Content**

The most accurate method to calculate shale volume ($V_{sh}$) of sandstone from well logs is to calibrate GR or SP responses of the logs using shale content values determined from core. Because I did not have core analyses of shale content, I used the following method to calculate shale volume, after I completed GR normalization and defined sand and shale GR baselines.

First, I calculated $GR_{index}$ as: $GR_{index}= (GR-GR_{min})/ (GR_{max}-GR_{min})$, where GR is the log response in the shaly sand, $GR_{min}$ is GR response in a clean sand zone, and $GR_{max}$ is GR response in a 100% shale zone. I selected $GR_{min}$=70 API and $GR_{max}$=140 API. Then, I used Clavier's equation (**Eq. 2.2**) to calculate shale content, $V_{sh}$:

$$V_{sh}= 1.7-\left[3.38-(GR_{index}+0.7)^2\right]^{0.5} \quad \text{..... (2.2)}$$

**Correction of Neutron Porosity Shale Effect**

High shale content of SSPK sandstone causes the neutron porosity values to be approximately 2-times greater than core porosity values for the same interval (**Fig. 2.11a**)**.** Therefore, neutron porosity cannot be used directly when evaluating porosity of shaly sandstone reservoirs. To determine porosity using neutron porosity logs, the shale effect must be subtracted from the neutron log response to determine effective neutron

porosity. The equation (**Eq. 2.3**) used to calculate effective neutron porosity (PHIN_E) is:

$$PHIN\_E = PHIN - V_{sh}*0.45 \quad \text{..... (2.3)}$$

where PHIN is the well log neutron porosity value and 0.45 is neutron porosity of a 100% shale interval.

**Core-Log Data Depth Shift**

After correcting the neutron porosity response for shale effect, I analyzed SSPK petrophysical properties of 3 key wells (100012103412W4, 100083403312W4, and 100101603312W4) and depth-shifted core data to match well log responses. Initially, core porosity did not match well with effective neutron porosity (Fig. 2.11a), but after depth shifting core porosity to effective neutron porosity, effective neutron and core porosities matched well (**Fig. 2.11b**).

**Reservoir Porosity Calculation**

The most prevalent porosity logs in Garden Plains field are neutron logs. Thus, neutron porosity logs were used to evaluate SSPK porosity throughout the field. After normalization and depth shifting, I calibrated the effective porosity logs by cross-plotting the effective neutron porosity and core porosity. There was a good relationship between core porosity and effective neutron porosity (**Fig. 2.12a**), and thus, I calculated porosity using the following equation (**Eq. 2.4**).

$$Porosity = 0.5454*PHIN\_E+0.0147 \quad \text{..... (2.4)}$$

To verify the accuracy of calculated porosity values, I compared the calculated porosities with core porosities (**Fig. 2.12b**). The agreement between calculated porosity and core porosity is good. Therefore, I applied the above equation to calculate and map porosity throughout the field.

Using net sand cutoffs of 8% porosity and 105 API units on the gamma ray curve ($V_{sh}$) (See below, Cutoff Determinations), average reservoir porosity ranges from 8.9 to 14.8% for Unit A and from 7.6 to 14.6% for Unit B; mean porosities for the two units are 12.4% and 11.8%, respectively.

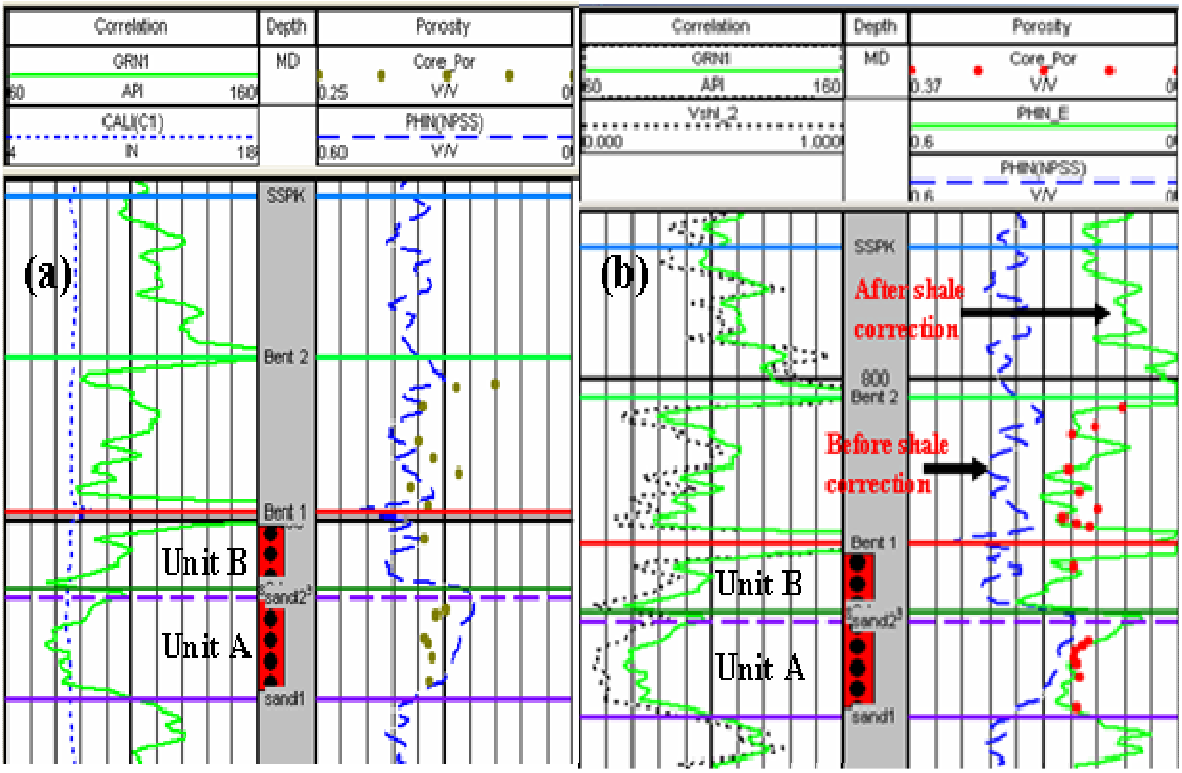


**Fig. 2.11— Core porosity vs. neutron porosity for well 100012103412W4. (a) Before depth shift. Owing to a shale effect, core porosity does not match neutron porosity. Note the difference in scales for core and neutron porosity. (b) After shale correction and depth shift.**

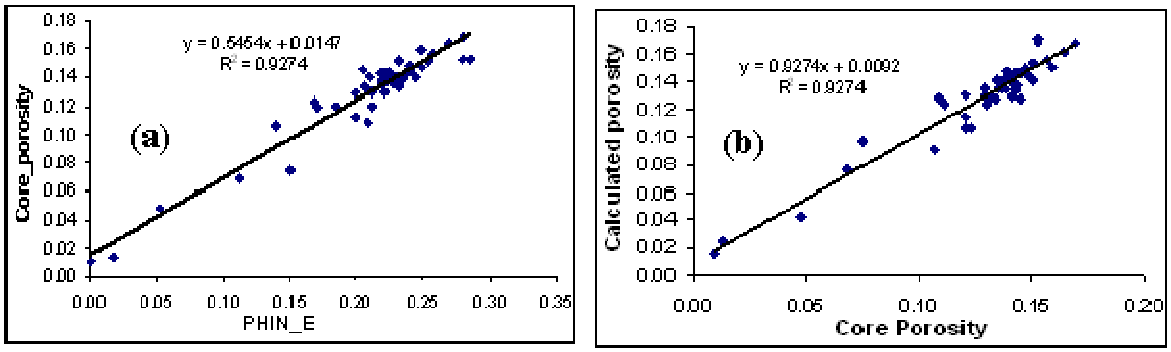


**Fig. 2.12— Porosity calculations. (a) Core porosity vs. effective neutron porosity after shaliness correction and depth shift. (b) Plot of core porosity vs. porosity calculated using logs corrected for shaliness and depth.**

## Permeability Determination

Core data were evaluated to establish a relation between porosity and permeability (**Fig. 2.13**). This relationship is given by **Eq. 2.5**:

$$\text{Permeability} = 464.69*(\text{Porosity})^{3.3028} \quad \ldots\ldots\ldots\ldots \quad (2.5)$$

Using net sand cutoffs of 8% porosity and 105 API units on the gamma ray curve ($V_{sh}$) (See below, Cutoff Determinations), average reservoir permeability ranges from 0.18 to 0.96 md for Unit A and from 0.05 to 1.17 md for Unit B; mean permeability values for the two units are 0.54 and 0.35 md, respectively.

## Cut-off Determinations

Shale volume and porosity cutoffs were used to determine net sandstone thickness in well logs. Net-sand thickness is defined as that part of the gross rock thickness that contributes to hydrocarbon production. Incorrect cutoffs will result in anomalously high or low calculated reservoir volume. However, there is no universal method for determining the correct cutoff. In this study, I evaluated the effects of a

number of possible cutoffs for approximately 168 wells that have digital GR curves, and I defined net sand thickness as those sands intervals having porosity > 8% and gamma ray response <105 API units (equals $V_{sh}$ of 31%) (**Fig. 2.14**).

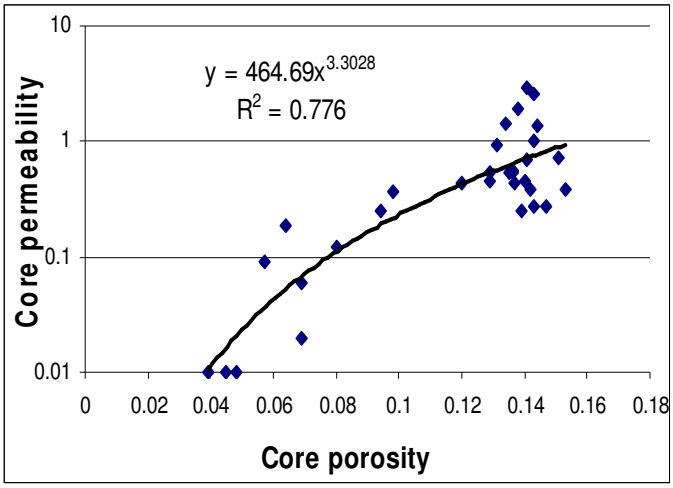


**Fig. 2.13— Core porosity vs. core permeability of net sand intervals, Units A+B, SSPK formation.**

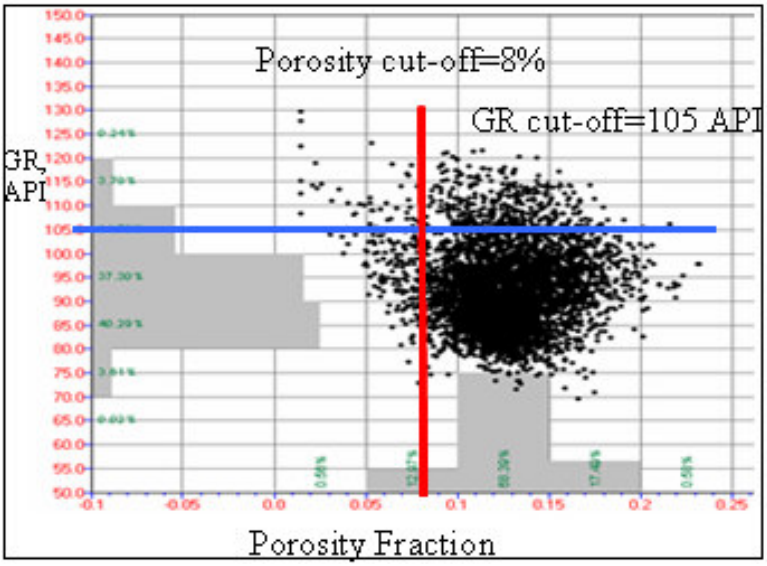


**Fig. 2.14—Determination of net sand cut-offs of 8% porosity and gamma ray of 105 API units.**

## 2.5 RESERVOIR FACIES AND PROPERTIES MAPS

After completing the petrophysical analysis and determining cutoffs, I mapped net sandstone thickness, average porosity, average permeability, and porosity-thickness product of the SSPK Units A and B in Garden Plains field. For some areas of the maps (especially in the south) I interpolated reservoir properties in the absence of data, because there were potential infill well locations, and thus, it was necessary to characterize reservoir properties.

### Net Thickness and Net/Gross Ratio

After applying petrophysical cutoffs, I mapped net thicknesses of Unit A, Unit B, Units A and B combined (Units A+B), and net/gross thickness of Units A and B (**Figs. 2.15a – 15e**)**.** Although most Garden Plains wells are perforated in Units A and B, Unit A is the primary SSPK reservoir. Reservoir properties of Units C and D were not mapped, owing to the limited number of wells completed in those units.

Unit A net sandstone thickness ranges between 7 and 15.8 ft (2.1 – 4.8 m) and averages 12.3 ft (3.8 m) (Fig. 2.15a)**.** The net sandstone thickness map depicts Unit A as a continuous, elongate, northeast-trending sand body, consistent with the gross thickness map (Fig. 2.8a). Net/gross ratio of Unit A is 55-95% (average = 85%) (Fig. 2.15d). The net/gross map shows a strongly developed northwest trend that contrasts with the well developed northeast trend of the net thickness map (compare Figs. 2.15a and 2.15d) and suggests greater reservoir heterogeneity than indicated by the net sand map.

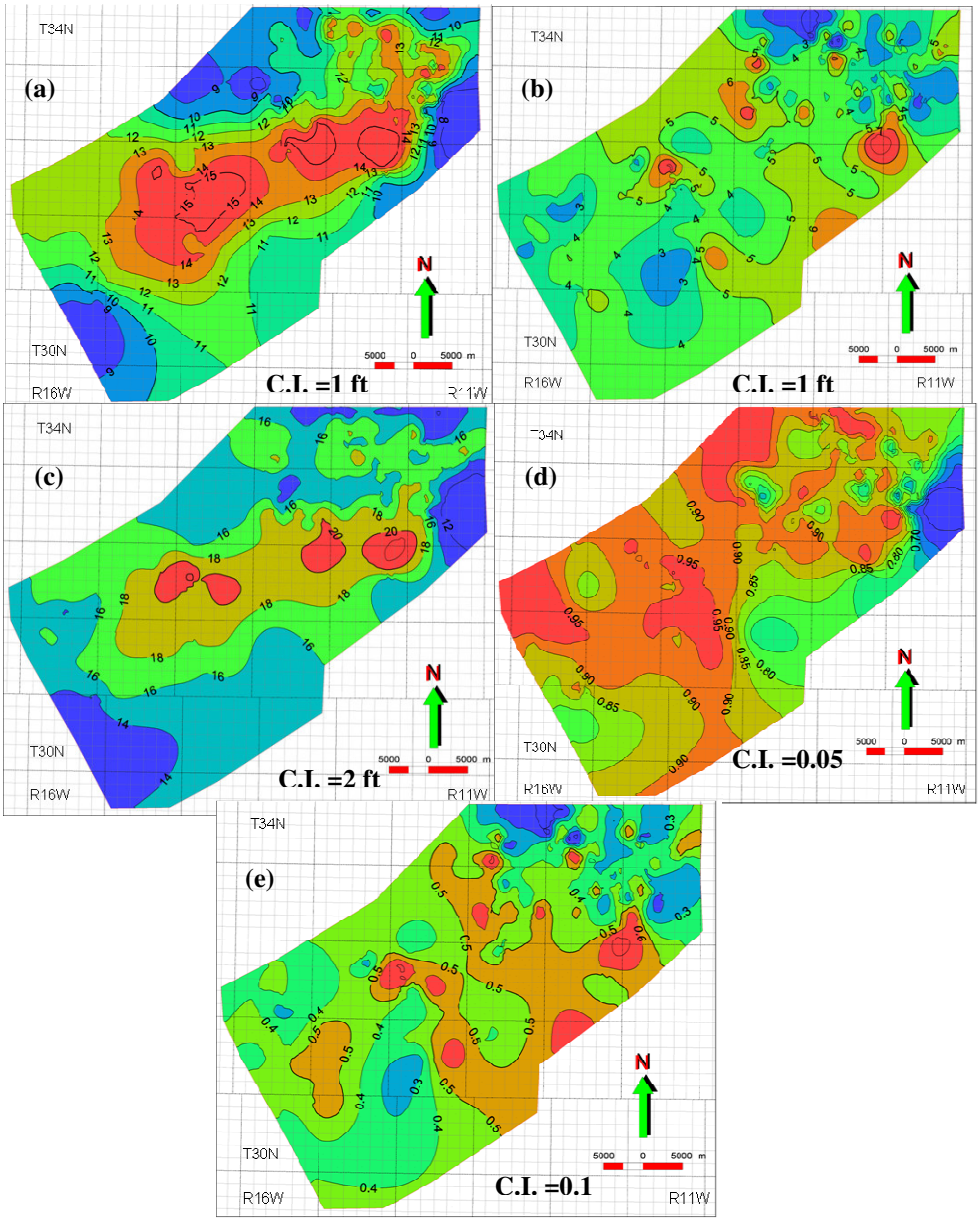


**Fig. 2.15— Net-sandstone thickness maps. Net-sandstone thickness (ft) of SSPK Unit A (a) and Unit B (b). (c) Net-sandstone thickness (ft) of Units A+B. Net/gross ratio of Unit A (d) and Unit B (e).**

Net sandstone thickness of Unit B ranges from 0.5 ft to 9 ft (0.15 – 2.7 m) and averages 4.2 ft (1.3 m) (Fig. 2.15b). Unit B is 10 to 70% sand (average ~45%) (Fig.

2.15e). In Unit B, strongly developed northwestward trends are apparent in both the net sandstone thickness and net/gross thickness maps (Figs. 2.15b and 2.15e).

Combined net sandstone thickness of Units A and B (A+B) ranges from 10.5 ft to 22 ft (3.2 – 6.7 m) and averages 16.5 ft (5.1 m) (Fig. 2.15c). This map suggests a continuous, homogeneous, northeast-trending SSPK reservoir, owing to the fact that net thickness of Unit A is generally 2-3 times greater than thickness of Unit B (compare Fig. 2.15a and 2.15b). There is no indication in either the net sandstone or net/gross maps that the syncline which crosses the west-central part of the field (Fig. 2.6) was active during sedimentation. Sandbody trends appear to be unaffected by that structural feature.

As noted above, the net/gross thickness (sandstone fraction) maps of Units A and B indicate greater reservoir heterogeneity than do net sandstone thickness or the gross thickness maps. To further assess reservoir heterogeneity, I mapped well log gamma ray patterns (electrofacies) of SSPK Units A and B.

**Log Facies**

GR well log patterns may indicate sedimentary facies and energy of the transporting medium. Commonly, in clastic depositional systems, high-energy facies have coarser grain size (low GR values) and greater primary porosity and permeability than do low energy facies (high GR values). Thus, the vertical changes in GR response may indicate changes of energy the transport medium. Because the magnitude of energy acting in a depositional system varies with the local depositional setting, log pattern maps may be used in conjunction with sedimentary facies maps to interpret paleogeography. Both Units A and B have strongly developed northwest well log facies

trends (**Figs. 2.16** and **2.17**). The areas of northwest-trending, upward fining and upward coarsening facies (high-energy well-log facies) coincide with the northwest-trending areas of greater sandstone percentage in the net/gross maps (compare Figs. 2.16a and 2.16b with Figs. 2.15d and 2.15e, respectively). Orientation of these high-energy facies orthogonal to the primary axes of the sandbody complexes reinforces the conclusion that SSPK reservoirs are more heterogeneous than indicated by the gross thickness and net sandstone maps (Figs. 2.8a, 2.8b, and 2.16a).

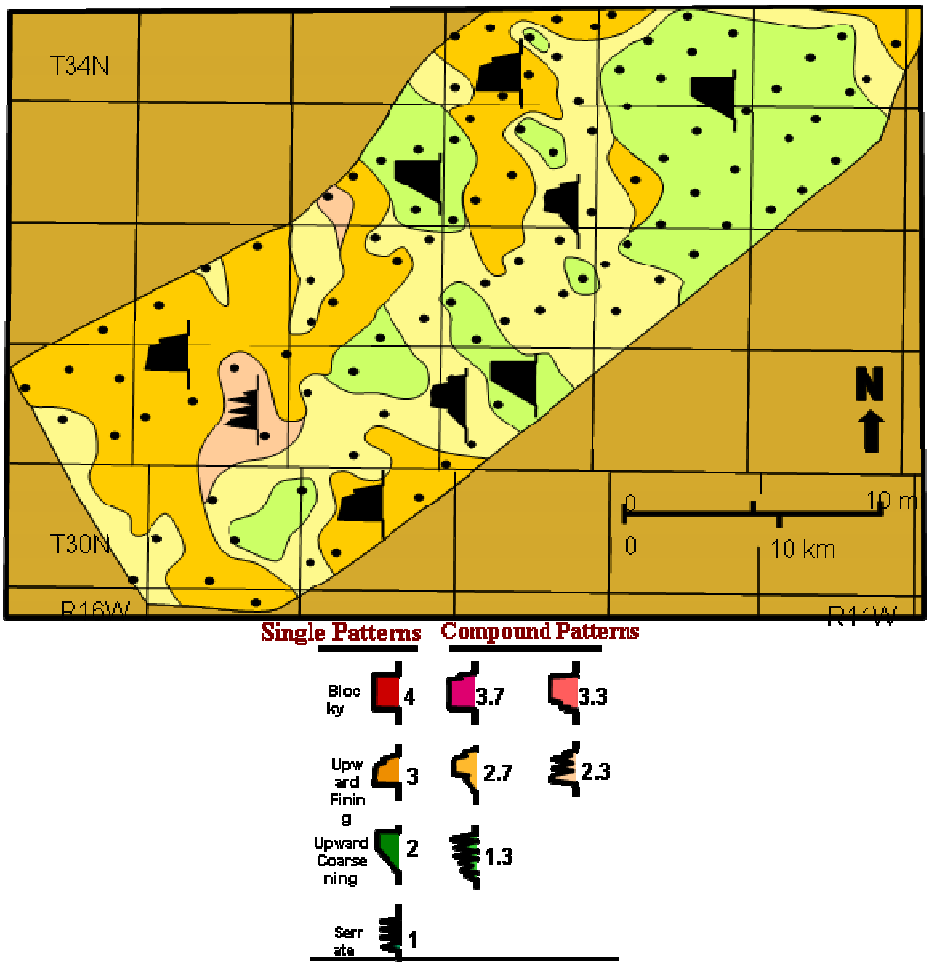


**Fig. 2.16—Well-log patterns/facies for SSPK Unit A. Generally, log facies are complex and trend northwestward. Log pattern classification is shown with a numerical classification that is sometimes used for computer contouring.**

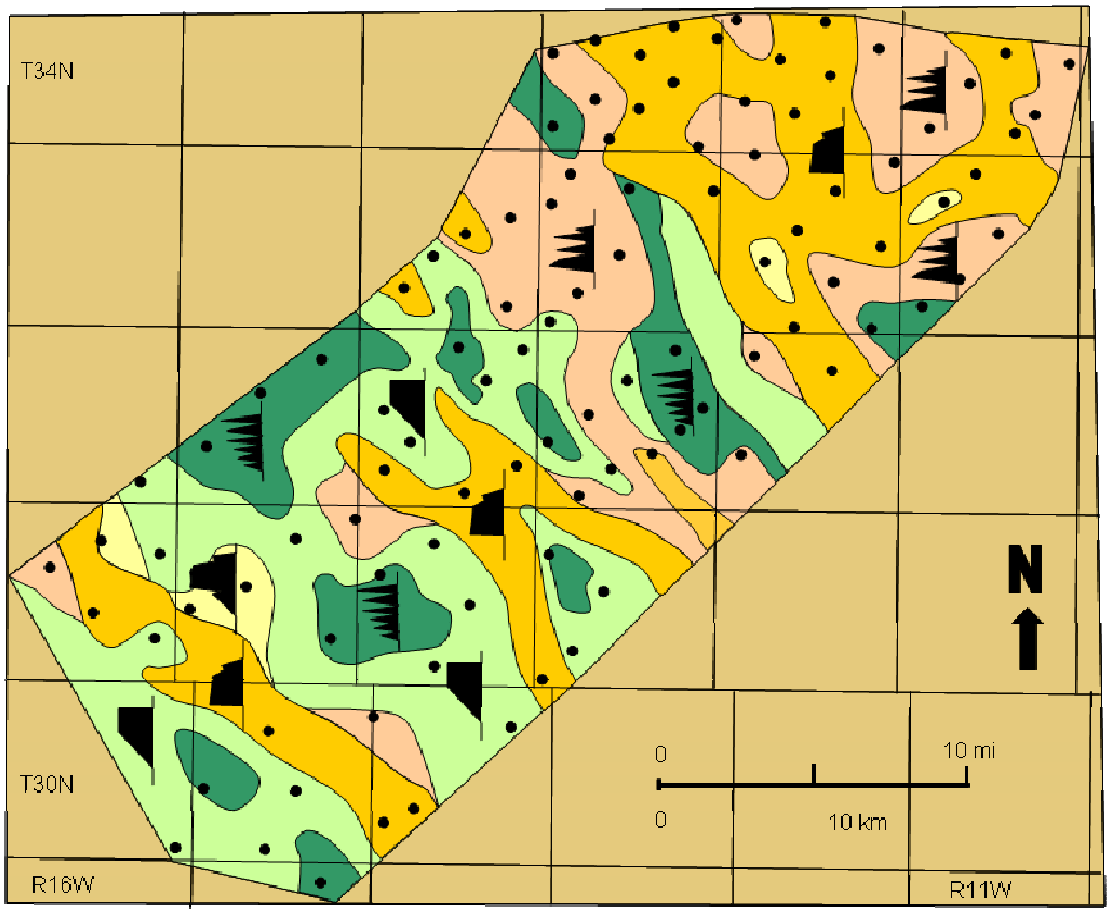


**Fig. 2.17—Well-log patterns/facies for SSPK Unit A.**

## Reservoir Porosity and Permeability

Using the petrophysical analysis described above, I calculated and mapped average porosity and average permeability for the combined net sandstone intervals of Units A+B (**Figs. 2.18a** and **2.18b**, respectively). High and low values porosity and permeability values coincide in these maps, because permeability was derived from the porosity-permeability transform. Porosity and permeability vary considerably across the field, suggesting significant reservoir heterogeneity.

**Porosity-Net Thickness Product**

To investigate effects of total pore volume on reservoir performance, I mapped the porosity-net-thickness product for the combined Units A+B, using data for each well that had digital log data (**Fig. 2.18c**). Porosity-net-thickness product of the combined Units A+B ranges between 1.4 and 2.6. Anomalously high and low values of porosity-net-thickness product trend northwestward and northeastward.

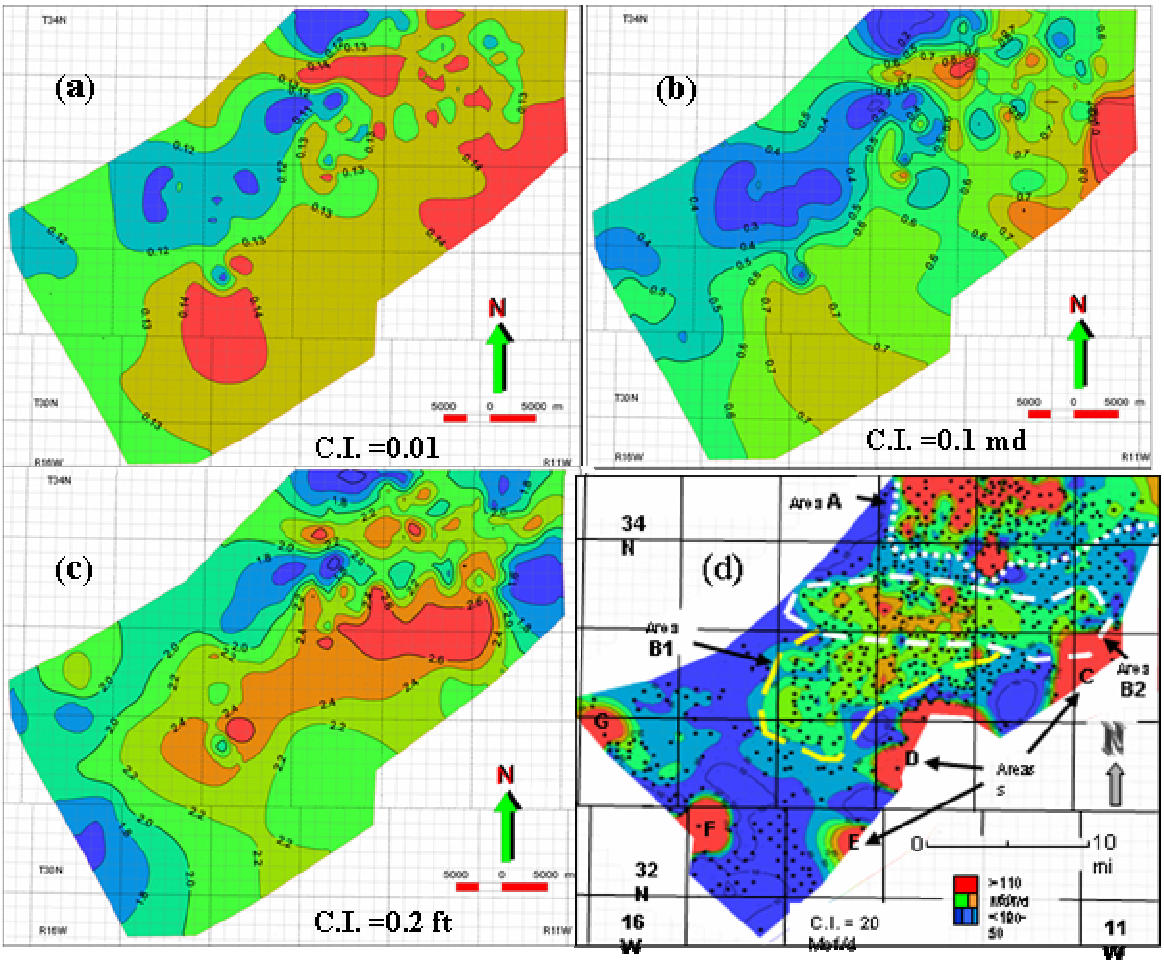


**Fig. 2.18— Geologic controls on gas production of SSPK reservoir in Garden Plains field. (a) Average porosity and (b) average permeability (md) of SSPK Units A+B. (c) Porosity-thickness product of SSPK Units A+B. (d) Best year production of SSPK reservoir in Garden Plains field. Best year production is defined as average daily production during the best 12 consecutive months of production.**

## 2.6 GEOLOGIC CONTROLS ON RESERVOIR PERFORMANCE

### Production Summary

In Garden Plains field, 772 gas wells have produced gas from only the SSPK. First production in this area was in April 1979. In August 2004, 741 wells reported gas production, whereas 31 wells had no reported gas production. Condensate yield is very limited from the field. Few wells have water production records. In Garden Plains field, 75% of the SSPK gas wells are stripper wells (production < 60 Mcf/d [1700 $m^3$/d]). Cumulative gas production for the field was 46 Bcf (1.3 x $10^9$ $m^3$) through December 31, 2004.

To assess geologic controls on reservoir performance, I calculated and mapped values of best year of gas production (BYG) (**Fig. 2.18d**), which was defined as average daily gas production during the best consecutive 12 months of production of each well. Also, I plotted values of BYG against the porosity-net thickness product (**Fig. 2.19**) and compared the BYG and structure maps (Figs. 2.6 and 2.18d). During the best year of production, SSPK average daily gas production from individual wells ranged from 0.7 to 175 Mcf/d (Fig. 2.19), and the average for all wells was 61 Mcf/d.

Generally, BYG is greater in the northeast 2/3 of Garden Plains field (> 50 Mcf/d) than in the west and southwest 1/3 of the field (generally, BYG < 30 Mcf/d) (Fig. 2.18d). BYG exceeds 50 Mcf/d and commonly is greater than 100 Mcf/d in an east-trending belt along the northwest margin of the field (Fig. 2.18d, Area A). In the center of the field, the 50 Mcf/d contour encloses higher producing wells that, in the south, form a northeast-trending pattern and on the north have a strongly developed, east-

trending pattern (Fig. 2.18d, areas B1 and B2, respectively). Three areas of high BYG that occur along the southeast margin of the field (Fig. 2.18d, Areas C, D, and E) result from a total of 4 data points, and the 2 bulls-eye patterns in the south part of the field (Fig. 2.18d, Areas F and G) result from one data point each. Thus, areas C-G are production anomalies that should be further investigated to determine whether they are due to either (a) anomalous reservoir character, such as natural fractures, or (b) erroneous data. These areas were not considered in our evaluation of geologic controls on gas production in the next section.

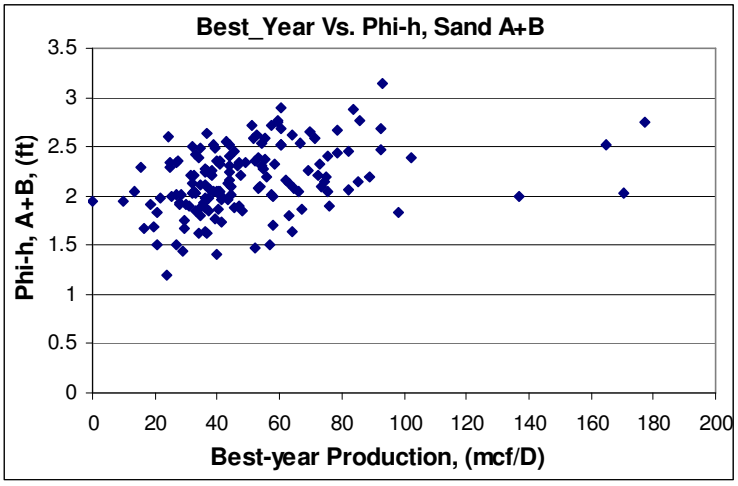


**Fig. 2.19—Porosity-thickness product of Units A+B vs. best year production.**

## Geologic Controls on Gas Production

*Structural Controls*

Elevation of the SSPK is highest (>40 ft [12 m] above SL) along the northeast margin of the field (T33-34N, R11W), which is an area of low to intermediate BYG. Structural position does not appear to be the sole determinant of reservoir performance. However, as noted above, wells in the structurally high east and northeast 2/3 of the field

have relatively high BYG (30-120 Mcf/d) in comparison to the structurally low west and southwest areas of Garden Plains field, where generally, BYG is <30 Mcf/d (Fig. 2.6 and Fig. 2.18d). Moreover, preliminary analysis indicates higher water/gas ratios in the west and southwest areas (MGV Energy, 2004). In several cases, local areas of high BYG appear to coincide with subtle structural closures having approximately 20 ft (6 m) of relief. These small structural closures and the west-trending syncline formed after deposition of Units A and B and during deposition of Units C and D, as demonstrated in isopach maps (Figs. 2.8a to 2. 8d). It is unclear whether the small closures are small folds or minor faults that may result in fracture-enhanced permeability or, whether they are products of soft-sediment deformation.

*Porosity-Net-Thickness Product*

High BYG values in areas B1 and B2 of Garden Plains field coincide with regions of greater than average net-sandstone thickness and high porosity-net-thickness product of Unit A and Units A+B (Fig. 2.15a and Fig. 2.15c, Fig. 2.18c, and Fig. 2.18d). It appears that net thickness of Units A+B (especially net thickness of Unit A) exercises primary control on gas production. However, the highest BYG occurs in an east-trending belt of along the northwest margin of the field (Fig. 2.18d, area A). This is an area of lower porosity-net-thickness product (Fig. 2.18c), but it is the site of the earliest wells in the field (MGV Energy, 2004) and may indicate higher production associated with high initial reservoir pressures. The east-trending area of low BYG between Areas A and B1 (Fig. 2.18d) coincides with low permeability (Fig. 2.18b).

# 3. EVALUATION OF RESERVOIR CONNECTIVITY AND DEVELOPMENT RECOVERY STRATEGIES IN MONUMENT BUTTE FIELD, UTAH

## 3.1 INTRODUCTION

### Background

Monument Butte oil field, located in the central Uinta basin, Utah (**Fig. 3.1**), was discovered by Diamond Shamrock in 1964 when they drilled the Walton Federal #1-11 well (Larsen and Zellitti, 1997). Initial oil discovery stimulated drilling activities in the area, but drilling slowed in late 1980s when the oil price was very low. To improve oil recovery, Lomax Exploration Company initiated a water flood in Monument Butte Unit in 1987. Success of this water flood prompted Lomax and its successor, Inland Resources, and the U.S. Department of Energy (DOE), to start the DOE Class I (Fluvial-Deltaic Reservoirs) demonstration project in 1992 (Deo et al., 1994). The demonstration project confirmed the economic feasibility of water flooding reservoirs of the middle and lower members of the Green River formation. Since then, the greater Monument Butte area has become a major oil producing region of the Uinta basin. In August 2004, Newfield Exploration Company purchased Inland Resources. Newfield planned to develop the field on 40-acre well spacing. As of December 31, 2006, there were 900 producing wells and 400 water injection wells in Monument Butte field. Included in these wells is a successful 20-acre infill drilling pilot program that was initiated in 2006. This pilot project indicates that the field could support an additional 1,000 wells, if developed with 20-acre well spacing. A major goal of this research was to evaluate

reservoir connectivity and optimal oil recovery strategies and well spacing in Monument Butte field.

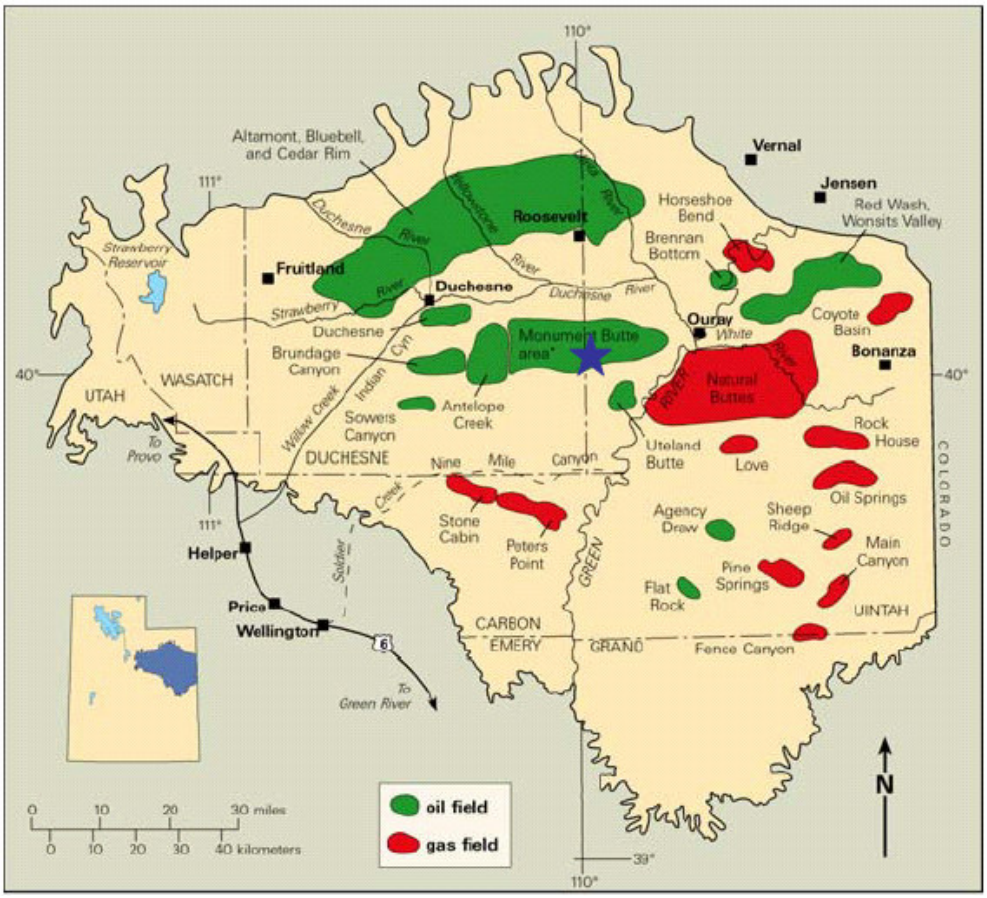


**Fig. 3.1—Location of Monument Butte field (star symbol) in central Uinta basin (from Chidsey et al., 2004).**

The Green River formation in the Uinta basin (Fig. 3.1) has produced more than 200 million barrels of oil. Cedar Rim, Altamont, Bluebell, and Red Wash fields produce oil from Green River formation sandstones that were deposited along the north shoreline of Lake Uinta during the Eocene, whereas the fields in the greater Monument Butte area (Fig. 3.1) produce from middle and lower Green River formation deltaic sandstones southern deposited along the southern margin of the lake (Morgan et al., 2002).

Monument Butte field produces from at least 22 different stratigraphically trapped sandstone reservoirs identified across a 2,200-ft stratigraphic interval from approximately 4,000 to 6,500-ft depth. Reservoirs are composed of very fine-grained sandstones and siltstones that are encased in shales, tight siltstones, and marlstones. The reservoir sands are lenticular, and they have limited aerial extent and questionable horizontal and vertical connectivity. Although individual wells may intersect 10 to 20 hydrocarbon-bearing sands, oil is produced mainly from 4 or 5 sands.

The primary production performance of the Monument Butte field was typical of an undersaturated reservoir close to its bubble point. The GOR increased quickly within a few weeks into the primary production process (Morgan et al., 2002). The increased gas production slowed the oil production significantly, causing low primary recovery (less than 5%). Initially, water-flood technology was not considered feasible for the marginally economic Monument Butte field. The Green River lacustrine fluvial-deltaic sandstones are highly heterogeneous and laterally discontinuous, and they have low porosity and permeability. The waxy nature of the crude oil further contributed to the preliminary assessment that water flooding was not a viable option for Green River formation reservoirs. However, primary recovery of less than 5% made the application of secondary recovery a necessity. The DOE Class I water-flood demonstration project was successful because it maintained the reservoir pressure above the bubble point (Deo et al., 1994). However, water flooding provides a poor sweep of this heterogeneous reservoir, resulting in an overall recovery of less than 5% of the OOIP by primary plus secondary production (Morgan et al., 2002).

A more detailed reservoir characterization and better assessment of secondary and tertiary recovery methods were needed to increase oil recovery efficiency in Monument Butte field. This study focused on Green River oil reservoirs in the northwest part of Monument Butte field (**Fig. 3.2**). The study area is a 35-well area that covers mainly the Wells Draw Unit and parts of the South Wells Draw and Travis units. Presently, 18 wells are oil producers and 17 wells are water injectors, with uniform 40-ac well spacing.

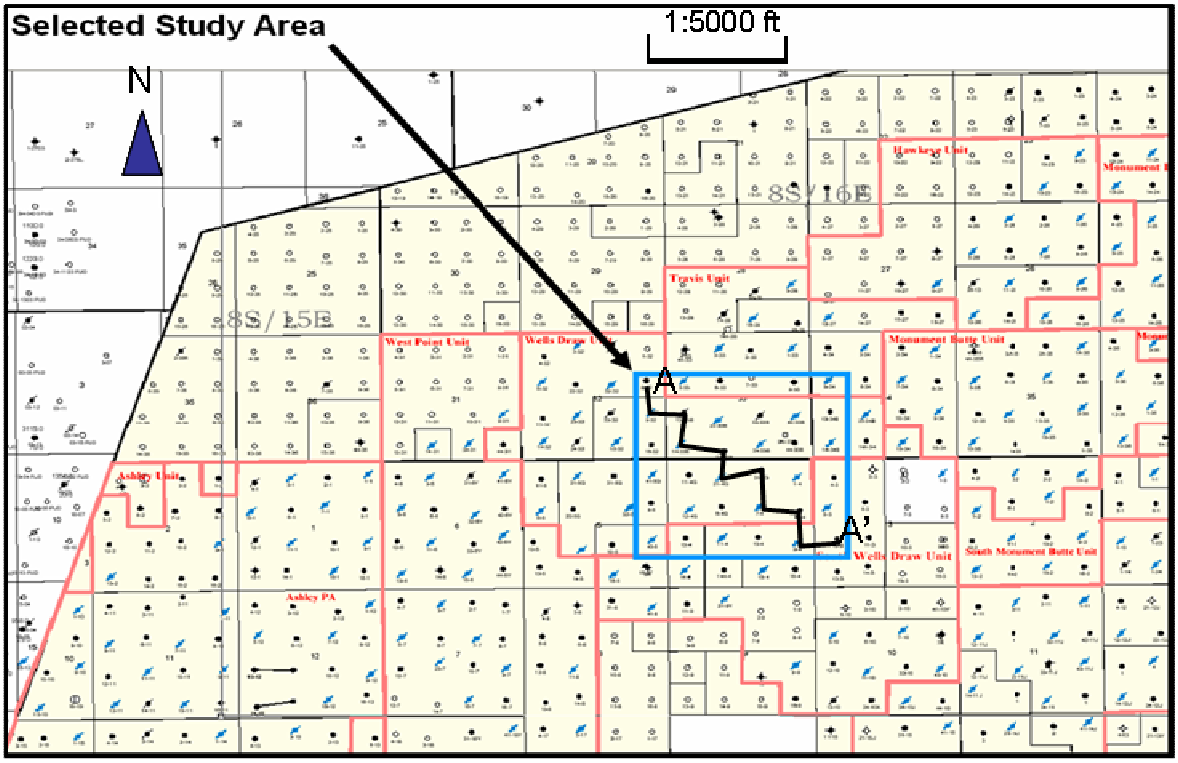


**Fig. 3.2— Location of the study area in the northwest part of Monument Butte Unit. It covers mainly the Wells Draw Unit and parts of the Travis and South Wells Draw units. See Figure 3.3 for cross section A-A'.**

## Present Status of the Questions and Literature Review

### *Geostatistical Reservoir Characterization and Interwell Connectivity*

Improving the water-flood performance requires an understanding of the uncertainty associated with reservoir heterogeneities and connectivity at the interwell scale, which can be achieved through reservoir modeling. There are several ways to evaluate reservoir heterogeneities and connectivity (Hill, 2004; Ainsworth, 2005), including 3D geostatistical characterization techniques (Journel and Alabert, 1990; Weber and van Geuns, 1990; Budding et al., 1992; Dubrule, 1998). This approach allows integration of multidisciplinary data at different scales and the generation of probabilistic 3D models of reservoir connectivity. In addition, geostatistical characterization techniques allow inclusion of uncertainty of reservoir connectivity in reservoir simulation assessments of development strategies for optimization of oil and gas recovery (Haldorsen and Damsleth, 1990; Wolcott and Chopra, 1991; Cosentino, 2001). Several authors have also proposed different methods for analyzing reservoir connectivity (Stauffer, 1985; Haldorsen and MacDonald, 1987; King, 1990; Yuan and Strobl, 1991; Ainsworth, 2005; Yousef et al., 2005). In this research, 3D geostatistical characterization techniques were used to generate probabilistic 3D models that reflect the uncertainty in heterogeneities and connectivity of Green River sandstones at the interwell scale.

*Ranking Geostatistical Reservoir Realizations*

During geostatistical reservoir characterization, it is common to generate a large number of realizations of the reservoir model to assess the uncertainty in reservoir descriptions and performance predictions. However, in practice only a small fraction of realizations can be used to perform full-scale simulation assessments due to expensive computation time required to do history matching on all realizations. Therefore, the number of realizations commonly is reduced through a ranking process.

Currently, there is no consensus as to what criteria should be used for model ranking. Ranking could be done by static or dynamic methods. A common static ranking method is 3D visualization of the geological models. During this process, the modelers and geologists will visually compare each model with the best knowledge of the geological features. This is very time consuming, and one could be misled by personal experience. Another common method is the use of statistical correlation between input and output data. Theoretically, all stochastic modeling algorithms are able to reproduce statistics of the input data (Isaaks and Srivastava, 1989). If there is a poor correlation between input and output data statistics in a particular model, this model could have problems. Since most realizations will reproduce statistics of the input data, this method can not identify the best realization. Also, pore volume can be used to rank geological realizations. It is common practice to avoid extreme values. The drawback of static ranking methods, such as pore volume, is that they do not account for dynamic flow behavior.

One of the most common dynamic ranking methods is sweep efficiency ranking (Idrobo et al., 2000; Vasco and Datta-Gupta, 2001; Ates et al., 2003). The model that gives the best sweep efficiency is the best realization. However, better sweep efficiency does not necessarily mean that the realization best represents the actual geology of the reservoir. If production data are available, integration of these data with geostatistical realizations can reduce the uncertainty. A good geological model should reproduce production history in a simulation run, so I ranked these realizations based on their match to production history. Dynamic ranking can be done with conventional finite-difference simulation; however, this is not practical due to the extensive time needed for all realizations (Scheepens, 2003). Streamline simulation, which has gained rapid acceptance over the past 10 years (Datta-Gupta and King, 1995; Datta-Gupta, 2000; Vasco and Datta-Gupta, 2001), helps to rapidly rank a large number of realizations. because it is much faster than a conventional finite-difference simulator. In this research project, a streamline simulator (FrontSim) (FrontSim, 2007) was used for model ranking.

*Reservoir Simulation and History Matching*

A simulation model represents an oil or gas reservoir in its size, shape and physical characteristics. Its main use is to numerically duplicate reservoir performance by incorporating physical parameters that dictate subsurface flow in porous media (Rietz and Palke, 2001). Reservoir simulation is usually the only way to quantitatively describe the flow of multiple phases in a heterogeneous reservoir having a production schedule determined not only by properties of the reservoir, but also by market demand, investment strategy, and government regulations (Mattax and Dalton, 1990). The value

of reservoir simulation to field management is the ability to predict future reservoir performance under a specified development scenario. However, the simulation model must be verified, because one can not observe, measure, and test every aspect of a hydrocarbon reservoir. The most useful way to verify the model is to simulate past performance of the reservoir and compare the simulation with actual, historical performance. The input data usually must be adjusted in this process to match past performance. This calibration process provides a more accurate reservoir model for forecasting.

One limitation of history matching is that it does not provide a unique solution. That is, more than one outcome may fit the field performance data. It is the engineer's responsibility to judge among the different outcomes. In making this judgment, the engineer should analyze other sources of data, such as well logs, production tests, core analyses, and geological interpretation (Lee and Wattenbarger, 1996).

Currently, most history matching is done by trial and error (manual history matching), with the engineer using analysis and judgment to modify the reservoir data and then rerun the simulator. Engineers often use local or regional multipliers to adjust reservoir properties to achieve matching. In general, the data that are matched are pressure, water/oil ratio (WOR), gas/oil ratio (GOR), water/gas ratio (WGR), water and gas arrival times, and fluid saturations. Matching historical WOR, GOR, or WGR is usually the best way to validate estimates of effective zonation and reservoir connectivity (Mattax and Dalton, 1990). Manual history matching by trial and error in most cases is very tedious and time consuming. The selection of parameters to be

adjusted is often subjective and depends upon engineering experience or intuition, so that a history-matched reservoir model may not be realistic or compatible with the geological model.

In recent years, automatic history matching has increased in popularity. The principal advantages of this approach are that it can significantly reduce the time necessary to obtain a history match and it removes some of the dependence on experience of the engineer. The quality of the match is quantified in terms of an objective function, the sum of squares of the differences between observed and calculated production response. The goal is to minimize the objective function to match historical production responses. The approaches to such minimization can be classified into three categories: gradient-based methods, sensitivity-based methods, and derivative-free methods. The derivative-free approaches, such as simulated annealing or genetic algorithms, require numerous flow simulations and thus can be computationally prohibitive for field-scale applications (Oliver et al., 2001). Gradient-based methods have been used widely for automatic history matching, although the convergence rates of this method are typically slower than sensitivity-based methods such as Gauss-Newton or the LSQR methods (Bissel, 1994; Oliver et al., 2001). The gradient of the objective function is calculated to find the search direction to minimize the objective function (Chu et al., 1995). Sensitivity-based methods calculate sensitivity coefficients, which are the gradients of production responses with respect to the model parameters (Chu et al., 1995; Landa and Horne, 1997; Wen et al., 1998). Based on the coefficients, a system of

equations called the “inverse system” can be constructed and solved to minimize the objective function.

Inverse problems are typically ill-posed and can result in non-unique and unstable solutions. Most current automatic history matching methods become computationally prohibitive when a large number of parameters and observed data are involved. In complex reservoirs, the relationship between the production responses and reservoir properties can be highly nonlinear. This often causes the solution to converge to a local minimum.

Both manual and automatic history matching methods have their respective advantages and disadvantages. In this project, I proposed to combine manual and automatic history matching methods to rapidly achieve an accurate history match. First, field-wide matching was performed using manual matching methods by changing local and regional multipliers. Then, an automatic method was used to match individual well production responses. By following a proper procedure, the history matching process was much shorter than using either manual history matching or automatic history matching.

*Optimization of Oil and Gas Recovery*

Once the model is built, history matched, and thus verified, it can be used predict future performance. The objective of a field simulation study usually is to test alternative development scenarios for a field to optimize either recovery or economic returns (Coats, 1982). This is an attempted optimization, because no one ever knows the best depletion scenario. Optimization is usually accomplished by comparing reservoir

performance to a base case, which usually represents continuing current operations. Then, other cases are run that represent alternative operations, such as changing the water-flood patterns, changing recovery strategies (e.g., water alternating gas), or infill drilling (Christian et al., 1981; Wendschlag et al., 1983).

The DOE Class I demonstration project at Monument Butte field (Deo et al., 1994) showed that, by starting a water flood soon after drilling the wells in a unit, the reservoir pressure could be maintained above the bubble point, resulting in greatly increased oil recovery. It is now common practice in the Monument Butte area to drill on 40-acre well spacing, produce all the wells initially for a few months, and then convert every other well to a water injection well. Although water flooding in Monument Butte field was reportedly successful in maintaining reservoir pressure (Deo et al., 1996), it provides a poor sweep of the reservoir because of low permeability and porosity, unfavorable oil-water mobility ratio due to high oil viscosity, and significant reservoir heterogeneity and unmatched perforation intervals between injectors and producers, which result in poor interwell connectivity. With a combined recovery of less than 5% by primary and secondary recovery methods, it may be possible to improve oil recovery in the greater Monument Butte area using tertiary recovery methods that feature miscible displacement. Candidate tertiary methods are WAG, $CO_2$ flooding, or gas (methane) injection. Infill drilling may be another effective way to improve oil sweep efficiency in the reservoir.

A pilot $CO_2$ flood was attempted in Red Wash field in the 1980's, when $CO_2$ was injected in four wells producing from the Douglas Creek member of the Green River

formation (Morgan et al., 2002). Breakthrough $CO_2$ reached neighboring wells almost instantly in two of the tests. As a result, the pilot program was abandoned (there are no detailed descriptions available of the $CO_2$ project in Red Wash field).

**Objectives**

Specific objectives of the Monument Butte research are to (1) assess reservoir connectivity via geological modeling and reservoir simulation history matching, (2) determine optimal oil recovery strategies, including secondary and tertiary methods, for existing and future development areas, and (3) evaluate infill drilling potential in Monument Butte field.

**Research Approach**

Below is an outline of the research strategies that were used to assess oil recovery strategies in Monument Butte field.

1. Characterize static reservoir properties.
    - Define the major geometry and architecture of the reservoirs in the Wells Draw area by correlation of stratigraphic markers in the Green River formation.
    - Evaluate petrophysical properties and determine cut-offs.
    - Conduct a 3D geological modeling using sequential Gaussian simulation.
2. Build reservoir simulation model.
3. Rank geological realizations using streamline simulation.

4. Conduct history matching. This required developing a workflow to combine manual and automatic history matching methods to achieve accurate and rapid history matching.
    - First stage: overall pressure matching of the study area by adjusting local or regional pore volume multipliers and individual-well productivity indices
    - Second stage: phase ratios (GOR, WCT) matching by adjusting regional permeability multipliers and relative permeabilities
    - Third stage: individual well performance matching using automatic history matching by adjusting local permeability multipliers (SimOpt, 2005)
5. Evaluate and compare interwell connectivity results with geological evaluation (Abiaze, 2008).
6. Evaluate development strategies (primary, secondary, and tertiary) for optimization of future oil and gas recovery.
    - Compare primary-then-water-flood and water-flood only strategies.
    - Conduct compositional PVT matching of experiments performed by the PVT laboratory on the fluid sample.
    - Conduct compositional simulation to evaluate $CO_2$, $N_2$, and $CH_4$ injection strategies.
7. Assess the potential of infill drilling.

## 3.2 DATABASE

Digital log curves were provided for all 35 wells in the study area. The geophysical log suite included combinations of gamma ray, neutron porosity, density porosity, caliper, and resistivity. Logs were sampled in 0.5-ft increments. All logs were normalized. Core analysis reports of sidewall and whole cores were available for 12 wells (Morgan et. al., 2000). Among the 12 cored wells, 2 wells are in the Wells Draw area, and 10 wells are near the study area. The core analysis data included porosity, permeability, grain density, and water saturation. For the 12 cored wells, sandstone porosity range is 1-20.5%, and the permeability range is 0.01-170 md. Production data for wells in the Wells Draw study area were available for the period of June 1, 1982 to December 31, 2006. These data included monthly oil, gas, and water production rates. Water injection data were available from January 1, 1995 to December 31, 2006. Perforation data were used to help identify sandbodies and set up simulation model. There are 380 total perforations in the 35 wells of the Wells Draw study area PVT, relative permeability, and capillary pressure data also were available to conduct PVT analysis and reservoir simulation.

## 3.3 RESERVOIR CHARACTERIZATION AND 3D GEOLOGIC MODELING

### Reservoir Geology

The Green River formation in the Greater Green River area consists of fluvial-deltaic rocks deposited in open- to marginal-lacustrine environments along the southern margin of Eocene-aged Lake Uinta, in northeastern Utah (Morgan et al., 2002). Reservoir rocks are primarily fluvial and delta, distributary channels-fill sandstones, distributary-mouth bars, and nearshore bars (Ryder, 1976). Carbonates were deposited in marginal lacustrine environments. The southern shore of Lake Uinta was broad and flat. Therefore, climatic- and tectonic-induced rise and fall of the lake caused large transgressive and regressive shifts of the shoreline that resulted in cyclic sedimentation and numerous stacked deltaic deposits.

The oil-productive lower and middle members of the Green River formation in the southwest Uinta basin are divided into five distinct intervals. These intervals in stratigraphically ascending order are Uteland Butte, Castle Peak, Lower Douglas Creek, Upper Douglas Creek, and Garden Gulch (**Figs. 3.3** and **3.4**). This study was restricted to reservoir characterization of only four of the intervals. These are the (1) Castle Peak, (2) Lower Douglas Creek, (3) Upper Douglas Creek, and (4) Garden Gulch intervals. The top of the sandstone reservoirs is defined by the Second Garden Gulch (GB-2) marker, and the bottom is defined by a limestone marker bed (BSCARB) (Fig. 3.3), a consistent log marker throughout the Monument Butte area (Larsen et al. 1997). Detailed correlations were completed for all the wells in the Wells Draw study area. Thirty-three

sandstone layers were delineated by correlating 68 markers from the base of Castle Peak interval to GB-2 of Garden Gulch interval in the Wells Draw study area (Fig. 3.4).

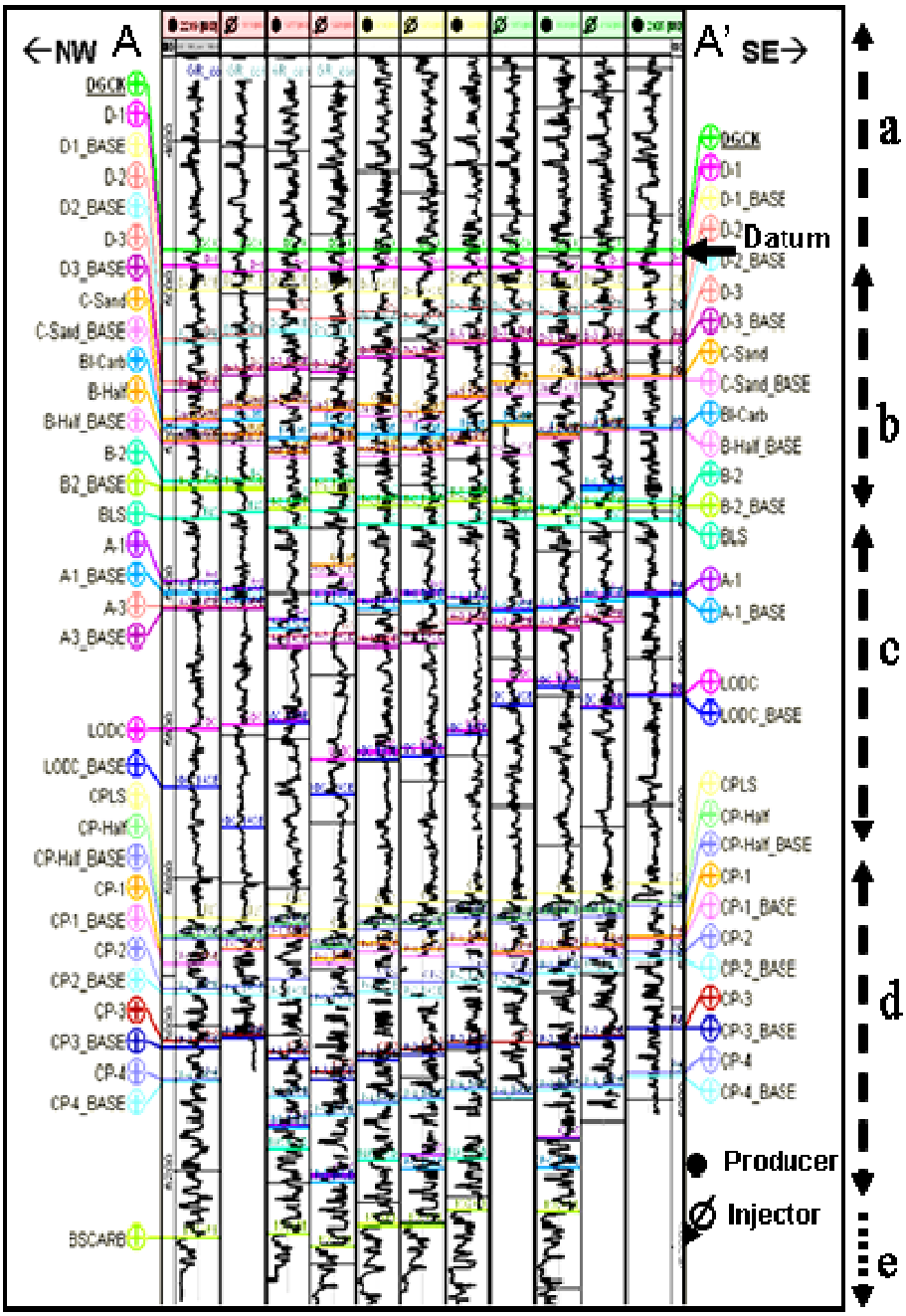


**Fig. 3.3—Cross section A-A' of the lower and middle members of the Green River formation. See Fig. 3.2 for location. Figure shows correlated sand tops and bases below the Douglas Creek marker bed (DGCK), using gamma ray logs; datum is DGCK.**

| Zones | Horizons | Layer Index |
|---|---|---|
| Zone 1 | GB-2 | 1 |
| | GB-2 Base | 2 |
| | GB-3 | 3 |
| | GB-3 Base | 4 |
| | GB-4 | 5 |
| | GB-4 Base | 6 |
| | GB-6 | 7 |
| Zone 2 | GB-6 Base | 8 |
| | Pt-3-MKR | 9 |
| | GB Base | 10 |
| Zone 3 | PB-7 | 11 |
| | PB-7 Base | 12 |
| | PB-8 | 13 |
| | PB-8 Base | 14 |
| | PB-10 | 15 |
| | PB-10 Base | 16 |
| | PB-11 | 17 |
| Zone 4 | PB-11 Base | 18 |
| | X MKR | 19 |
| | Y MKR | 20 |
| Zone 5 | D-S2 | 21 |
| | D-S2 Base | 22 |
| | D-S3 | 23 |
| Zone 6 | D-S3 Base | 24 |
| | DGCK | 25 |
| Zone 7 | D-1 | 26 |
| Zone 8 | D-1 Base | 27 |
| Zone 9 | D-2 | 28 |
| | D-2 Base | 29 |
| | D-3 | 30 |
| Zone 10 | D-3 Base | 31 |
| Zone 11 | C-Sand | 32 |
| | C-sand Base | 33 |
| | Bl-Carb | 34 |
| | B-Half | 35 |
| Zone 12 | B-Half Base | 36 |
| Zone 13 | B-1 | 37 |
| | B-1 Base | 38 |
| | B-2 | 39 |
| Zone 14 | B-2 Base | 40 |
| | BLS | 41 |
| | BLS Base | 42 |
| Zone 15 | A-Half | 43 |
| | A-Half Base | 44 |
| | A-1 | 45 |
| | A-1 Base | 46 |
| | A-3 | 47 |
| Zone 16 | A-3 Base | 48 |
| Zone 17 | LODC | 49 |
| | LODC Base | 50 |
| | LODC2 | 51 |
| Zone 18 | LODC-2 Base | 52 |
| Zone 19 | LODC3 | 53 |
| Zone 20 | LODC3 Base | 54 |
| Zone 21 | CPLS | 55 |
| | CP-Half | 56 |
| | CP-Half Base | 57 |
| | CP-1 | 58 |
| | CP-1 Base | 59 |
| | CP-2 | 60 |
| | CP-2 Base | 61 |
| | CP-3 | 62 |
| | CP-3 Base | 63 |
| | CP-4 | 64 |
| Zone 22 | CP-4 Base | 65 |
| | CP-5 | 66 |
| | CP-5 Base | 67 |
| | BSCARD | |


**Fig. 3.4—Zonation of the 33 sandstone layers into 13 sand zones (yellow) and 9 significant shale zones (green). Figure shows correlated sand tops and bases and zone names in the studied interval. Note: a: Garden Gulch; b: Upper Douglas Creek; c: Lower Douglas Creek; d: Castle Peak; e: Uteland Butte.**

Sandstone intervals are separated by one or more shale layers, thus resulting in 67 layers. Among the 33 sandstones, reportedly, D1 and C sands are relatively good quality sands, and they are laterally more continuous than others sands (Deo et al., 1996). Green River formation reservoir sandstones consist of individual and amalgamated sandbodies, and thus, reservoir thickness and width vary greatly. Reservoir thickness ranges from 3 to 120 ft (1-35 m) but more commonly is 10 to 15 ft (3-5 m); reservoir width ranges from 25 to 800 ft (7-245 m) but more commonly is 90 to 600 ft (25-180 m) (Taylor, 2004). Sands less than 3 ft (1 m) thick are usually non-commercial. The main pay consists of D1, C, and A sands of the Upper Douglas Creek interval (Figs. 3.3 and 3.4). Assigning a simulation layer to each layer would result in a large reservoir model, which would make simulation computationally expensive. Also, the complicated geologic model may introduce more uncertainties in flow simulation, especially history matching. Therefore, the model was simplified (upscaled) by grouping the 33 sandstone and their interbedded shale intervals into 13 dominantly sand zones (according to sand characteristics and depositional environment) and 9 significant shale zones (Fig. 3.4). This gives the simulation model 22 zones.

**Petrophysical Analysis**

The most prevalent porosity logs in Monument Butte field are density porosity logs. Normalized and calibrated density porosity logs were used to evaluate porosities of the 4 producing Green River intervals. Thickness-weighted average porosity was calculated for each interval. To evaluate permeability, I cross-plotted core porosity and permeability data from 12 cores (**Fig. 3.5**). Then, permeability was calculated at each

density porosity sample point using **Eq. 3.1.** Thickness-weighted average permeability was then calculated for each interval.

$$\kappa = 0.003 * e^{(0.515*\varphi)}. \ldots\ldots\ldots\ldots (3.1)$$

Upon recommendation of the operator, I initially used a 10% density porosity cut-off to discriminate between reservoir and non-reservoir quality rock. However, I found that some perforated reservoirs are low quality sands that were excluded by the 10% cut-off. Also, some wells have limited perforated intervals after using 10% cut-off, which is not reasonable compared with their production histories. To include all perforated sands, a range of gamma ray and density-porosity log cut-offs were investigated. Gamma ray logs were observed to be less effective for identifying reservoir quality sandstones than were density-porosity logs, a conclusion consistent with that of Morgan et al. (2002). Ultimately, I selected cutoffs of 8% density porosity and 80-API-units gamma ray response, because these parameters preserved the perforated low-quality sandstones. These cutoffs were used to identify potential zones for future perforations and to estimate reservoir quality at unperforated locations for reservoir simulation purposes. Net sand thickness, net-to-gross ratio (NTG), net porosity (average porosity of the net reservoir thickness), and net permeability (average permeability of the net reservoir thickness) were calculated for each interval at each well location, using the selected cut-offs.

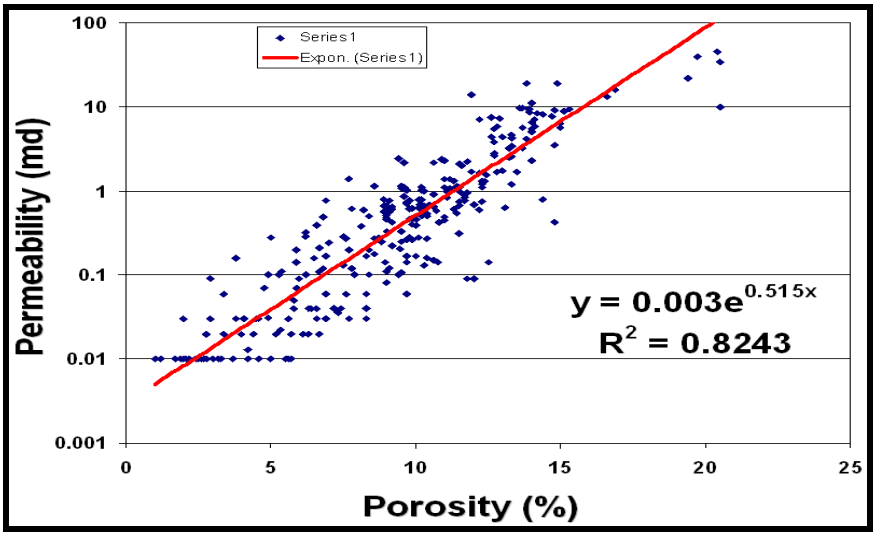


**Fig. 3.5— Relation between porosity and permeability from 12 cores. Porosity ranges from 1-20.5%, and permeability ranges from 0.01-170 md.**

## 3D Geological Modeling

*Methodology*

A numerical model of the reservoir requires accurate representation of reservoir heterogeneities and connectivity. Improving the water-flood performance requires an understanding of the reservoir heterogeneities and connectivity at the interwell scale and its associated uncertainty. 3D geostatistical characterization techniques provide a better way to represent interwell heterogeneities and connectivity of the reservoirs. For this study, we combined deterministic and geostatistical techniques to develop a 3D reservoir model. We used a deterministic method to populate the net-to-gross ratio model, because the 40-ac well spacing in the study area was considered to be sufficient for building a deterministic model. Porosity was populated at interwell locations using sequential Gaussian simulation coupled with collocated co-kriging (**Eq. 3.2**), conditioning each

porosity realization with the NTG property. With this algorithm, standard kriging with the primary data dominates where there is enough primary data within the variogram range. The method requires a variogram of the primary variable, only, and secondary data must exist at all primary locations. This approach allowed us to quantify the uncertainty of porosity at interwell locations by generating multiple realizations of the net porosity distribution. The contribution of the secondary data (NTG) was controlled by a correlation coefficient between porosity and NTG in each zone. Finally, the generated porosity realizations were used to calculate corresponding permeability realizations, using the correlation between core porosity and core permeability.

$$Z_{CCOK}(x_0) = \sum_i \lambda_i Z(x_i) + \mu Y(x_0) \qquad \text{……..…..} \quad (3.2)$$

Where,

$Z_{CCOK}(x_0)$ is the calculated property value at location $x_0$.

$\mu$ is the correlation coefficient between primary and secondary data.

$Y(x_0)$ is the secondary data value at location $x_0$.

*Results of 3D Geological Modeling*

The moving average algorithm (Chopra et. al., 1990) was used to populate deterministic net-to-gross ratio values. This algorithm uses the square of inverse distance in a search radius neighborhood in weighting data points to determine average value at interwell locations. Thus, distant points have lesser influence on the determined average. **Fig. 3.6** is a NTG ratio map for the zone 7 (D1 sand). Semivariogram analysis was performed on normal score transforms of net-porosity for each sand zone. **Fig. 3.7** shows sample and modeled semivariograms along major axes of net porosity in zones 7, 11, 15

and 17 (Abiazie, 2008). The semivariance is plotted on the y-axis as a function of the separation distance on the x-axis. **Table 3.1** shows net porosity anisotropy models for the 13 sand zones, including horizontal major range, horizontal minor range, vertical range, and direction of the horizontal major range. Crossplots were used to determine the correlation between net-to-gross ratio and net porosity for each sand zone (**Fig. 3.8**). The correlation coefficients are generally low (less than 0.5) for most of the sands. Only the D1 sand has a relatively high correlation coefficient, 0.69. This indicates that using this colocated co-kriging method, for laterally continuous sands, NTG controls porosity distribution at interwell locations, whereas low correlation coefficients mean NTG has less control on porosity distribution at interwell locations.

Porosities were populated at interwell locations using sequential Gaussian simulation coupled with collocated co-kriging, conditioned with the NTG property. Twenty-one equiprobable porosity realizations were generated to account for the uncertainty in porosity distribution. **Fig. 3.9** shows four net porosity realizations for the D1 sand (zone 7). Permeability was calculated using the porosity-permeability correlation (Fig. 3.5). **Fig. 3.10** shows the corresponding horizontal permeability models derived from the net-porosity realizations for the D1 sand (Zone 7). The calculated horizontal permeability ranges (1 to 13 md) for all 21 realizations fall within the permeability range from the core analysis data (1 to 21 md).

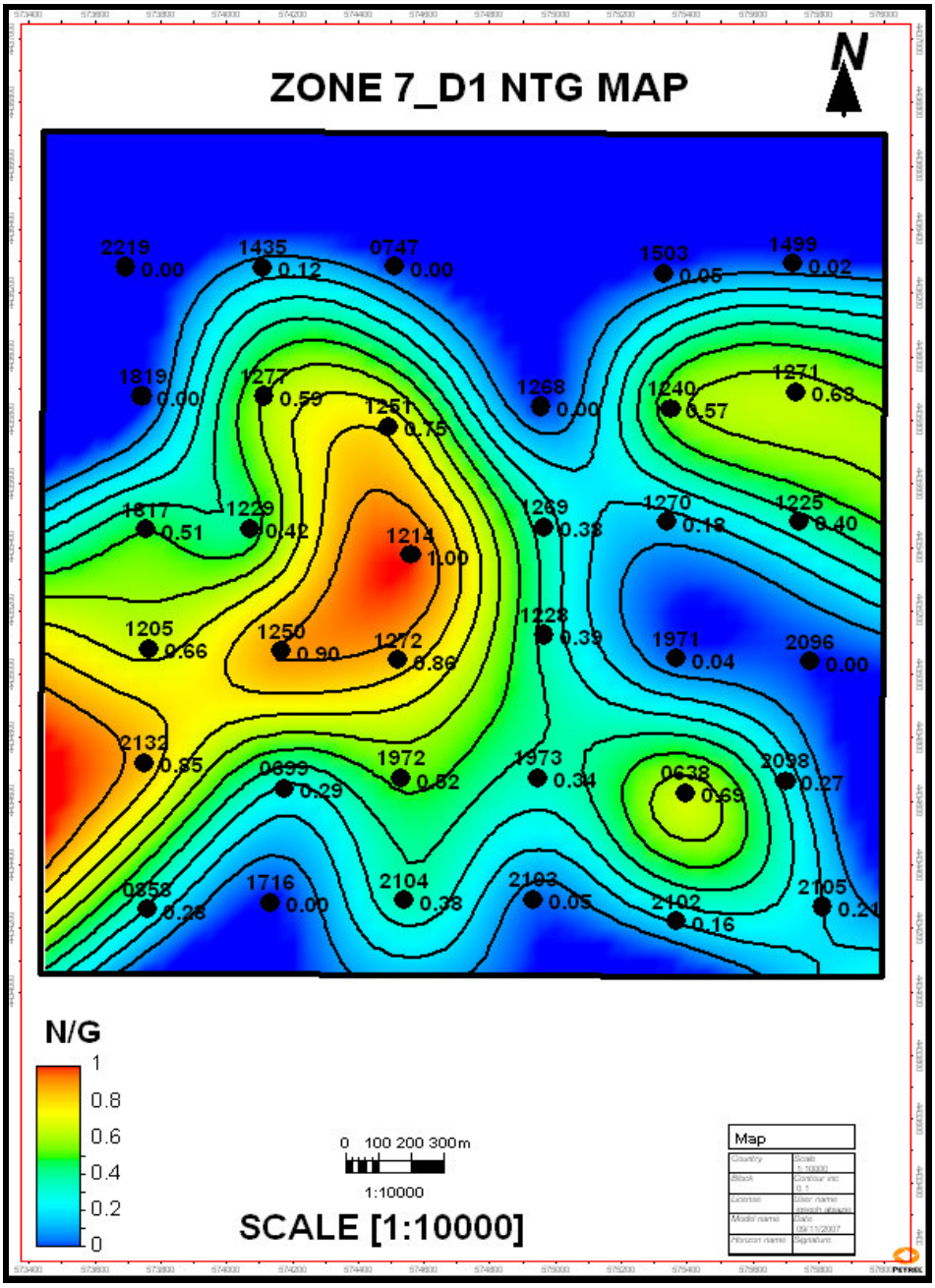


**Fig. 3.6—Map of net-to-gross ratio for the D1 sand, determined using the moving average algorithm (from Abiazie, 2008).**

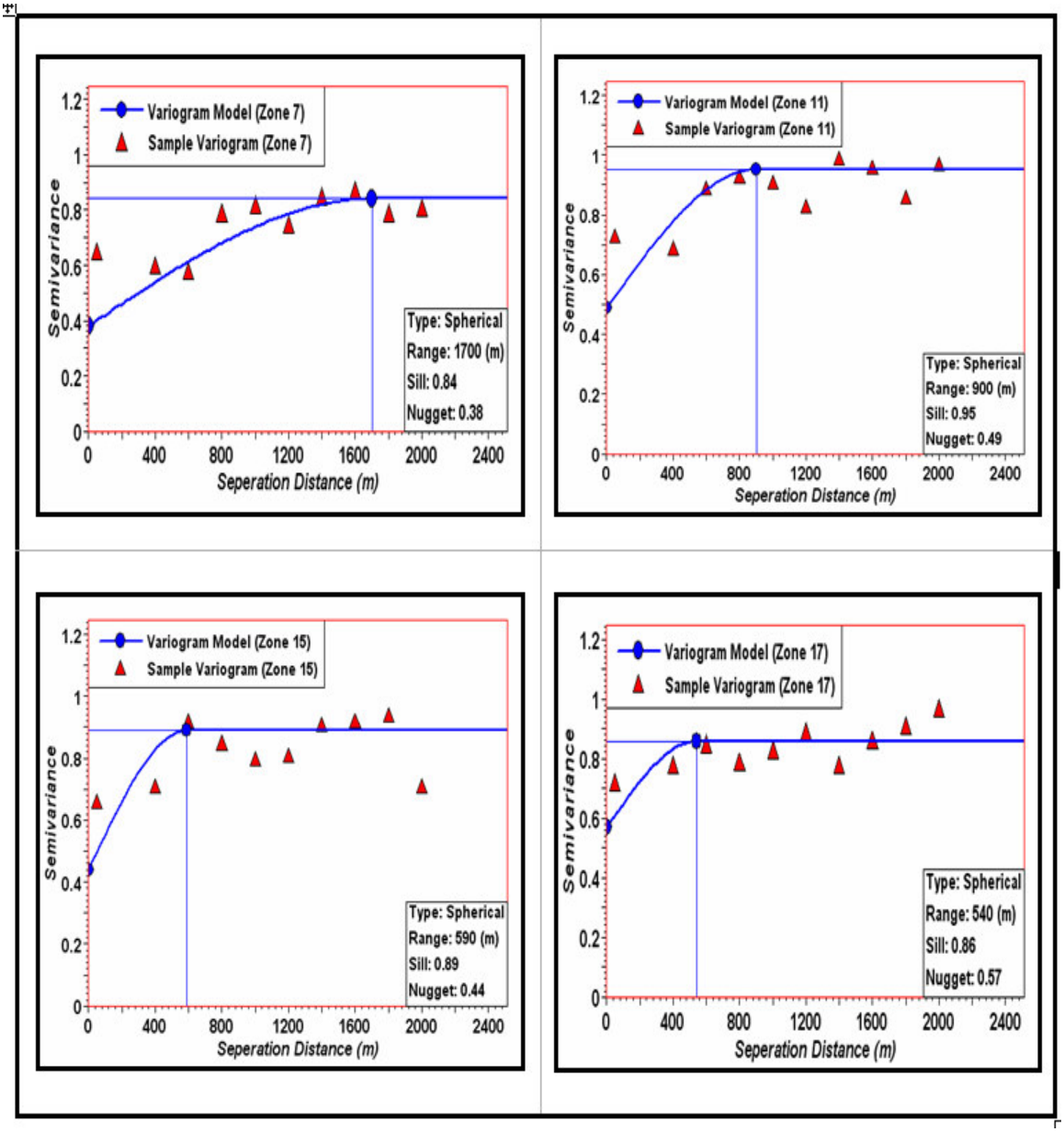


**Fig. 3.7— Sample and modeled semivariograms of net porosity along major axes in zones 7, 11, 15 and 17 (from Abiazie, 2008). Triangles are sample points.**

**Table 3.1—Net porosity anisotropy models for the 13 sand zones (from Abiazie, 2008).**

| Zone # | Major Range (m) | Minor Range (m) | Vertical range (m) | Dip (deg) | Azimuth (deg) |
|---|---|---|---|---|---|
| 1 | 1050 | 500 | 11 | 0 | 80 |
| 3 | 300 | 200 | 10 | 0 | -30 |
| 5 | 350 | 170 | 6 | 0 | 7 |
| 7 | 1700 | 500 | 12 | 0 | 75 |
| 9 | 900 | 350 | 6 | 0 | 5 |
| 11 | 900 | 590 | 5 | 0 | 93 |
| 13 | 800 | 300 | 7 | 0 | -3 |
| 15 | 590 | 430 | 13 | 0 | 2 |
| 17 | 540 | 350 | 37 | 0 | 129 |
| 19 | 520 | 310 | 15 | 0 | 105 |
| 20 | 410 | 370 | 12 | 0 | 15 |
| 21 | 380 | 220 | 13 | 0 | 23 |
| 22 | 280 | 150 | 9 | 0 | 21 |

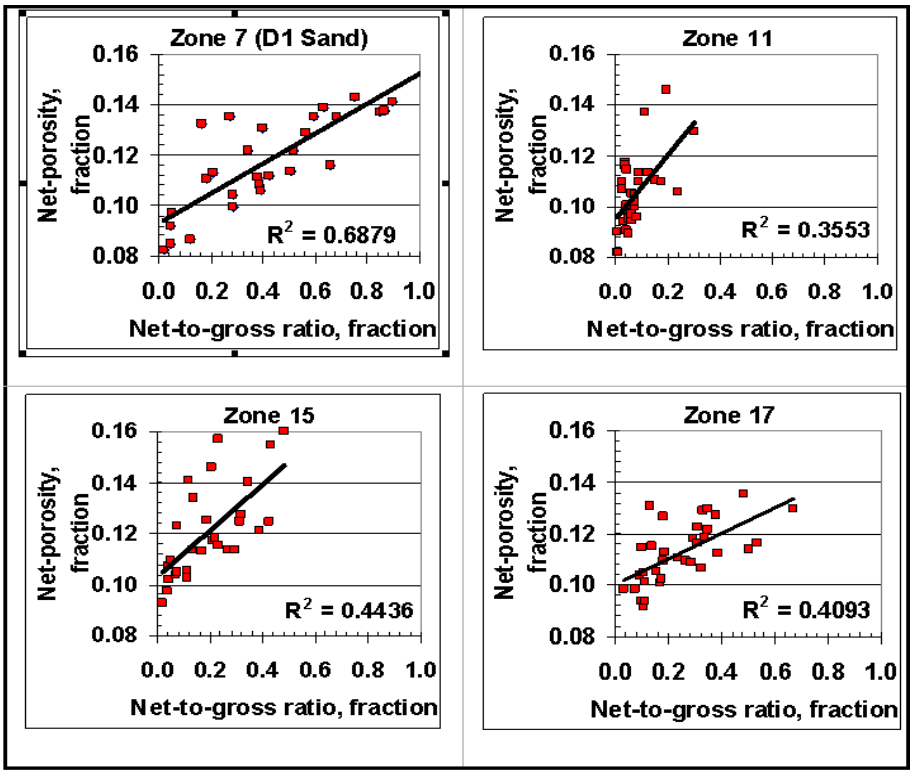


**Fig. 3.8—Correlation between net-to-gross ratio and net porosity for sand zones 7, 11, 15 and 17 (from Abiazie, 2008).**

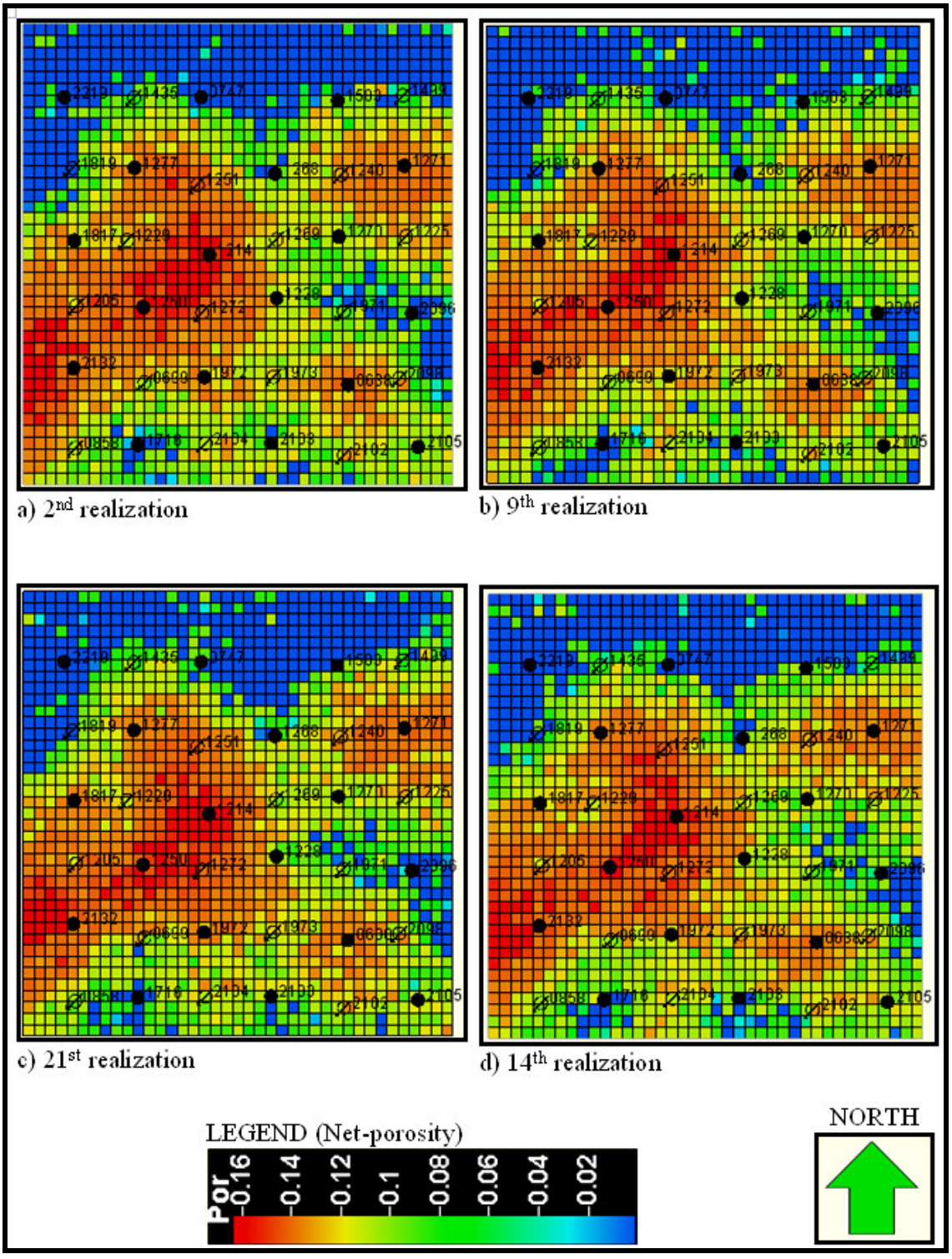


**Fig. 3.9—Four realizations of net porosity distribution in the D1 sandstone (from Abiazie, 2008).**

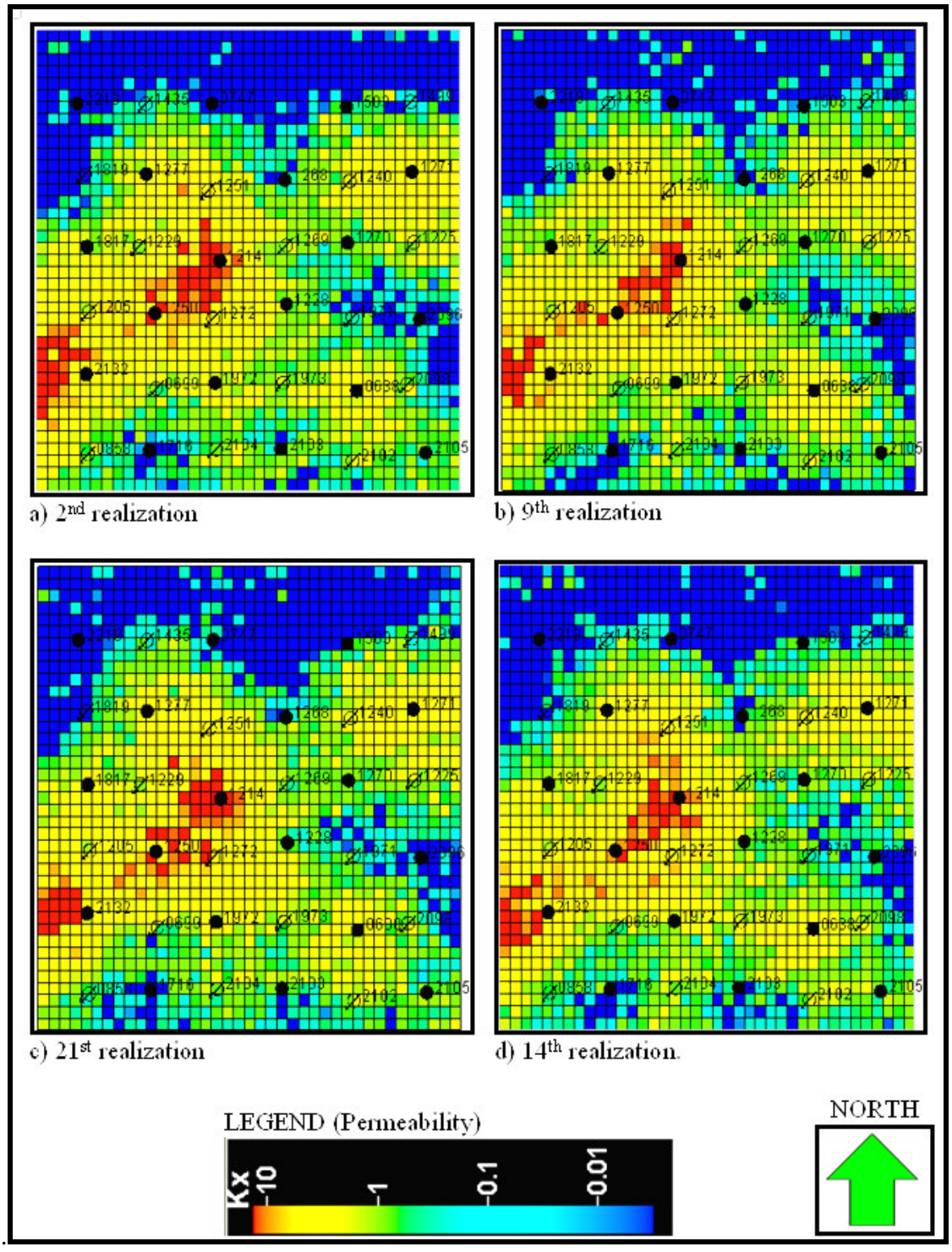


**Fig. 3.10—Four realizations of permeability distribution in the D1 sand (from Abiazie, 2008).**

## 3.4 GEOLOGICAL INTERWELL CONNECTIVITY EVALUATION

We evaluated interwell reservoir connectivity first by analyzing well data. Sandstone net thickness and perforation data were analyzed for more than 33 sandstone reservoirs to quantify interwell connectivity as a function of well spacing. “Static connectivity” in a layer is assumed to exist between two adjacent wells if sandstone net thickness is identified in both wells. “Hydraulic connectivity” is assumed to exist between two adjacent wells in a layer if net thickness and perforations are present in both wells. Thus, a condition for the presence of hydraulic connectivity is that static connectivity is present. Note that both measures may overestimate connectivity since they assume that if non-zero net thickness exists in a zone in both wells of the pair, then non-zero net thickness exists at all locations between the two wells (i.e., the wells are connected in that zone). Despite this assumption, we have found this methodology helpful in assessing connectivity in the Monument Butte field.

**Fig. 3.11** shows static connectivity visualizations for D1, D2 and D3 sandstone layers. For each layer, the maximum possible number of well-pair connections between the 35 wells in the study area is 105. In the D1 sandstone layer, the number of well-pair connections with static connectivity is 78. Taking the ratio of 78 to 105 yields a static connectivity value of 0.74 for the D1 sandstone layer. In a similar manner, static connectivity values for the D2 (Fig. 3.11) and D3 (not shown) sandstone layers were obtained. The D1 sandstone is the most connected (0.74) of the 3 D sandstones. This agrees with Deo *et al.*, who reported that the D1 sandstone is laterally continuous. The D2 and D3 sandstones have poor static connectivity (<0.3).

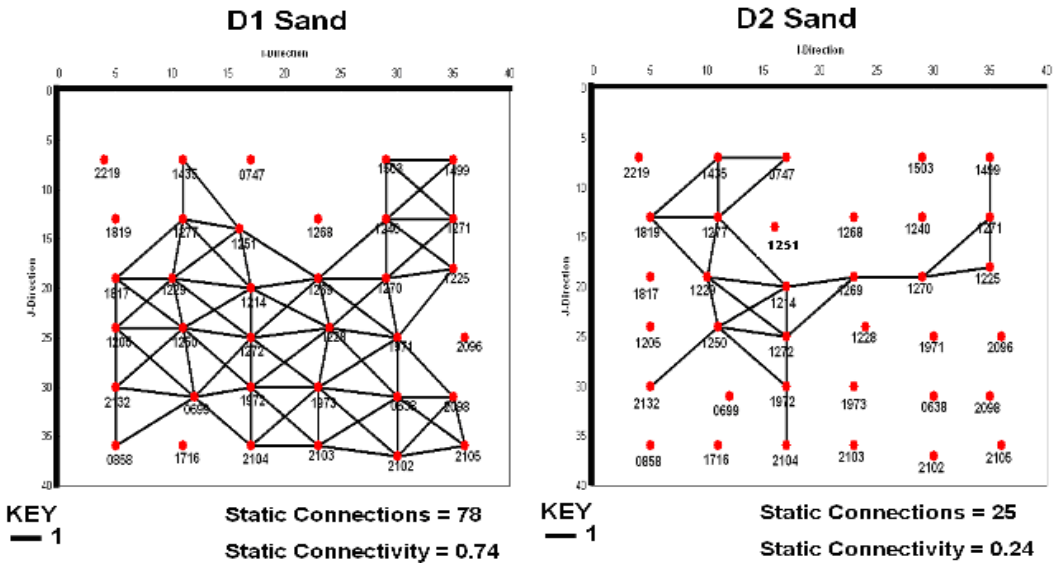


**Fig. 3.11—Static connectivity visualization in the D1, D2 and D3 sands.**

**Fig. 3.12** shows hydraulic connectivity visualizations for 4 of the 13 sand zones in the 3D model. Hydraulic connectivity assessments show that 10 sand zones in the 3D model have non-zero hydraulic connectivity. They include zones 1, 5, 7, 9, 11, 13, 15, 17, 19 and 21. Zone 7 (D1 layer) has the highest hydraulic connectivity (0.63). Twelve of the total 22 zones have zero hydraulic connectivity, including sand zones: 3, 20 and 22. It is important to note that zero hydraulic connectivity in a zone does not indicate the absence of perforations. Rather, it indicates that there are no adjacent well pairs in which both wells have perforations and non-zero net thickness in that zone. These results can help us define flow barriers in the simulation model for history matching purpose. Those zones that have zero or very low connectivity indicate that waterflooding might not be a good choice for them.

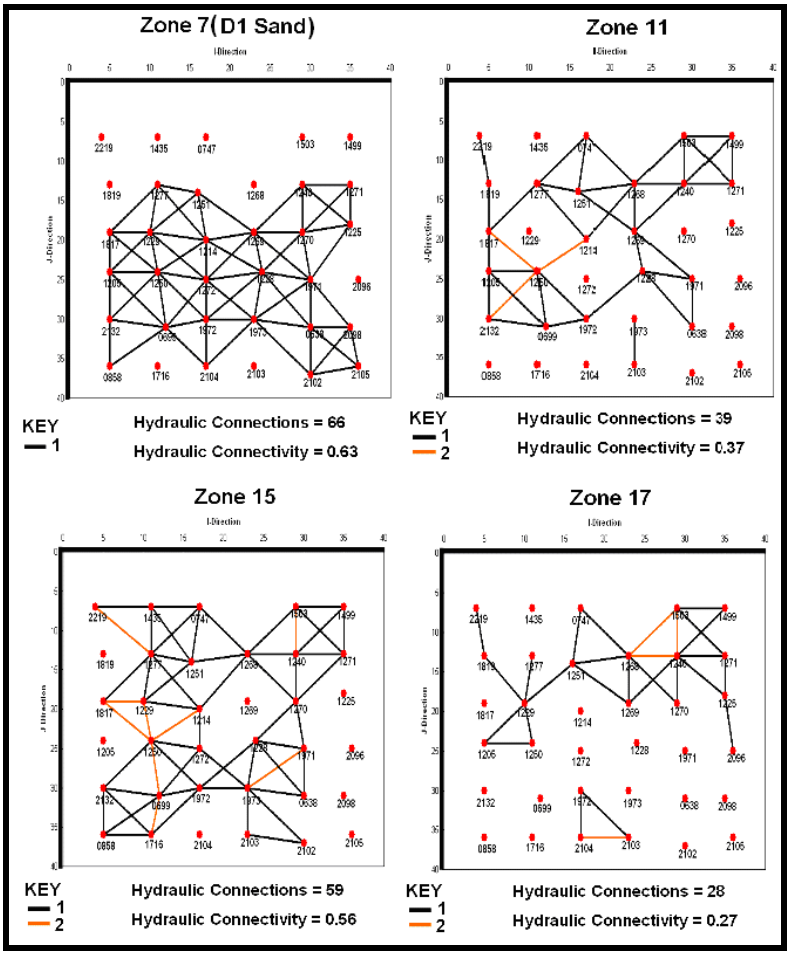


**Fig. 3.12—Hydraulic connectivity visualization of four zones in the 3D model.**

Static and hydraulic connectivity as a function of well spacing (40, 80, 160 and 360 acres per well) was evaluated for D1 and D2 sandstone layers, and the combined 22 zones (**Fig. 3.13**). Connectivity evaluation at spacings of 80, 160, and 360 acres was achieved by evaluating well pairs an appropriate distance apart, instead of adjacent well pairs. For the combined 22 zones, the connectivity values were calculated by dividing the sum of connections from all evaluated layers by the product of the number of layers

evaluated and total well-pair connections considered. Sixty-seven layers were evaluated for the combined 22 zones.

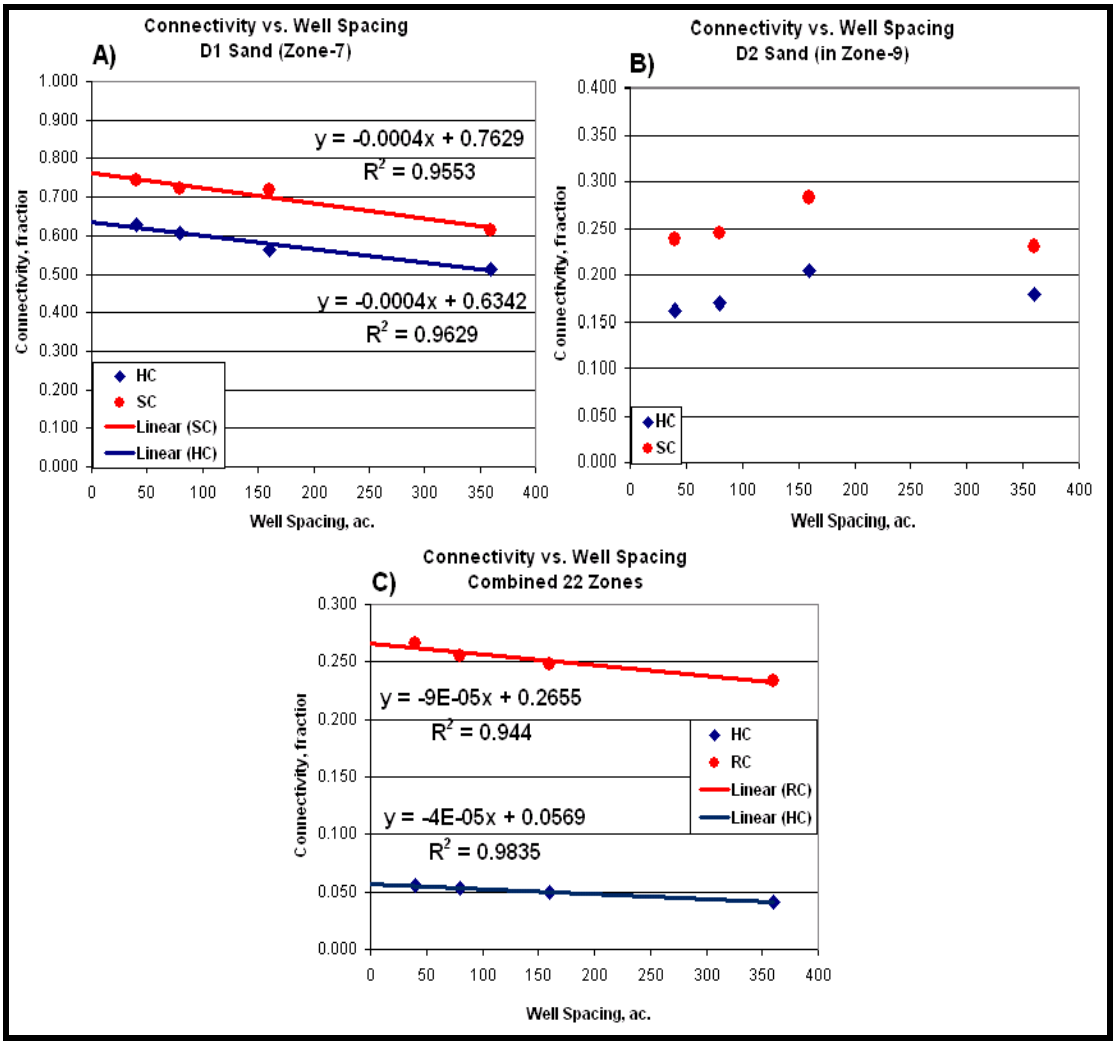


**Fig. 3.13—Static and hydraulic connectivity versus well spacing for three cases. SC = static connectivity; HC = hydraulic connectivity.**

The D1 and D2 sandstones were separately evaluated as single layers. For the D1 sandstone layer and the combined 22 zones, there is a strong negative correlation ($R^2$>0.94) between well spacing and connectivity—static and hydraulic connectivity increase as well spacing decreases, as expected. This relationship is not observed in the D2 sandstone, likely because of its poor connectivity. At the current well spacing of 40 acres, static connectivity in the D1 sandstone is very good (>0.7) compared to the combined 22 zones, where it is poor (<0.3) (Fig. 3.13, A and C). Also, hydraulic connectivity at 40 acres in the D1 sandstone (0.629) is ten times more than the hydraulic connectivity for the combined 22 zones (0.056).

In all three cases shown in Fig. 3.13, the hydraulic connectivity curve falls below the static connectivity curve. Thus, hydraulic connectivity could be increased by adding perforations in zones in adjacent well pairs in which both wells have non-zero net thickness but do not both have perforations currently. The curves of static connectivity represent the hypothetical upper limit for which hydraulic connectivity can be improved by adding perforations. If hydraulic connectivity can be increased, then it may be possible to improve reservoir performance by perforating additional zones. However, this is not guaranteed since this simplified analysis assumes that if there is non-zero net thickness in a zone in a pair of adjacent wells, then the wells are connected in that zone. If this is not the case, then drilling infill wells may be necessary to access those commercial oil accumulations in isolated, lensoid sandstone reservoirs.

## 3.5 SIMULATION MODEL INITIALIZATION

### Study Area Performance Review

Monthly oil, gas, and water production rates in the Wells Draw study area were available from first production in June 1, 1982, to December 31, 2006. Water injection data were available from the start of water flooding in January 1, 1995, to December 31, 2006. **Fig. 3.14** shows the profiles of historical oil, gas and water production rates, water injection rate, GOR, water cut, producer well count, and injector well count from the 35 wells in the Wells Draw area.

The monthly production from the four producing intervals as of August 1, 1982 was 5144 STB (1 producer) of oil with a solution gas-oil ratio (GOR) of 625 SCF/STB and 178 STB of water. In January 1, 1995 when water injection was started, oil production had dropped to 3166 STB and 384 STB of water with a GOR of 7524 SCF/STB from 18 producers. After water flooding started, the GOR of the study area decreased quickly, indicating good water-flood response. Since January 2006, the GOR of the study area has been less than 500 scf/stb, indicating the average reservoir pressure increased to above the initial bubble point pressure of 2020 psia (from PVT lab data). From the profiles of oil rate, water rate, and GOR, and also from well logs, I concluded that this reservoir is a solution gas drive reservoir.

Perforation data were used to set up the simulation model. The only directly applicable pressure data available were recently measured pressure data for one well that

is near the study area. Recent pressure data for other Monument Butte areas with good and bad waterflooding response were also available for comparison to the study area.

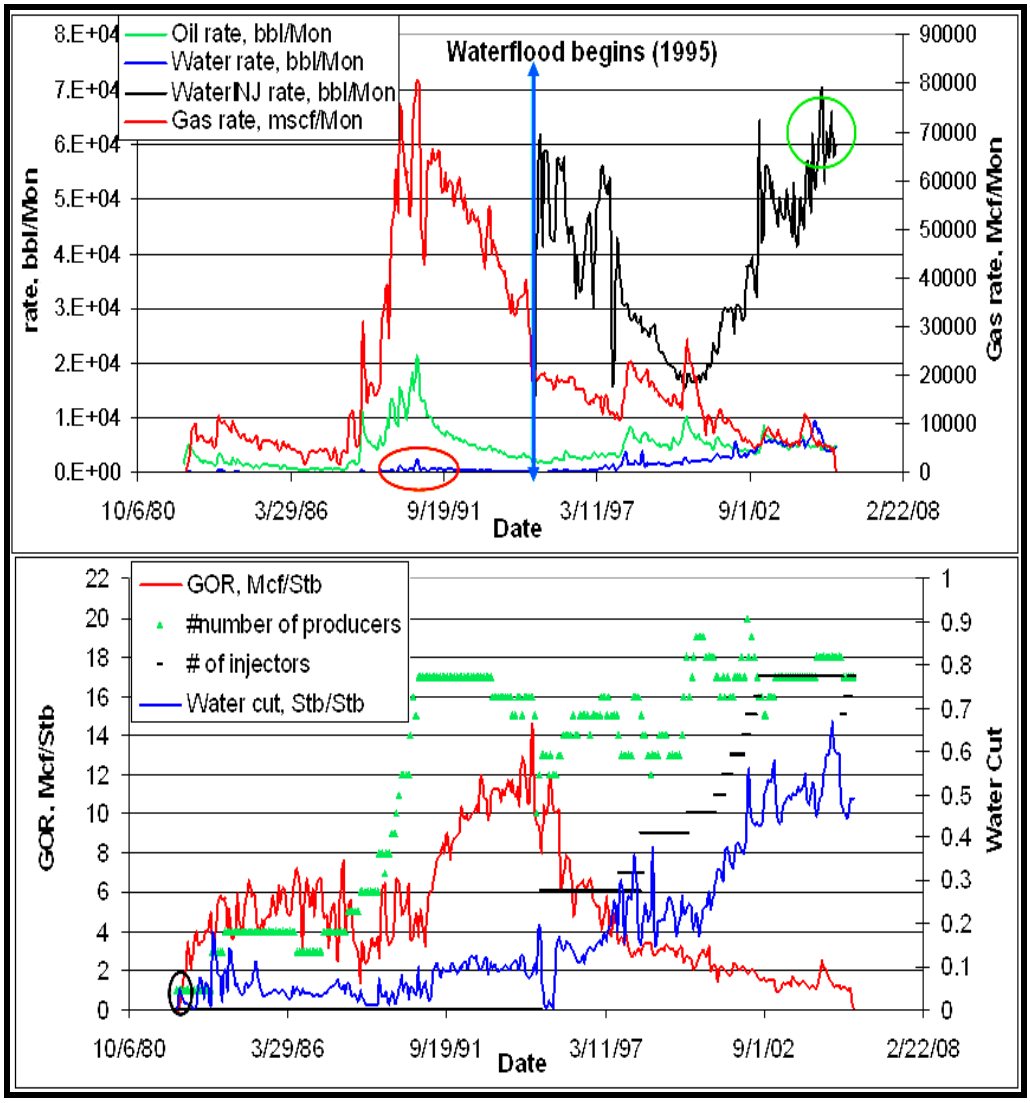


**Fig. 3.14—Production and injection data from the 35 wells studied.**

## Fluid and Saturation-Dependent Properties

PVT data were provided by the operator. The PVT data were adjusted to separator conditions for use in reservoir simulation (**Table 3.2**). **Figs. 3.15** and **3.16**

show pressure dependent properties (oil formation volume factor, solution gas-oil ratio, and oil and gas viscosities). The initial bubble point pressure was 2020 psia, and the reservoir temperature is 131 ˚F. Solution gas-oil ratio above bubble point pressure is 408 scf/stb. The oil has 33$^{o}$ API gravity and relative high viscosity (7 cp) at surface conditions. Oil-water relative permeability data (**Fig. 3.17)** were measured using core samples by Core Lab using the steady-state method. Gas-liquid relative permeability data (**Fig. 3.18)** were obtained from a previous simulation study (Morgan et al., 2001) conducted by the U.S. Department of Energy (DOE) and Utah Geological Survey (UGS). Capillary pressure data were also measured using high speed centrifuge method on core samples.

**Table 3.2— Calculated PVT table, from D-sand sample. $\rho_o$ and $\rho_g$ are dimensionless.**

| Pressure | Bo(rb/stb) | $\rho_o$ | $\mu_o$ (cp) | Co | Rs(scf/stb) | Bg(rb/mcf) | $\mu_g$(cp) | $\rho_g$ |
|---|---|---|---|---|---|---|---|---|
| 4000 | 1.1862 | 0.7852 | 2.812 | | 408 | | | |
| 3750 | 1.1884 | 0.7823 | 2.751 | 7.3158 | 408 | | | |
| 3500 | 1.1906 | 0.7795 | 2.690 | 7.4472 | 408 | | | |
| 3250 | 1.1928 | 0.7765 | 2.628 | 7.5858 | 408 | | | |
| 3000 | 1.1951 | 0.7736 | 2.567 | 7.7713 | 408 | | | |
| 2750 | 1.1975 | 0.7706 | 2.506 | 7.9833 | 408 | | | |
| 2500 | 1.1999 | 0.7674 | 2.445 | 8.2165 | 408 | | | |
| 2250 | 1.2024 | 0.7642 | 2.381 | 8.5001 | 408 | | | |
| 2020 | 1.2048 | 0.7612 | 2.322 | 8.8118 | 408 | | | |
| 1700 | 1.2071 | 0.7659 | 2.430 | | 357 | 1.51 | 0.016 | 0.682 |
| 1400 | 1.1893 | 0.7712 | 2.713 | | 308 | 1.867 | 0.015 | 0.665 |
| 1100 | 1.1719 | 0.7761 | 3.100 | | 256 | 2.411 | 0.014 | 0.663 |
| 800 | 1.1549 | 0.7808 | 3.630 | | 204 | 3.411 | 0.013 | 0.671 |
| 500 | 1.1360 | 0.7860 | 4.400 | | 148 | 5.642 | 0.012 | 0.701 |

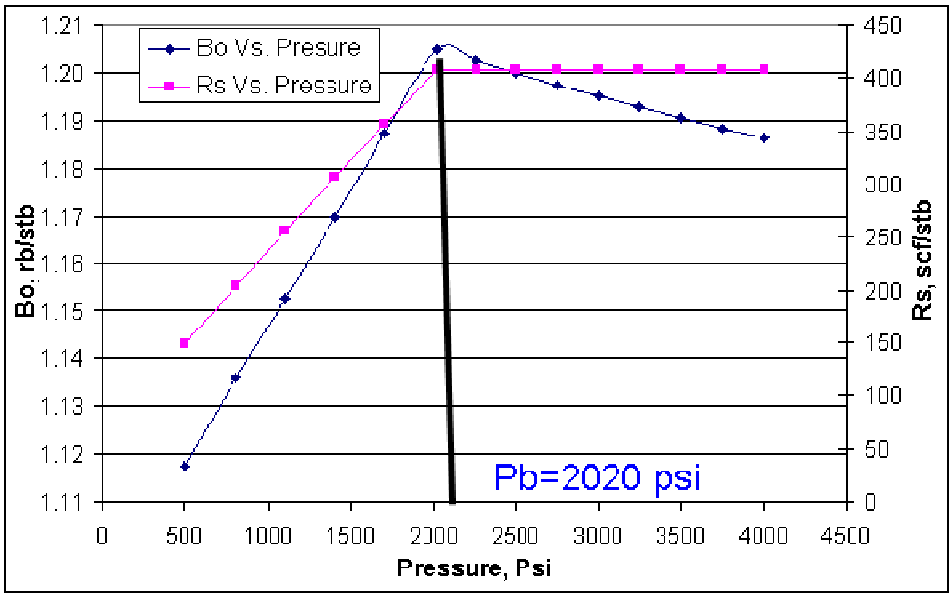


**Fig. 3.15—Oil formation volume factor and solution gas oil ratio vs. pressure.**

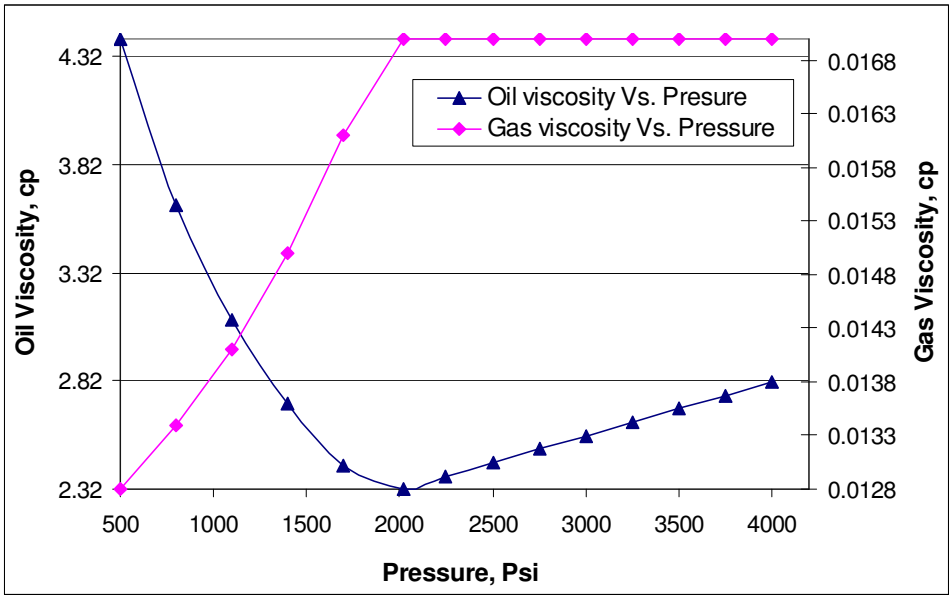


**Fig. 3.16—Oil and gas viscosities vs. pressure.**

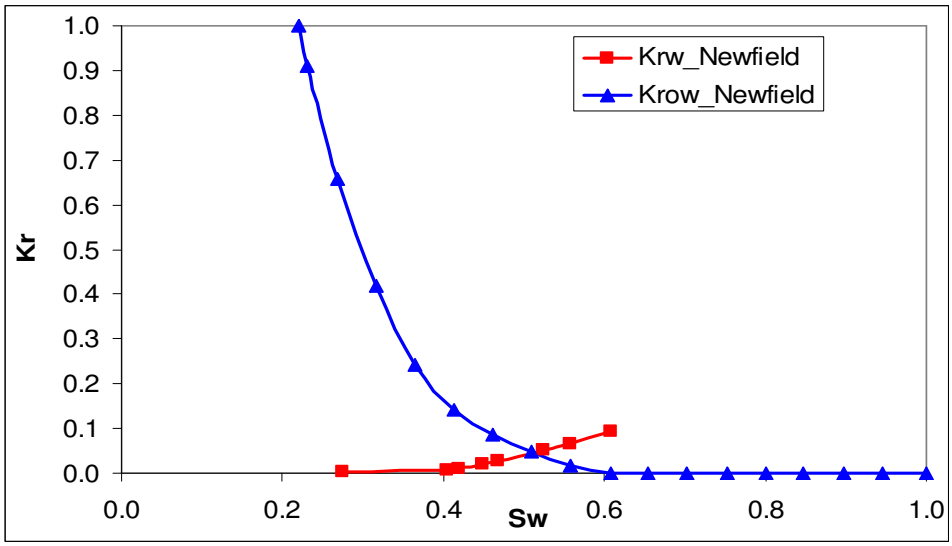


**Fig. 3.17—Oil-water relative permeabilities.**

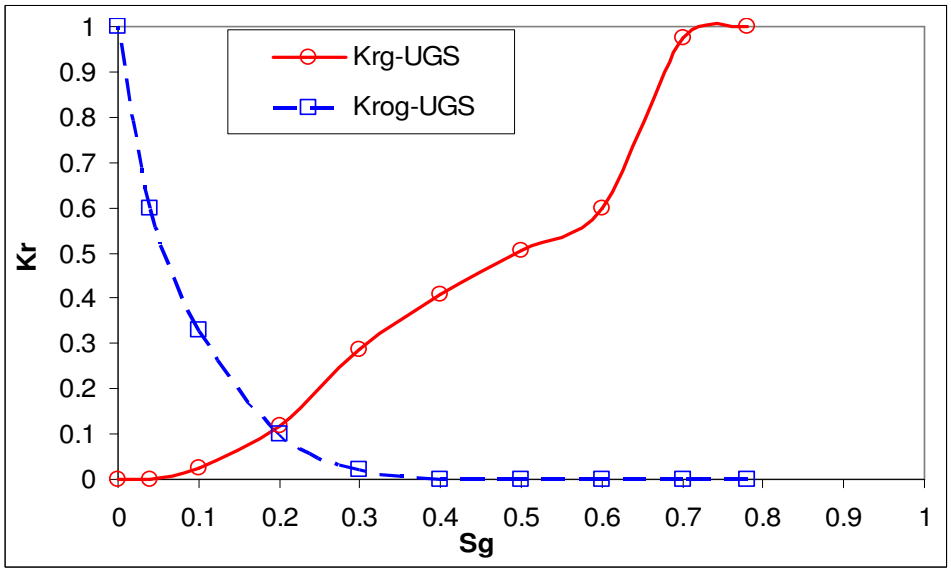


**Fig. 3.18—Gas-liquid relative permeabilities (from Morgan et al., 2001).**

## Simulation Model Description

The reservoir simulation grid is 39x39x22, a total of 33,462 grid cells. Each cell is 216.5 ft by 223 ft, and cell thickness varies according to zone thickness. Permeabilities

in the *x* and *y* directions are assumed equal. I assumed that vertical permeabilities are one-tenth of corresponding horizontal permeabilities. According to well logs and previous studies there is no aquifer, so the oil-water contact (OWC) was set far below the base of the reservoir. The oil saturation distribution was initialized using the capillary pressure data provided. Preliminary simulation runs had stability (convergence) problems because some cells had very small pore volumes. To address the problem, net-to-gross ratio cut-offs of 5%, 3%, and 1% were used to define inactive cells for the simulation model. Finally, I selected a net-to-gross cut-off of 1%, which resulted in 9818 inactive cells. **Fig. 3.19** shows the gridded gross thickness and active cells in the model.

**Initial Reservoir Pressure Estimation**

Initial reservoir pressure data were not available. Assuming the reservoir was normally pressured, the initial static pressure in the D sand was 2132 psia. I believe that this is a reasonable assumption, for the following reasons. First, the initial GOR of the study area in the first 3 months of production was approximately 450 scf/stb. At a pressure of 2132 psia, which is above the initial bubble point pressure of 2020 psia, the PVT data indicate a GOR of 408 scf/stb. Second, previous project reports (Deo et al., 1994; Pawar et al., 1996; Morgan et al., 2002) indicate the initial reservoir was around and slightly above bubble point pressure (2020 psia). Third, abnormal reservoir pressure was not reported.

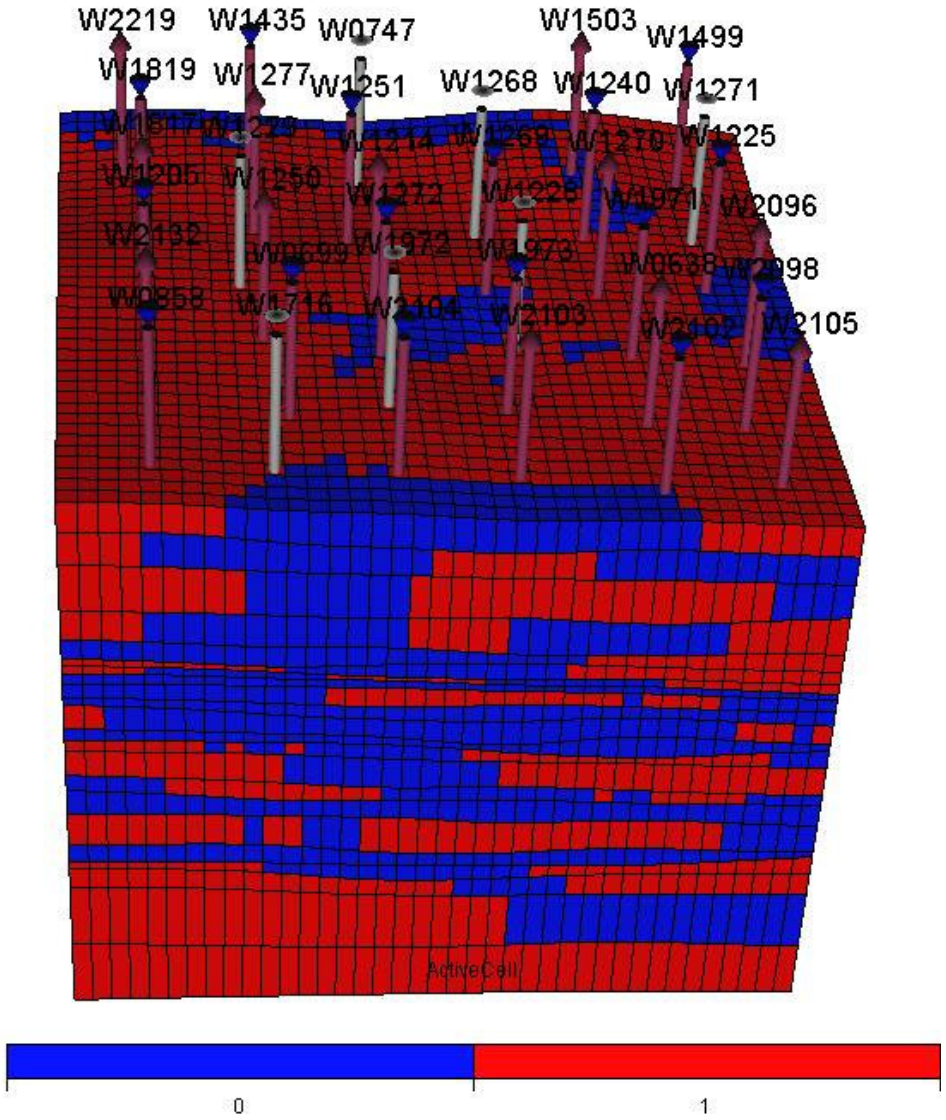


**Fig. 3.19—3D view of gridded gross thickness and active cells of the study area. Red represents active cells and blue represents inactive cells.**

## 3.6 RANKING GEOLOGICAL REALIZATIONS USING STREAMLINE SIMULATION

In this study, we generated 21 realizations of net porosity and net permeability to account for the heterogeneity of the reservoir properties and to quantify the uncertainty in the geological model. Flow simulation results using these realizations varied widely. A good geological model should reproduce production history in a simulation run, so I ranked these realizations based on their match to production history. Ranking can be done with conventional finite-difference simulation; however, this is not practical due to the extensive time needed for all realizations (Scheepens, 2003). Streamline simulation, which has developed rapidly over the past 10 years (Datta-Gupta and King, 1995; Datta-Gupta, 2000; Vasco and Datta-Gupta, 2001), helps to rapidly rank a large number of realizations because it is much faster than a conventional finite-difference simulator. In this research, a streamline simulator (FrontSim) (FrontSim, 2007) was used for ranking.

First, I defined a data mismatch function as the sum of the squares of the difference between simulated and observed data, divided by the measurement error, for all data points and all wells. **Eqs. 3.3** and **3.4** represent the GOR and water-cut mismatch functions, respectively. The total mismatch (**Eq. 3.5**) is the weighted sum of the GOR and water cut mismatches.

$$f(x)_{GOR} = \sum_{j=1}^{N_{well}} \sum_{i=1}^{m_{data}} \left( \frac{GOR_i^{cal} - GOR_i^{obs}}{\sigma_j^{GOR}} \right)^2 \qquad \text{…….. ……..….} \quad (3.3)$$

$$f(x)_{WCT} = \sum_{j=1}^{N_{well}} \sum_{i=1}^{m_{data}} \left( \frac{WCT_i^{cal} - WCT_i^{obs}}{\sigma_j^{WCT}} \right)^2 \qquad \text{…….. ……..….} \quad (3.4)$$

$$f(x)_{tot} = W_{WCT} f(x)_{WCT} + W_{GOR} f(x)_{GOR} \qquad \text{…….. ……..….} \quad (3.5)$$

$N_{well}$ and $m_{data}$ are number of wells and data points, respectively.

$i$ and $j$ are indices for data points and wells, respectively.

$GOR^{cal}$ and $GOR^{obs}$ are calculated and simulated GOR, respectively.

$\sigma_j$ is the measurement error of the jth well.

$WCT^{cal}$ and $WCT^{obs}$ are calculated and simulated water cut, respectively.

$W_{WCT}$ and $W_{GOR}$ are weighting factors for water cut and GOR, respectively.

Then, I used a root-mean-square (RMS) index to represent the average value of the deviation between simulated and observed data (**Eq. 3.6**), where $m$ is the total number of observed data points for all wells.

$$RMS = \sqrt{\frac{2f_{tot}}{m}} \qquad \text{…….. ……. (3.6)}$$

**Fig. 3.20** shows the RMS values of all 21 realizations. Realization number 8 has the lowest RMS value, so it was used for subsequent history matching and flow simulation.

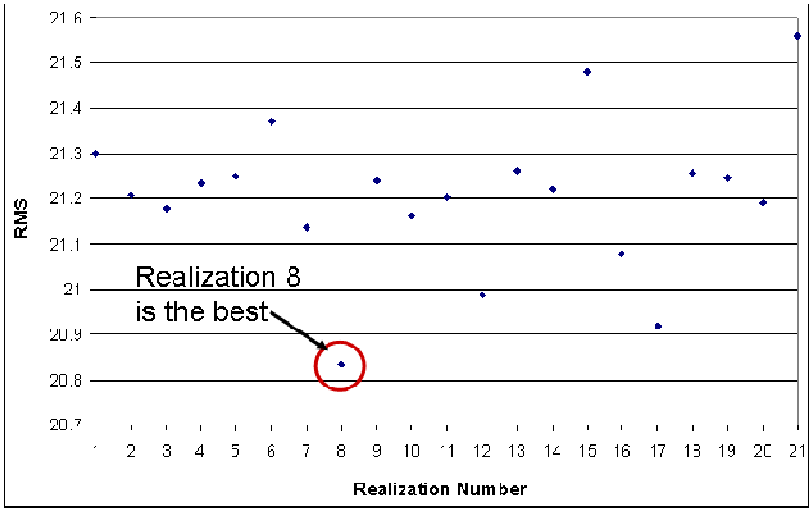


**Fig. 3.20—RMS values of all 21 realizations.**

## 3.7 HISTORY MATCHING RESERVOIR PERFORMANCE

Both manual and automatic history matching methods have their respective advantages and disadvantages. In this project, I developed a workflow to combine manual and automatic history matching methods to rapidly achieve an accurate history match. In the first stage, overall pressure behavior of the study area was matched by adjusting local or regional pore volume multipliers and individual-well productivity indices. In the second stage, phase ratios (GOR, WCT) were matched by adjusting regional permeability multipliers and relative permeabilities. In the third stage, individual well performance was matched using automatic history matching by adjusting local permeability multipliers (SimOpt, 2005). I believe the history matching process was much shorter than using only manual history matching or only automatic history matching.

### Manual History Matching

In general, the data that are matched are pressure, water/oil ratio (WOR), gas/oil ratio (GOR), water/gas ratio (WGR), water and gas arrival times, and fluid saturations. Matching historical WOR, GOR, or WGR is usually the best way to validate the estimates of effective zonation and reservoir connectivity (Mattax and Dalton 1990).

In the first stage of history matching, the simulation was run under reservoir voidage (total fluid rate) control for individual wells. Using historical reservoir total fluid rate (production and injection) as the constraint will make the wells produce the correct amount of total fluid from the reservoir before the mobility ratios are fully

matched. This enables a match of the pressure decline prior to a saturation match. However, in our study, some wells could not produce the observed total fluid rates from the reservoir, indicating potential problems with pore volume, *kh*, or well productivity. At this point in the process, if the well could not produce the reservoir voidage rate, the well productivity index was adjusted. Then, pore volume was adjusted slightly to match the estimated resent reservoir pressure reported by the operator. **Fig. 3.21** shows the simulated pore-volume-weighted average pressure profile and GOR history of the reservoir in the study area. The pressure profile is reasonable given the GOR profile and the expected pressure response suggested by the field operator.

The next step was to match overall GOR and water cut for the study area. After conducting sensitivity analysis of GOR and water cut with respect to permeability, porosity, and relative permeability, I could not improve the history match significantly. **Fig. 3.22** shows the best matches of GOR, gas rate, oil rate, and water rate at this point in the history match. The simulated GOR is far below the observed GOR. The gas rate match is good, while the simulated oil rates are much higher than observed oil rates. The water match is fair. The results indicate that the pressure support near each well is too high, preventing enough gas from coming out of solution. A possible explanation was that the reservoir model was too continuous (i.e., there was too much connectivity), likely resulting from upscaling from 67 layers in the geological model to 22 simulation layers.

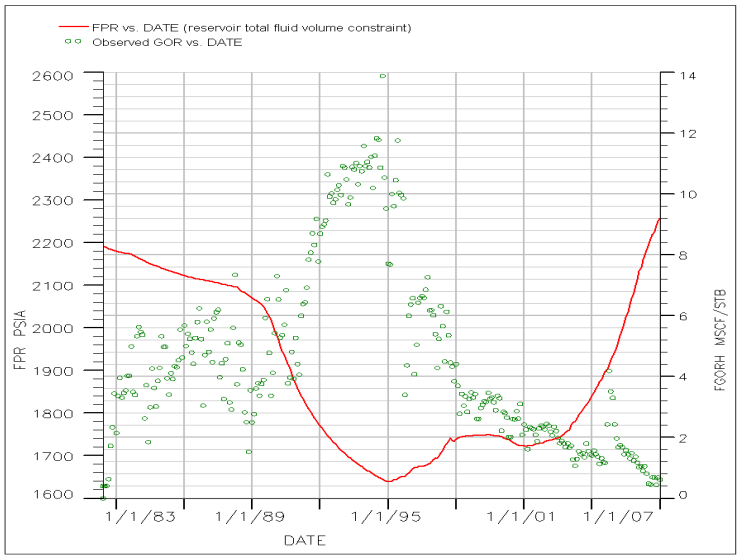


**Fig. 3.21—Simulated pore-volume-weighted average reservoir pressure profile and GOR history of the study area.**

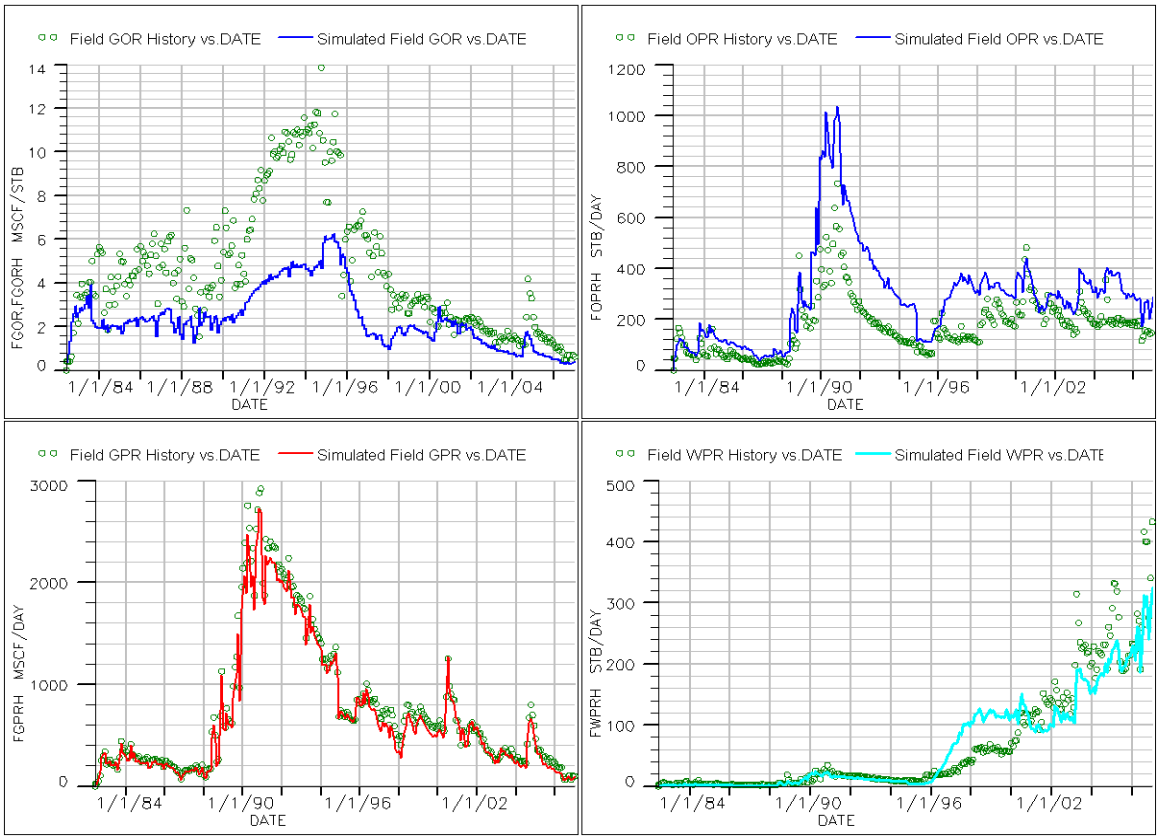


**Fig. 3.22—Intermediate matches of GOR, gas rate, oil rate, and water rate, prior to inclusion of barriers in the model.**

Including additional barriers to connectivity into the reservoir simulation model was investigated at this stage. The barriers were generated by including zero-transmissibility barriers between pairs of adjacent wells where no hydraulic connectivity was indicated (see Geological Interwell Connectivity Evaluation section above). **Fig. 3.23** shows the hydraulic connectivity model of zone 17 and *x*-direction barriers applied in the model. There are also y-direction barriers that are not shown on Fig. 3.23. In addition to the hydraulic barriers, I used a connection factor to alter the transmissibility between pairs of adjacent wells (Fig. 3.23). The connection factor was derived from the connectivity and perforation status of individual sub-layers that were upscaled to a particular simulation layer.

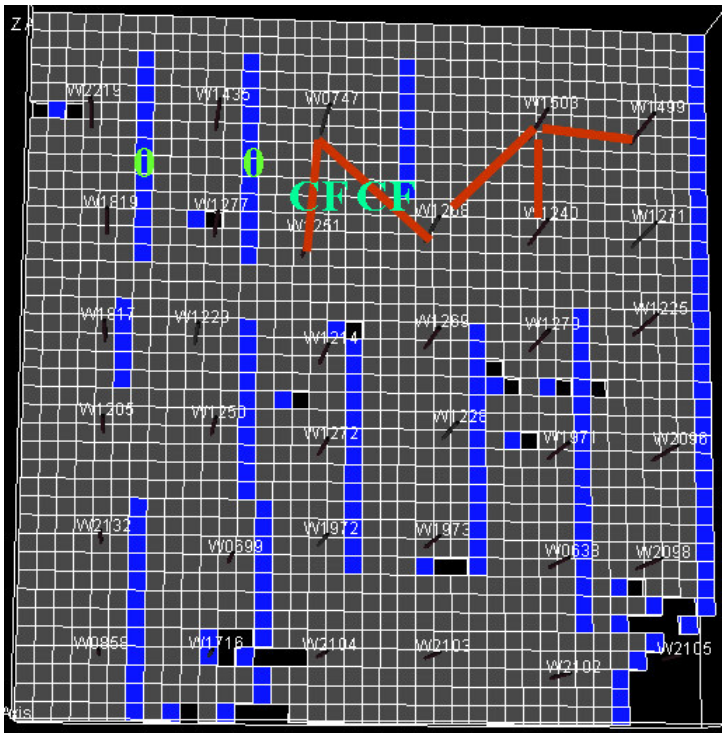


**Fig. 3.23— The hydraulic connectivity model of zone 17 and an example x-direction barrier model. Blue bars represent zero connectivity barriers and red bars represent non-zero hydraulic connectivity. CF means there is a connection factor that modifies the degree of connectivity between two wells.**

Several barrier models were constructed. The first one was based on static connectivity. This model does not improve history matching of GOR compared with the no-barrier base reservoir model (**Fig. 3.24**). The second barrier model was based on hydraulic connectivity. This model slightly improves history matching of GOR (Fig. 3.24). The third barrier model I tried had zero connectivity. In this model each well is sealed by barriers in each layer, and thus, yields zero connectivity for the reservoir model. The simulated GOR (Fig. 3.24) indicates a great improvement in the GOR history match, but only prior to water flooding.

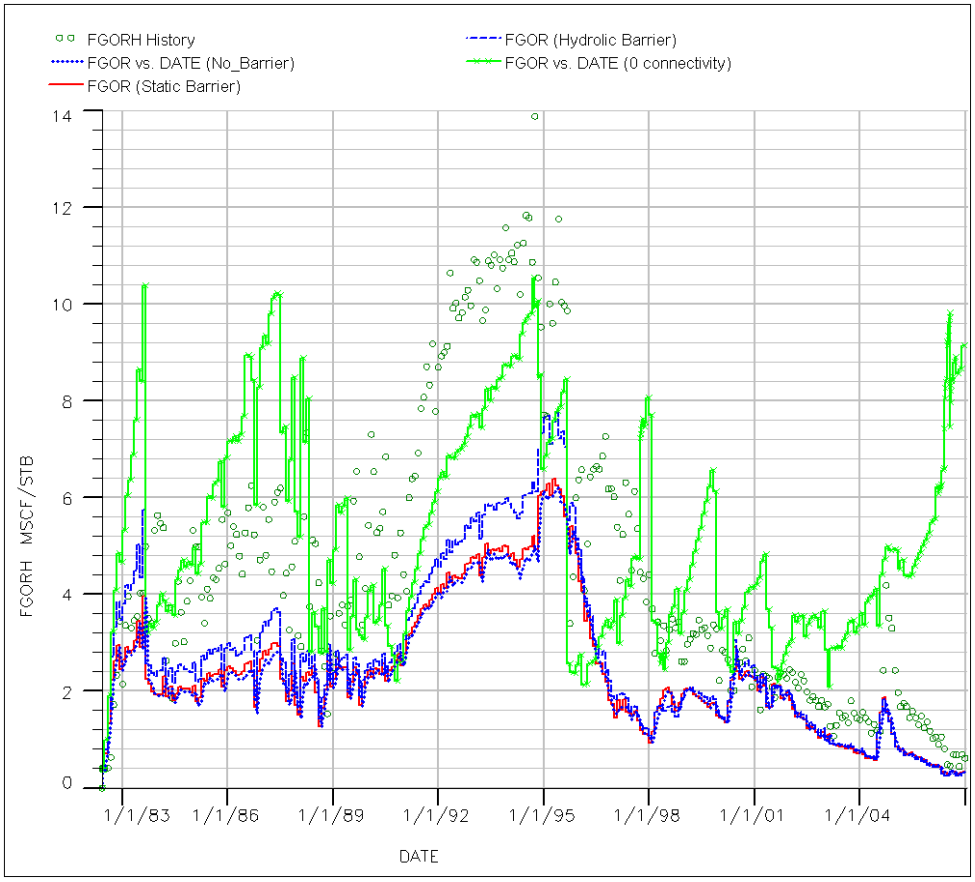


**Fig. 3.24—Effects of including different barrier models on history matching.**

In the fourth barrier model, I used a connection factor to alter the transmissibility between pairs of adjacent wells (Fig. 3.23). The connection factor is equal to the total connected and perforated sub-layers divided by the total sub-layers in a particular zone. This barrier model improves the GOR history match a lot (**Fig. 3.25**), but it is still not good enough. Connection factors were divided by 10 and 100 to further investigate interwell connectivity. The GOR history match was improved with decreasing connectivity (Fig. 3.25), and seems to indicate that connectivity is close to zero for most, but not all, of the sand zones. This conclusion is also supported by well logs. According to the geology, zone 7 (D1 sand), zone 11 (including C sands), and zone 15 (including A sands) are the most continuous zones, especially zone 7 (Deo et al, 1996).

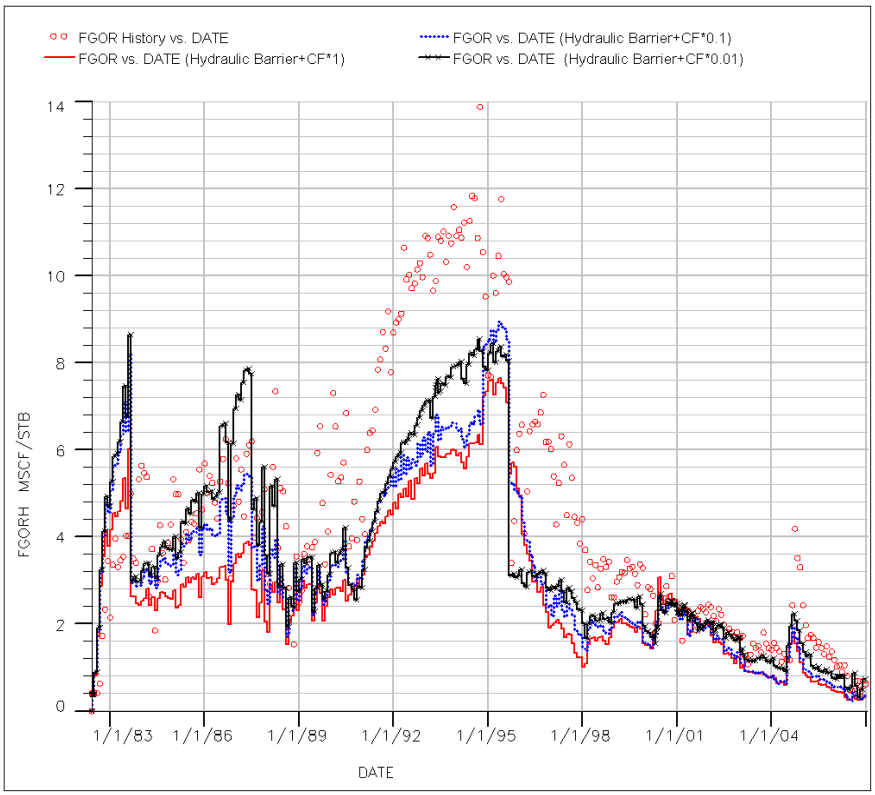


**Fig. 3.25—Effects of hydraulic barriers and connection factors on history matching.**

After several iterations of adjustments, the best history match had barriers where zero hydraulic connectivity was indicated and modified connection factors where non-zero hydraulic connectivity was indicated. I divided the connection factors by 5 for the C and A sands, and 10 for all the other sands. The connection factors of the D1 sands were not changed. A significantly improved history match of the study area's performance data was achieved. **Figs. 3.26** and **3.27** show the study area GOR, water cut, gas rate, oil rate, water rate, and water injection rate history matches.

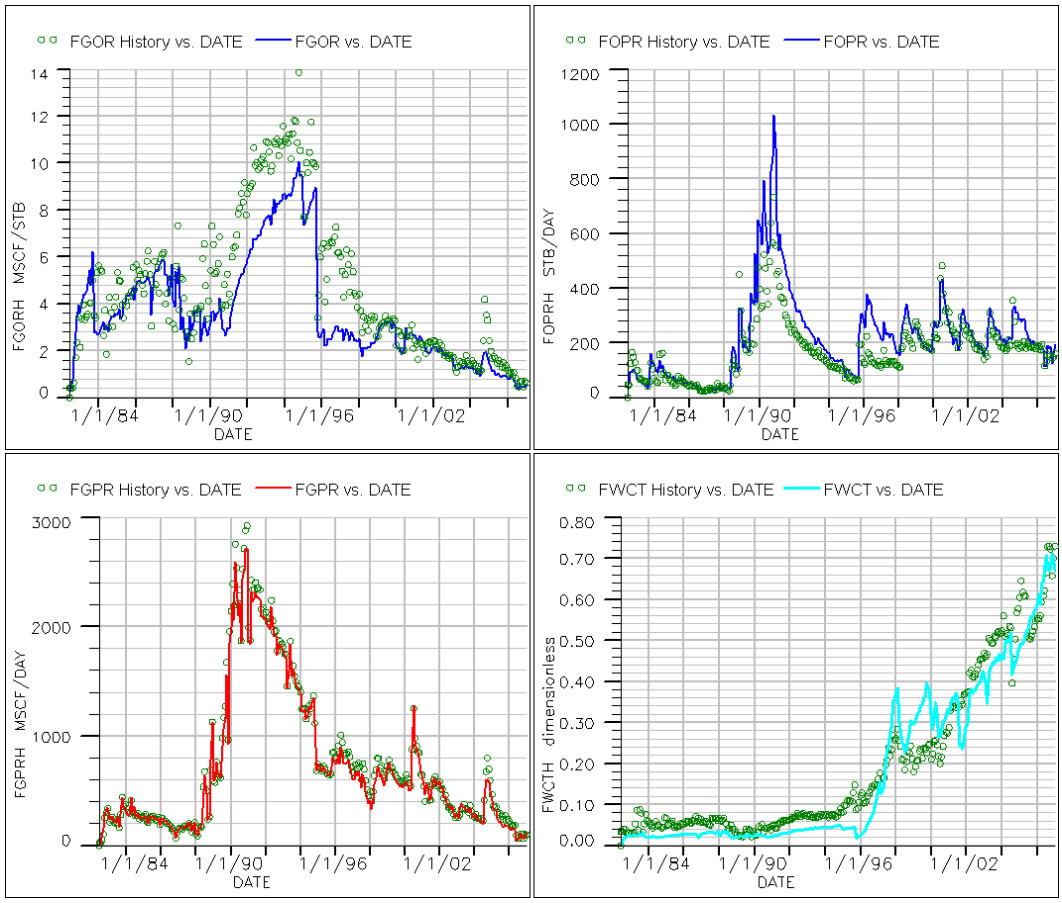


**Fig. 3.26— Best manual study area matches of GOR, gas rate, oil rate, and water cut.**

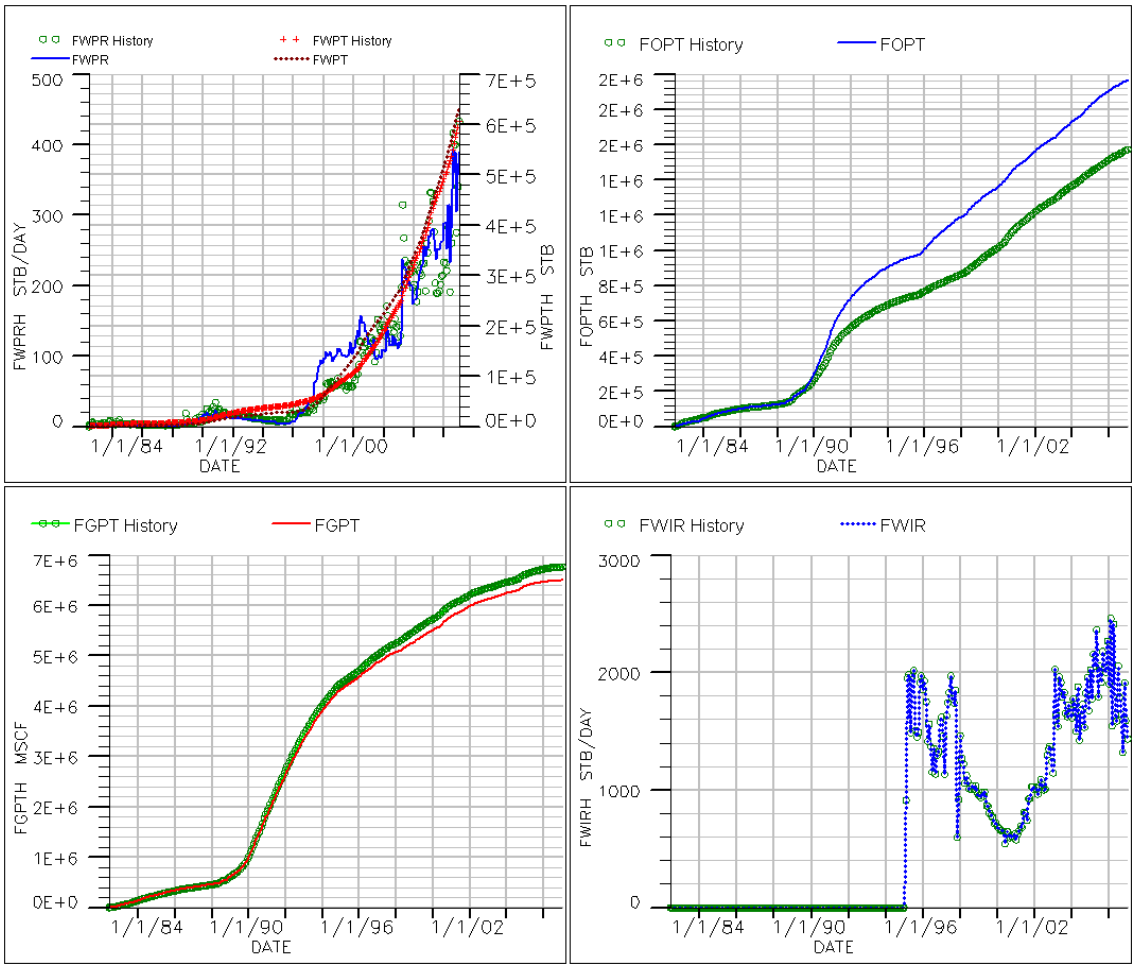


**Fig. 3.27— Best manual study area matches of water rate, cumulative water rate, cumulative gas rate, cumulative oil rate, and water injection rate.**

The manual history matching results were fairly good, but gas rates were still slightly low and oil rates were still slightly high. Also, some wells on the edge of the study area and some inner wells had poor matches. This is not surprising, due to inability to properly model boundary conditions in a sector model like this. For this reason, I checked the match for the group of wells consisting of only inner wells. **Figs. 3.28** and **3.29** show GOR, water cut, gas rate, oil rate, water rate, and water injection rate history matches for those inner wells. The matches are better. **Fig. 3.30** shows simulated pore

volume weighted average reservoir pressure profiles for the whole study area and inner-well region respectively.

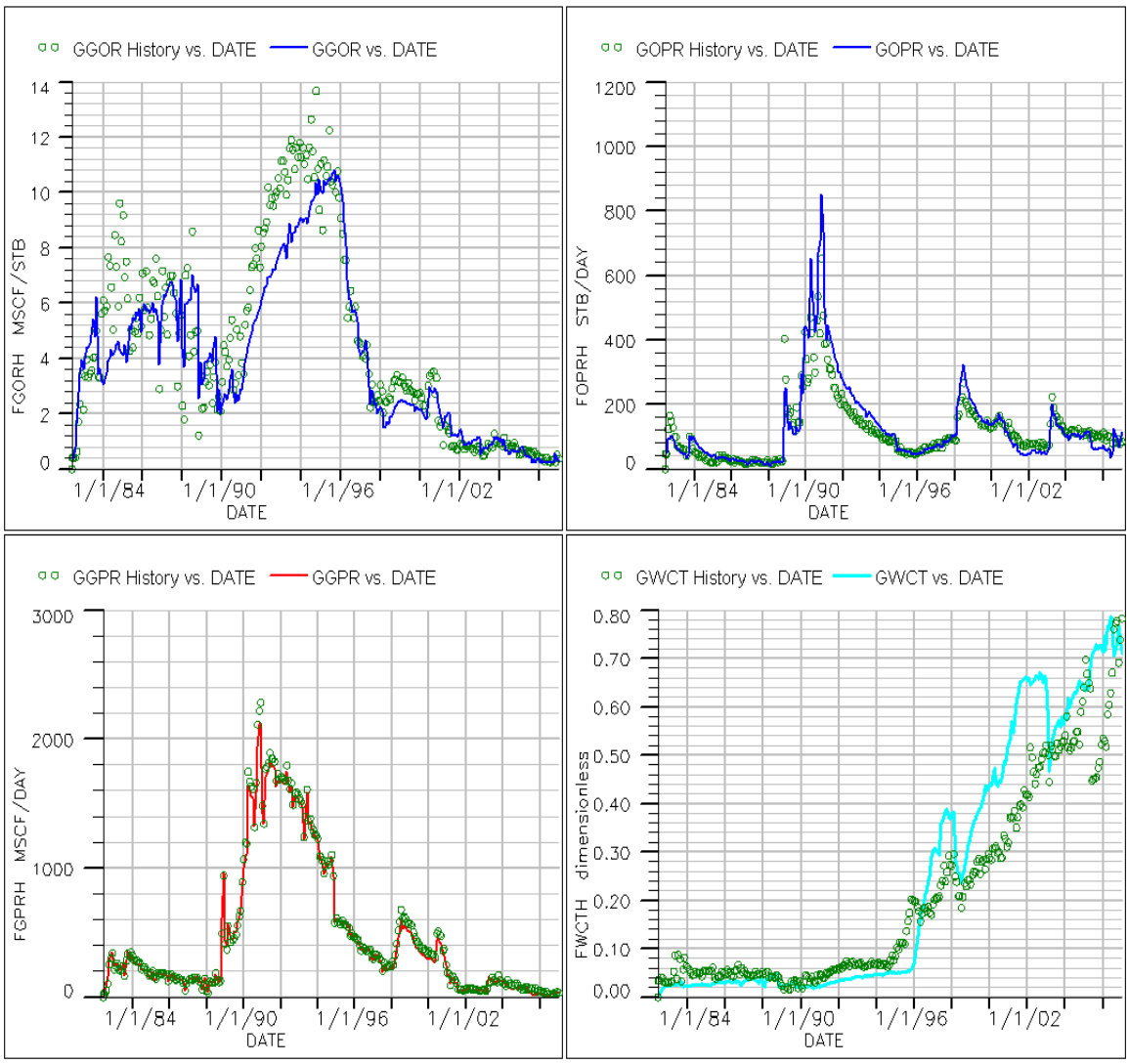


**Fig. 3.28—Study area inner-wells best matches of GOR, gas rate, oil rate, and water cut.**

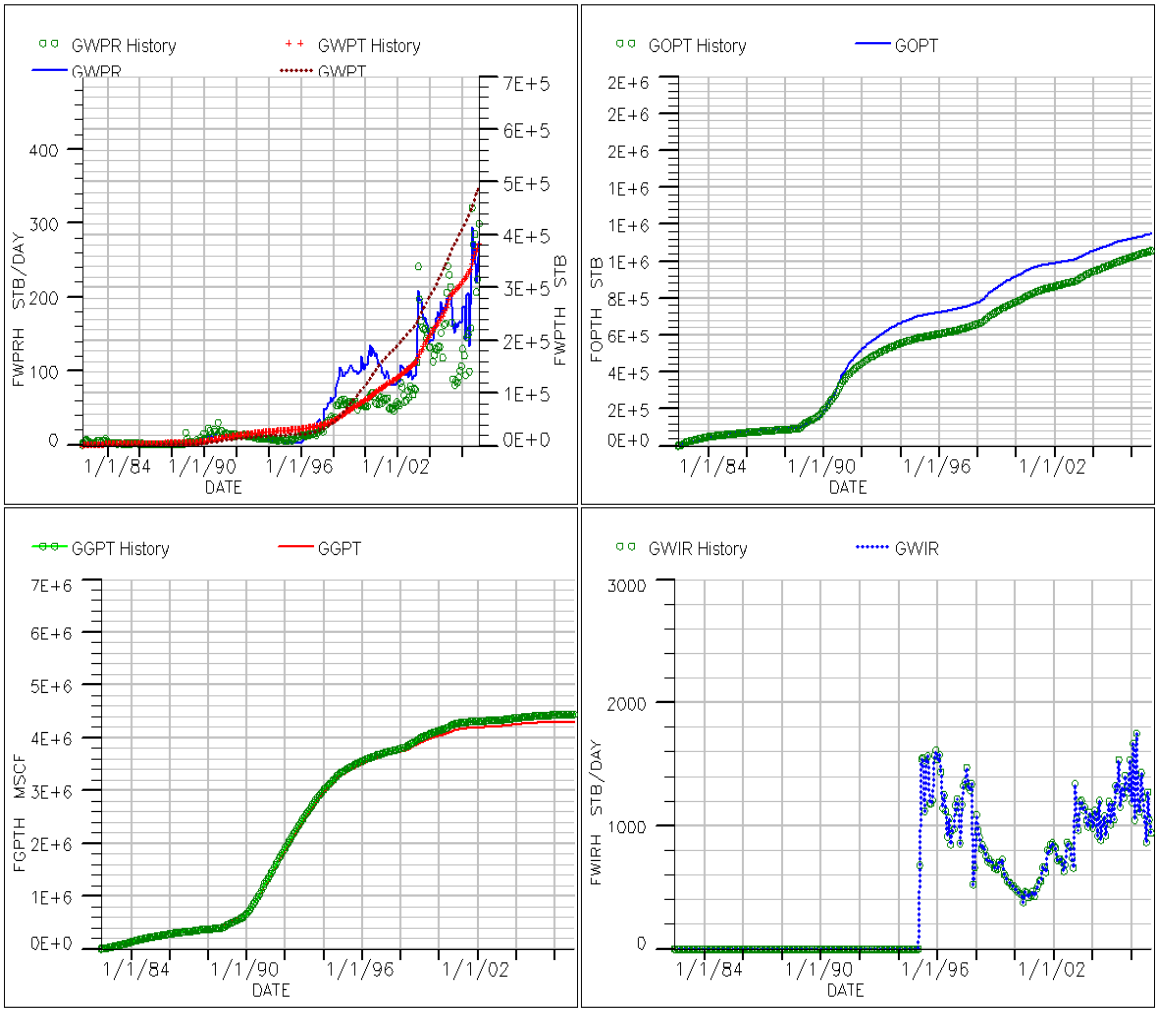


**Fig. 3.29—Study area inner-wells best matches of water rate, cumulative water rate, cumulative gas rate, cumulative oil rate, and water injection rate.**

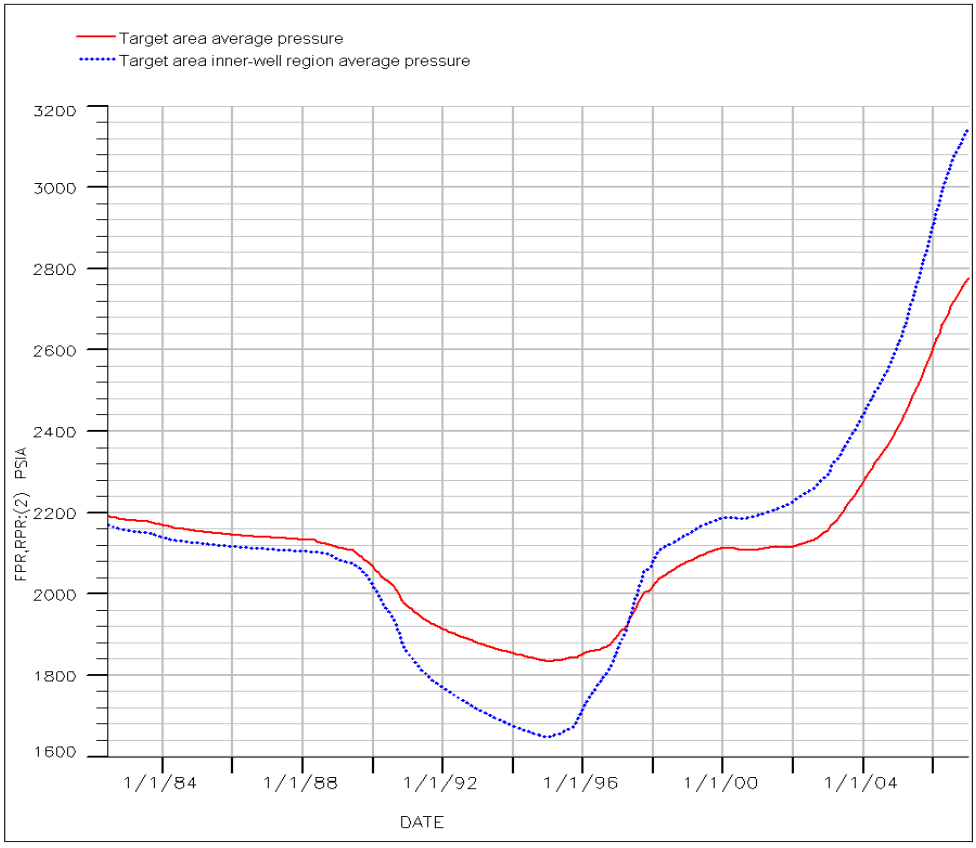


**Fig. 3.30—Simulated pore-volume-weighted average reservoir pressure profiles for the whole study area and inner-well region, respectively.**

**Assisted History Matching**

To improve the matches both for the entire study area and individual wells, I conducted assisted history matching using SimOpt (SimOpt, 2005).

*Principle of Assisted History Matching Using Simopt*

In automatic history matching, the quality of the match is quantified in terms of an objective function (**Eq. 3.7**), the sum of squares of the differences between observed and calculated production responses. The goal is to minimize the objective function to match historical production responses. To preserve geologic information, a prior term (**Eq. 3.8**) is included in the objective function, so that the change of reservoir parameter modifier (porosity, permeability, etc.) is constrained by the statistical distribution of the prior geological property.

$$f = \gamma \bullet f_{prior} + \frac{\alpha}{2} r^T r \quad \text{…….. ……..…} \quad 3.7$$

$$f_{prior} = \frac{1}{2} v^T B^T C_{prior}^{-1} B v \text{ …….. ……..…} \quad 3.8$$

Where

**r** is the vector of residuals for observed production data. Each element (**Eq. 3.9**), $r_i$, in the vector of residuals is the normalized and weighted difference between an observed production value and the corresponding simulated value.

$$r_i = w_d w_i \frac{(o_i - c_i)}{\sigma_d} \text{…….. ……} \quad 3.9$$

$$v = \frac{\lambda - \bar{\lambda}}{\sigma} \quad \text{…….. ……..…} \quad 3.10$$

$\alpha$ and $\gamma$ are the overall weights for production and prior terms, respectively;

$w_d$ is the overall weighting factor for the *d*'th production data set;

$w_i$ is the weighting factor for the *i*'th production data point;

$o_i$ and $c_i$ are the observed and calculated production values, respectively;

$\sigma_d$ is the measurement error for the *d*'th production data set;

$\nu$ is the vector of normalized parameter modifiers (**Eq. 3.10**);

$\lambda$ is the un-normalized parameter modifier;

$\overline{\lambda}$ is the mean value of the parameter modifier distribution;

$\sigma$ is standard deviation of the parameter modifier distribution;

*B* is the diagonal matrix of parameter modifier prior weights;

$C_{prior}$ is the parameter modifier prior correlation matrix.

The objective function is minimized using Levenberg-Marquardt algorithm, which is a combination of the Newton method and a steepest descent scheme. Denoting the vector of current parameter normalized modifier values as $\boldsymbol{v}^k$, then the algorithm estimates the change, $d\boldsymbol{v}^k$, required to minimize the objective function (**Eq. 3.11**)

$$dv^k = (H + \mu I)^{-1} \nabla f(v^k) \ldots\ldots\ldots\ldots\ldots \quad 3.11$$

Where, the Hessian matrix, *H*, is the matrix of second derivatives of *f* and *I* is the identity matrix. The parameter $\mu$ is free and is varied so that, away from the solution where the quadratic Newton model may have less validity, it takes large values and biases the step towards the steepest descent direction. While near the solution, it takes small values to make the best possible use of the fast quadratic convergence rate of the Newton step. For solving Eq. 3.11, SimOpt requires the first and second derivatives of

the objective function (Eq. 3.7) with respect to the normalized parameter modifiers. The first derivative (**Eq. 3.12**) is the gradient vector of the objective function.

$$\nabla f(v) = \alpha(\nabla r)^T r + \gamma \bullet \nabla f_{prior} \quad \ldots\ldots \ldots\ldots \ldots\ldots\ldots\ldots \quad 3.12$$

where each element in the $\nabla \boldsymbol{r}$ matrix is given by **Eq. 3.13**:

$$[\nabla r]_{ij} = \frac{\partial r_i}{\partial v_j} = -\frac{w_d w_i}{\sigma_d}\left(\frac{\partial c_i}{\partial v_j}\right) \quad \ldots\ldots \ldots\ldots\ldots\ldots\ldots \quad 3.13$$

The second derivative (**Eq. 3.14**) is the Hessian matrix of the objective function.

$$\nabla^2 f(v) = \alpha\left\{(\nabla^2 r)^T r + (\nabla r)^T (\nabla r)\right\} + \gamma \bullet \nabla^2 f_{prior} \quad \ldots\ldots \ldots\ldots \quad 3.14$$

It is common to ignore the term involving second derivatives of the simulated value in Eq. 3.14; this is the Gauss-Newton approximation. A justification for this is that it is frequently small in comparison to the first term. Also, it is pre-multiplied by a residual term, which is small near the solution, although the approximation is used even when far from the solution. Hence, the Hessian matrix is approximated by

$$\nabla^2 f(v) \cong \alpha(\nabla r)^T (\nabla r) + \gamma \bullet \nabla^2 f_{prior} \quad \ldots\ldots \ldots\ldots\ldots\ldots\ldots \quad 3.15$$

Thus, the problem can be solved with first derivatives of the simulated quantity with respect to the parameters. To calculate the first derivatives (Eq. 3.12), the matrix with elements of $\frac{\partial c_i}{\partial v_j}$ (Eq. 3.13) is needed. The Matrix is called sensitivity matrix, which is the first derivatives of calculated production data with respect to the normalized parameter modifiers. These sensitivities are obtained from the run of Eclipse 100 at the same time as the simulated quantities themselves, and in just one run. The sensitivity values indicate how the objective function will change with respect to perturbations in

the parameter modifier values. Positive sensitivities indicate that the parameter modifier should be decreased to improve the match, while negative sensitivities indicate that the parameter modifier should be increased (**Fig. 3.31**).

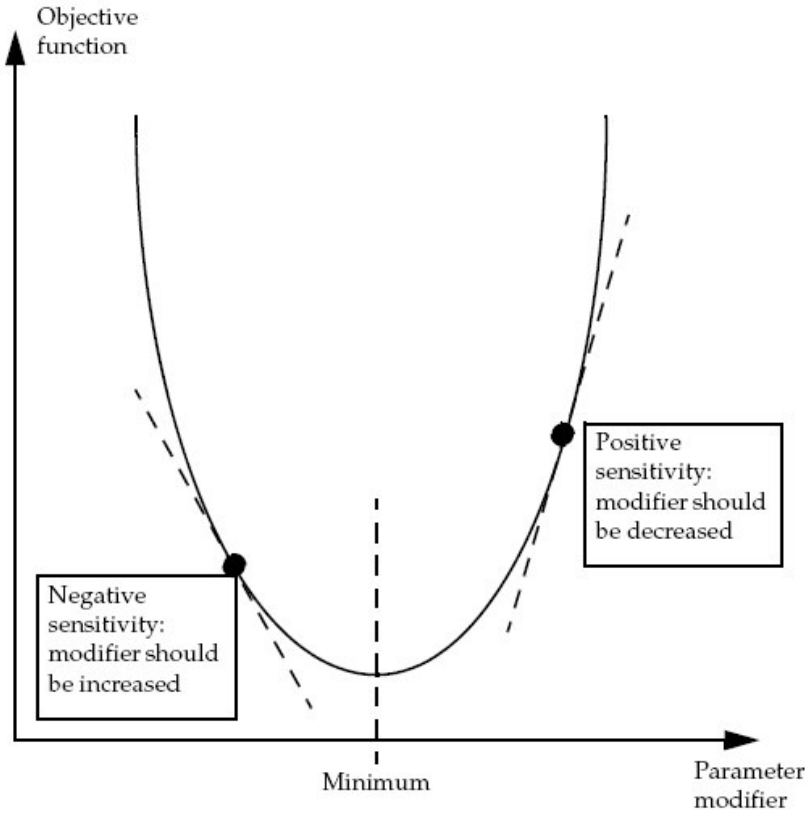


**Fig. 3.31—The relationship between sensitivities and an objective function (from SimOpt, 2005). To minimize the objective function parameter modifiers are changed according the sensitivities.**

SimOpt expresses the overall measure of a history match as a Root Mean Square (RMS) index (Eq. 3.6) formed from the regression of the objective function, where m is the total number of observations. This total RMS index provides an average value of the deviation between simulated and observed data for all data types in the objective function. In addition to the total RMS, SimOpt also calculates a data RMS index for each

data type (GOR or water cut), or each well. This is formed in the same way as the total RMS index except that the summation involved in calculating objective function *f* extends only over data points for a given data type.

*History Matching Settings*

Since in the manual history matching process I had already adjusted pore volume and well productivity index (PI), in SimOpt I selected horizontal permeability multiplier (PermXY) as the parameter to be adjusted. The simulation model has a total of 33,462 cells, so it was not computationally possible to history match on individual grid-block properties. I designated regions around individual wells in each zone and matched on the PermXY parameter in each region. There was no region designated if the well penetrates a null cell (resulting from net-to-gross ratio cut-off) in that zone. In shale zones, some wells shared a single region. The whole simulation model has a total of 362 regions. **Fig. 3.32** shows the designed regions for zone 7 (D1 sand). All the cells in one region share the same PermXY modifier.

The primary observed data matched were GOR and water cut. **Table 3.3** lists the measurement errors and weighting factors for GOR and water cut. Period weighting (**Fig. 3.33**) was used to emphasize later data, especially those data collected after water flooding began. It is essential to ensure that parameter modifier changes are within the model's geological uncertainty, which is constrained by the prior term of the objective function. I set the PermXY modifier to follow log-normal distribution, with a standard deviation of Ln(10) and a mean of Ln(1).

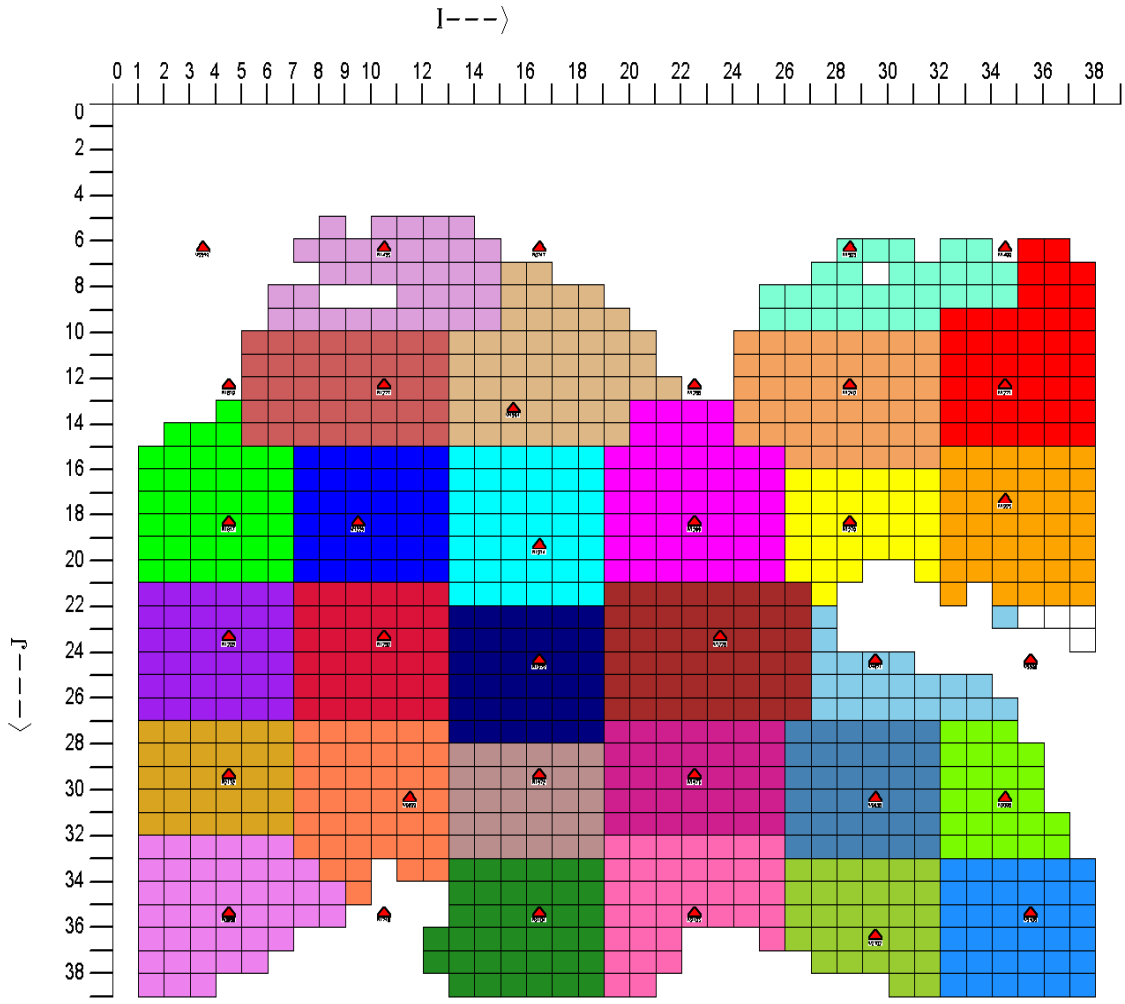


**Fig. 3.32—Designed regions for zone 7 (D1 sand). Blanks are inactive cells due to petrophysical cut-offs of 8% porosity and 80 API of gamma ray.**

**Table 3.3—Measurement errors and weighting factors for GOR and water cut.**

| | Measurement Error | Overall Weight |
|---|---|---|
| WGOR | 0.1 Mcf/stb | 0.6 |
| WWCT | 0.05 | 0.4 |

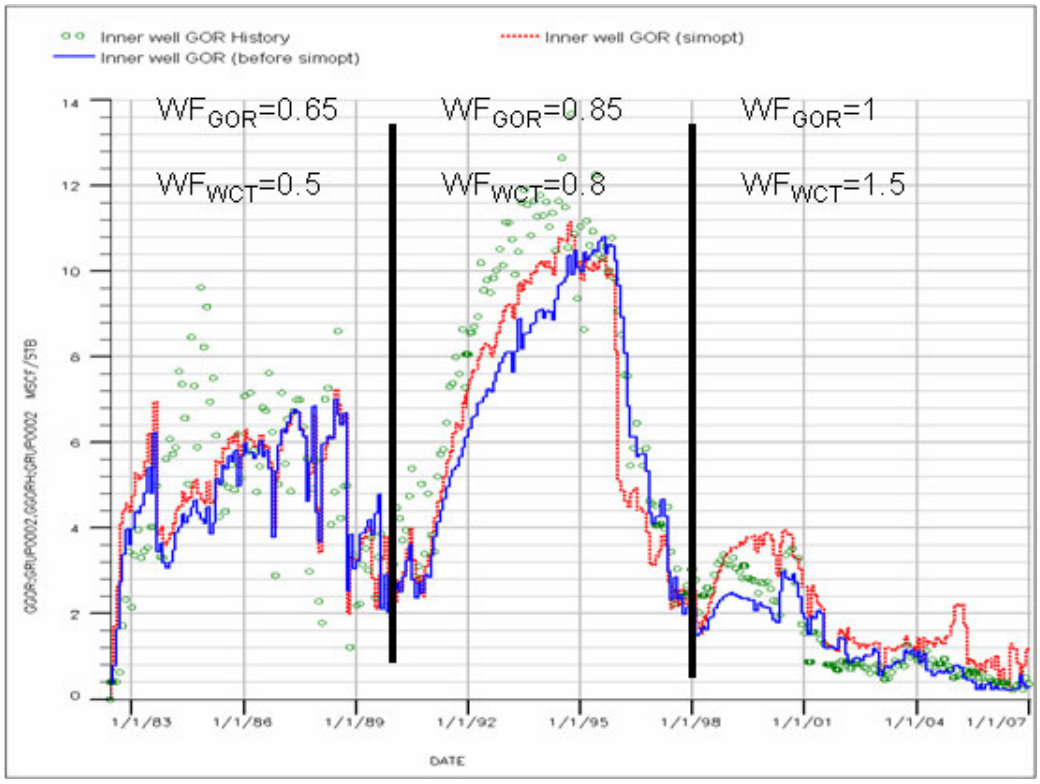


**Fig. 3.33—Period weighting factor (WF) for GOR and water cut (WCT).**

*History Matching Results*

With these parameters, the simulation model resulting from the best manual history match was run using SimOpt. The resulting model had a greatly improved match of not only the whole study area production performance, but also for individual wells. **Figs. 3.34** and **3.35** show GOR, water cut, gas rate, oil rate, water rate, and water injection rate history matches, and reservoir pressure profile in the study area.

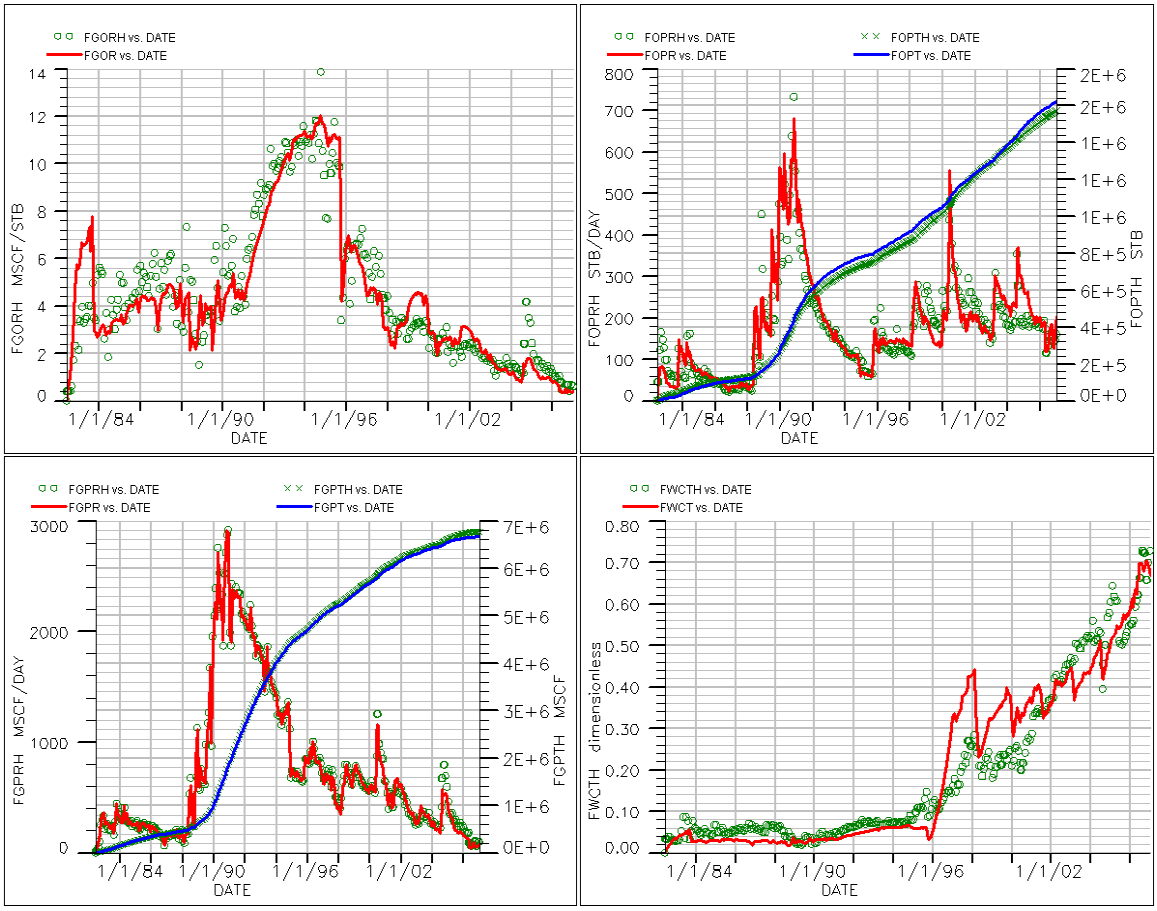


**Fig. 3.34—Study area GOR, water cut, gas rate, oil rate after assisted history matching.**

The matches range from satisfactory to quite good. The reservoir pressure profile is reasonable (Fig. 3.35). At the end of history matching (Dec. 2006), the reservoir pressure of the study area is approximately 2600 psia, which corresponds to a low history GOR of 0.5 Mcf/STB, indicating the reservoir pressure of the study area is above bubble point pressure. **Fig. 3.36** shows GOR and water cut matches for well 1269 and well 2132 before and after using SimOpt. The matches were greatly improved by assisted history matching. Overall, the history match at both the field and individual-well

levels was much improved over previous studies, and the final reservoir model was sufficiently accurate to evaluate reservoir development and recovery strategies.

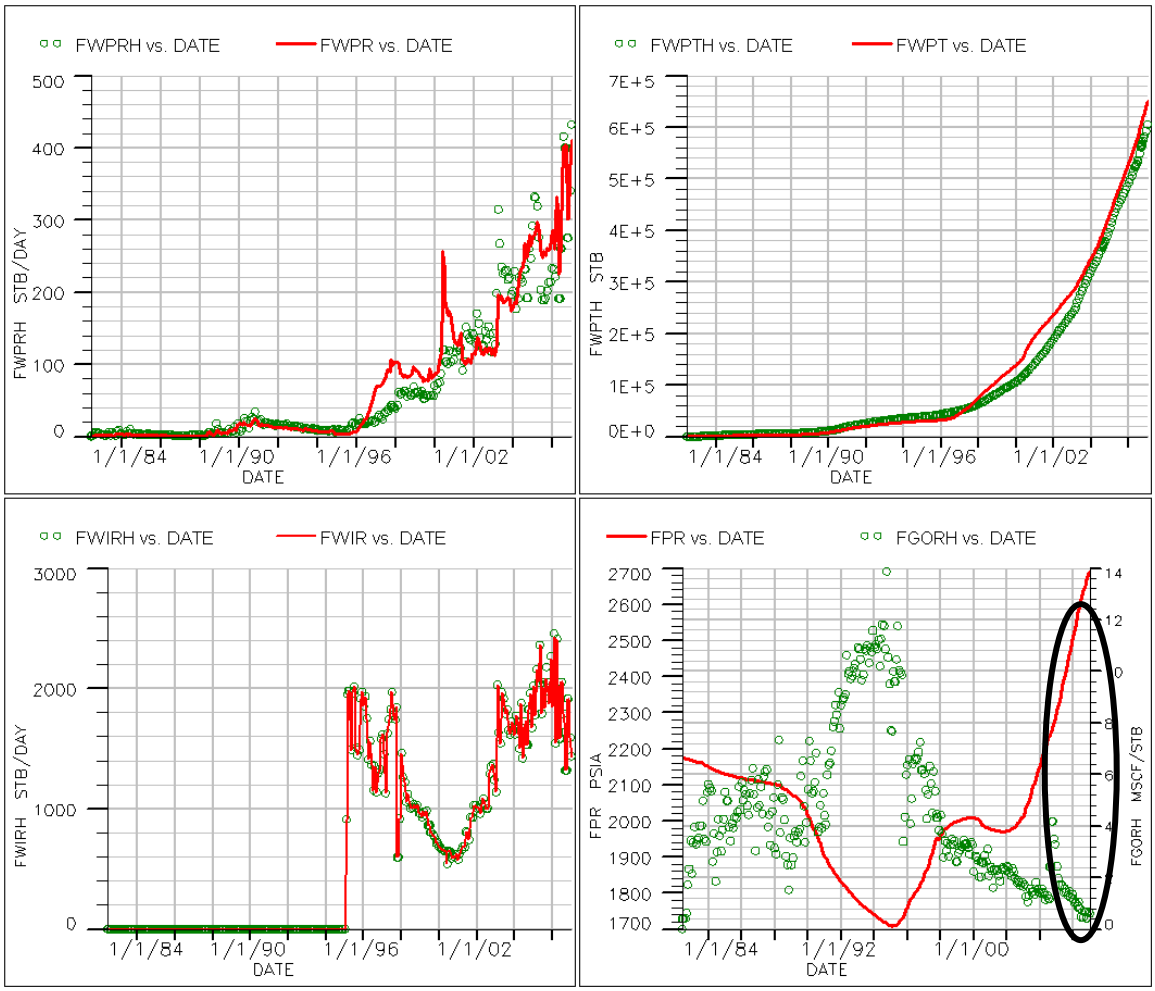


**Fig. 3.35—Study area water rate, water injection rate history matches, and reservoir pressure profile after assisted history matching.**

To check if the assisted history matching process preserved the permeability distribution of the original geological model, permeability distributions before and after history matching were compared. **Fig. 3.37** shows the permeability distribution of D1 sand (zone 7) of the original geological model. **Fig. 3.38** shows permeability distribution

of D1 sand (zone 7) after assisted history matching. Permeabilities from history matching are similar to permeability trends in the geologic model (Figs. 3.37 and 3.38). The map does not replicate exactly the original one because the regression was performed on regions, rather than on a cell-by-cell basis.

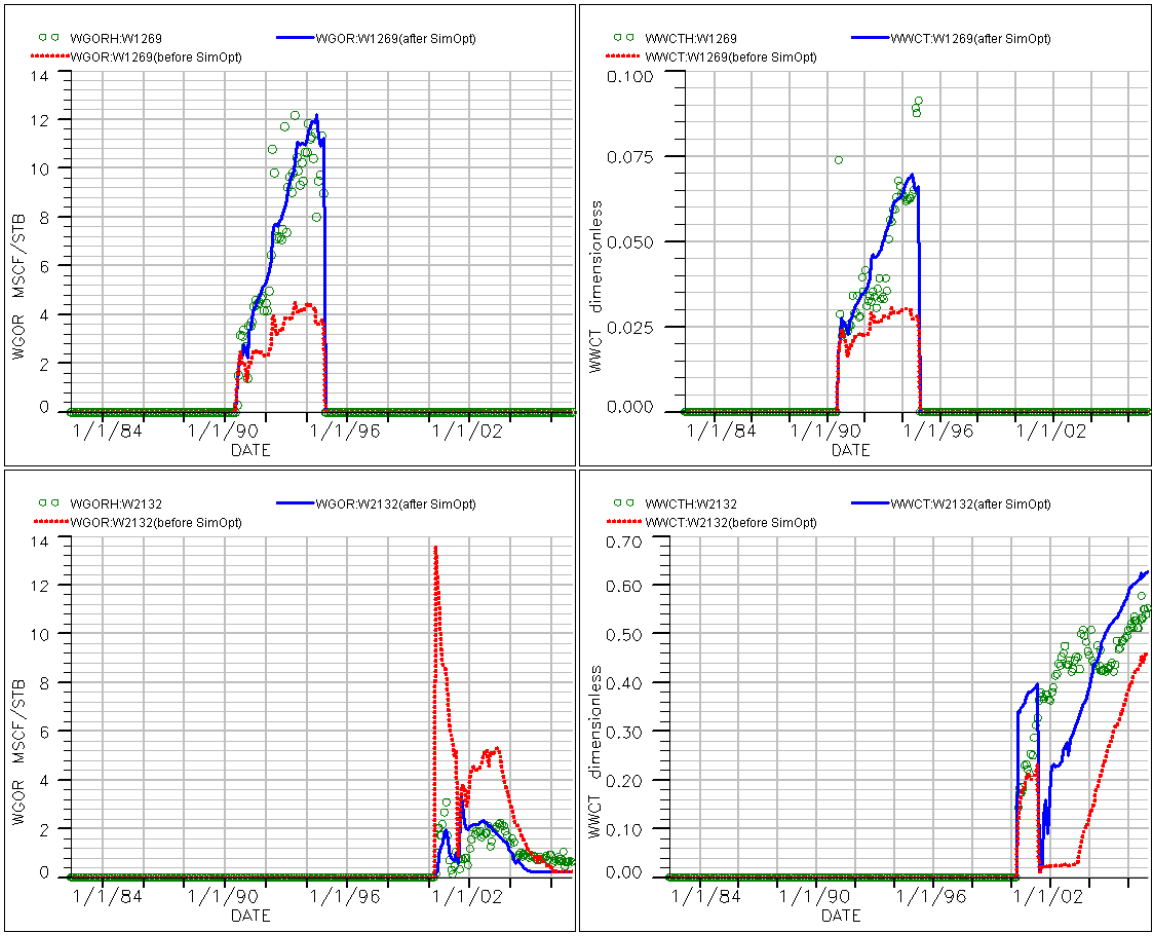


**Fig. 3.36—GOR and water cut matches for well 1269 and well 2132 before and after assisted history matching**

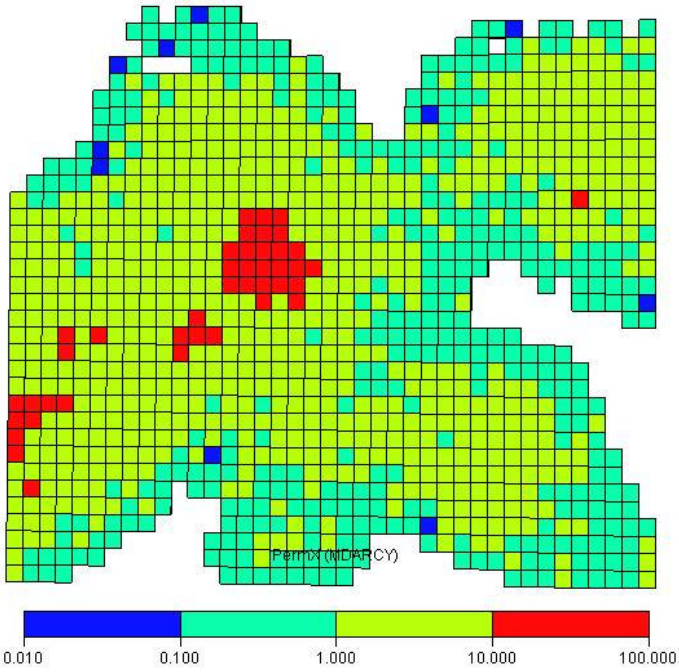


**Fig. 3.37—Permeability distribution of D1 sand of original geological model. Blanks are inactive cells due to petrophysical cut-offs of 8% porosity and 80 API of gamma ray.**

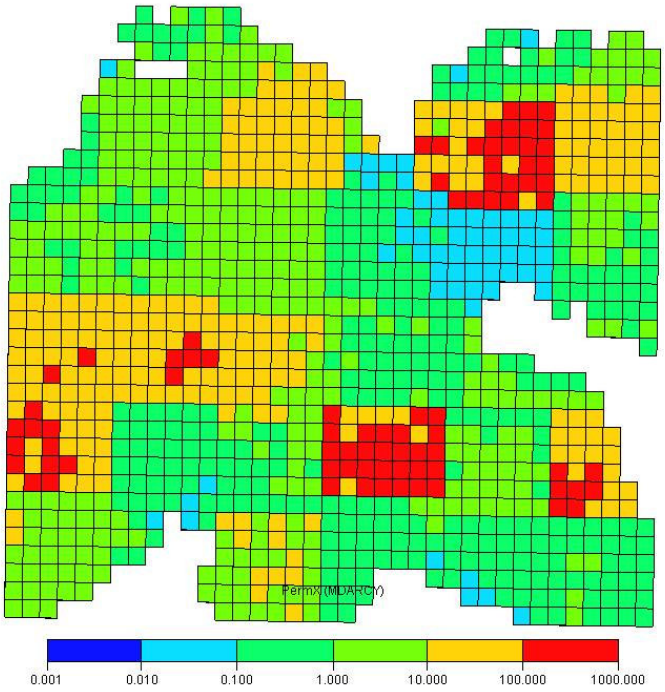


**Fig. 3.38—Permeability distribution of D1 sand (zone 7) after assisted history matching.**

The history-matched permeability distribution also was compared with the core permeability distribution to ensure that permeability values were not greatly altered. The core samples reports are from 12 sidewall and conventional cores published by (Morgan et. al., 2000). Two of the 12 cores are located in the study area, and the others are nearby. The average core permeability is about 5.53 md (**Table 3.4**), whereas the average history-matched permeability is approximately 6.8 md (**Table 3.5**). The maximum permeability value of the history-matched simulation model is 446 md, which is in the same order of the maximum permeability (170 md) of core permeability measurements.

**Table 3.4—Statistics of core permeability data.**

| *Bin* | *Frequency* | *Cumulative %* | *Percentage* | Min. | 0.01 |
|---|---|---|---|---|---|
| 0.01 | 23 | 9.66% | 9.66% | Max. | 170 |
| 0.1 | 45 | 28.57% | 18.91% | Avg. | 5.53 mD |
| 1 | 88 | 65.55% | 36.97% | | |
| 10 | 66 | 93.28% | 27.73% | | |
| 100 | 10 | 97.48% | 4.20% | | |
| 1000 | 6 | 100.00% | 2.52% | | |

**Table 3.5—Statistics of history matched permeability data.**

| *Bin* | *Frequency* | *Cumulative %* | *Percentage* | Min. | 0.002 |
|---|---|---|---|---|---|
| 0.01 | 7 | 0.04% | 0.04% | Max. | 446 |
| 0.1 | 1073 | 5.69% | 5.65% | Avg. | 6.8 mD |
| 1 | 7601 | 45.72% | 40.03% | | |
| 10 | 8854 | 92.35% | 46.64% | | |
| 100 | 1152 | 98.43% | 6.08% | | |
| 1000 | 297 | 100.00% | 1.57% | | |

Histograms of core permeabilities (**Fig. 3.39**) and history-matched permeabilities (**Fig. 3.40**) indicate very similar permeability distributions. **Fig. 3.41** and **3.42** show the RMS index distribution of well GORs before and after assisted history matching. Following assisted history matching, the GOR mismatches were greatly decreased for wells, with exception of some edge wells and one inner well (4301331277). Water-cut RMS indices (**Figs. 3.43** and **3.44**) also were decreased, to some degree, by assisted history match. Inner wells have reasonable water cut matches, with exception of wells 4301331277 and 4301331251.

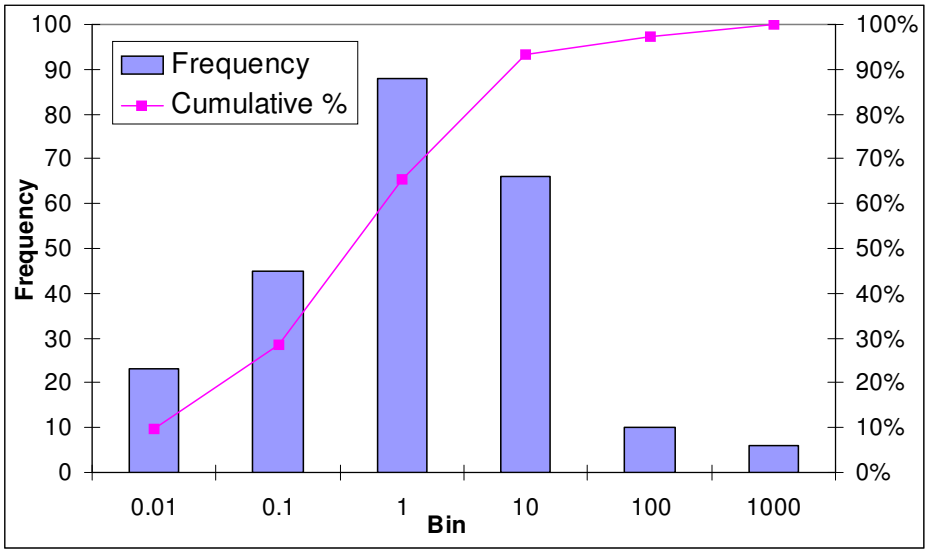


**Fig. 3.39—Histogram of core permeability data.**

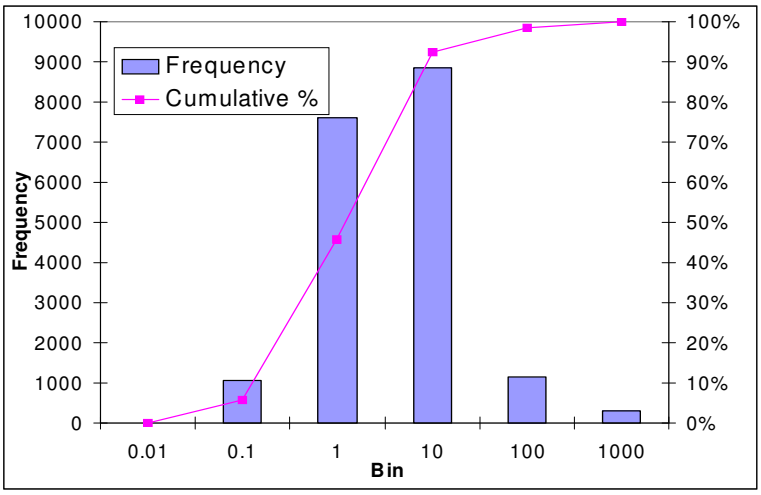


**Fig. 3.40—Histogram of history matched permeability data.**

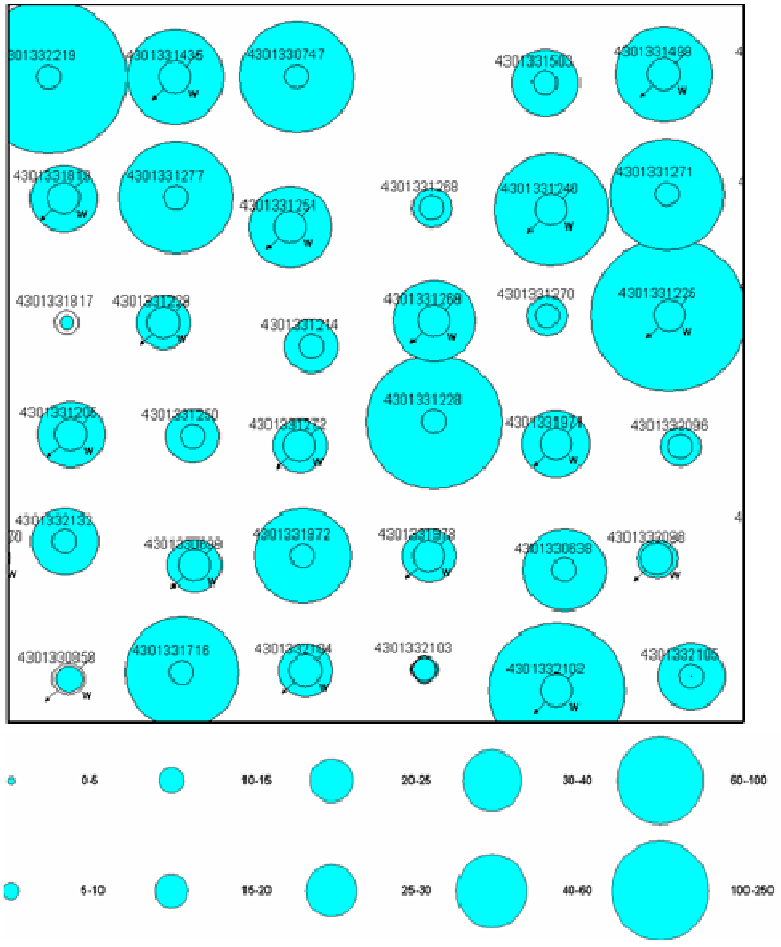

**Fig. 3.41—Well GOR RMS index distribution before manual history matching.**

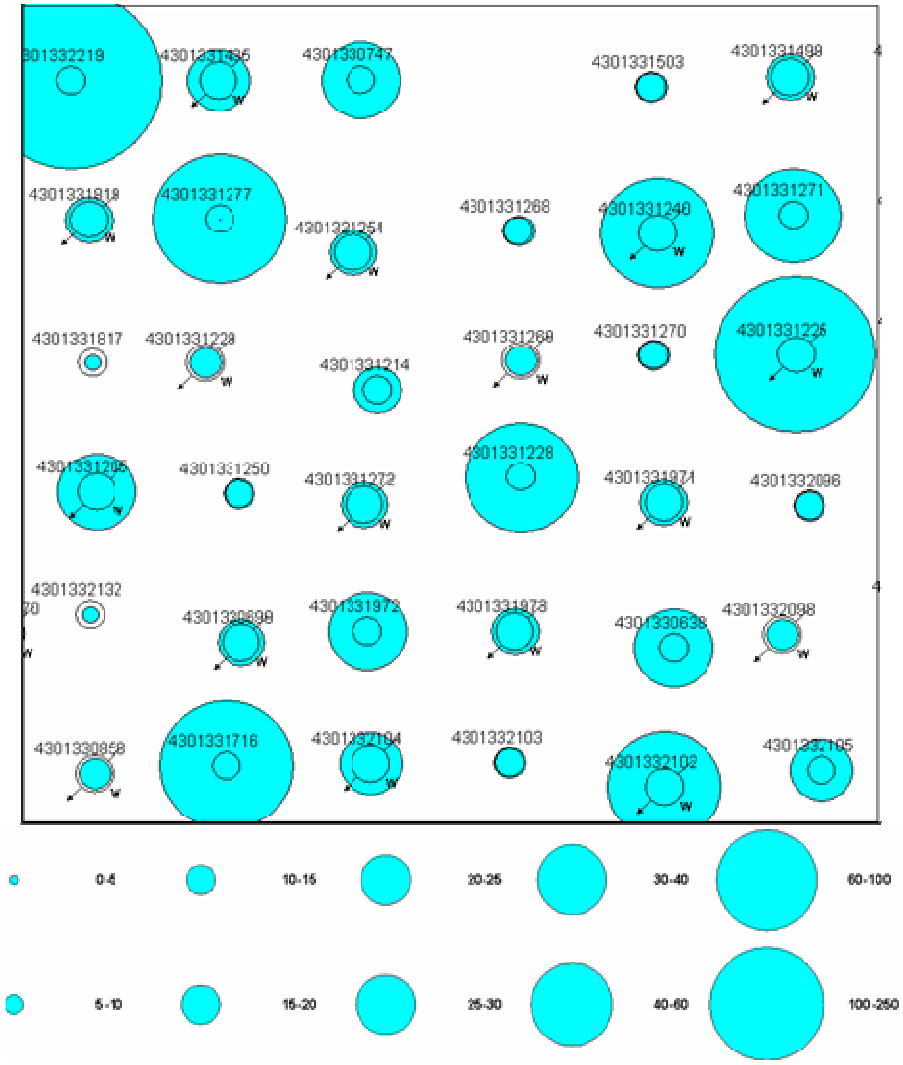


**Fig. 3.42—Well GOR RMS index distribution after assisted history matching.**

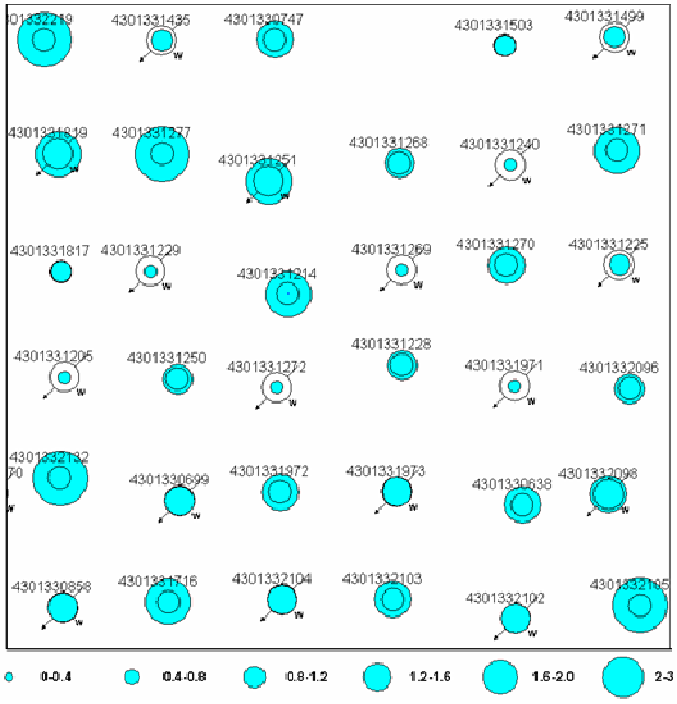


**Fig. 3.43—Water cut RMS indices after best manual history matching.**

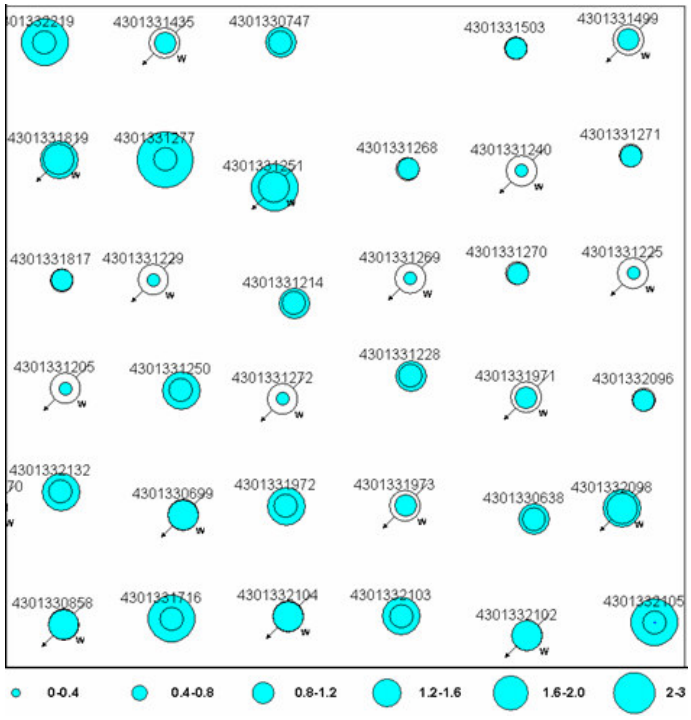


**Fig. 3.44—Water cut RMS indices after using assisted history matching.**

## 3.8 DYNAMIC INTERWELL CONNECTIVITY EVALUATION

In history matching, I used a barrier model that has zero transmissibility between two adjacent wells if hydraulic connectivity is 0 and has a connection factor that is between 0 and 1 if hydraulic connectivity is non-zero. During history matching, connection factors were usually decreased, sometimes significantly, to improve the match. After history matching, I recalculated connectivity values for each zone from the calibrated dynamic model and compared these connectivity values to the geological hydraulic connectivities calculated earlier using only static data (net thickness and perforations). The calculated "dynamic" connectivity factors were 0.63, 0.16, 0.23, and 0.01 for zone 7 (D1 sand), zone 11 (including C sand), zone 15 (including A sand), and zone 17 (LODC sands), respectively, compared to values of 0.63, 0.37, 0.56, and 0.27 for the same sand zones from the geological hydraulic connectivity evaluation described earlier. The dynamic connectivities are generally much lower than the hydraulic connectivities evaluated using net thickness and perforation data, especially in low quality sand zones. This indicates that our earlier assumption of continuity between adjacent wells both with net thickness and perforations in a particular zone may not be a valid assumption for many zones.

## 3.9 PVT MATCHING

It is vital to have a realistic physical model of reservoir fluid samples before using them in a compositional reservoir simulation, to anticipate how the fluids will behave in the reservoir over a wide range of temperatures and pressures. When gas is injected into the reservoir, it is necessary to know how the properties of the original reservoir fluid will change as the composition of the mixture changes. Black-oil simulation does not provide sufficient description of reservoir processes that involve a miscible displacement or large compositional changes in reservoir fluids.

In a black-oil model, the physical properties of the oil and the gas are functions of pressure, only. Therefore, the only input needed by a black-oil simulator is a table of physical properties versus pressure. In a compositional model, all we know is what components are present. First, we must calculate how many phases are present at reservoir (?) pressure and temperature. If there are oil and gas phases, the composition of each phase must be calculated. Given these compositions, we calculate the physical properties, such as oil viscosity.

To calculate the change of physical properties of the oil and gas with pressure and temperature, I calibrated an equation of state (EOS). This involved matching the main experiments performed by the PVT laboratory on the recombined fluid sample. In this study, measured PVT data were provided by the field operator. These data include compositional analyses of hydrocarbon samples, constant composition expansion (CCE) data, differential liberation (DL) data, and separator tests. **Table 3.6** gives compositional analysis of hydrocarbon samples of recombined well-stream fluids through C11+.

**Tables 3.7-3.9** provide constant composition expansion data, differential liberation data, and measured oil viscosity and calculated gas viscosity data, respectively.

Usually, PVT matching starts with splitting the heavy component, such as C11+, into two or three pseudo-components, because laboratories tend to give very limited analysis of the plus fraction and saturation pressure calculations can be extremely sensitive to mole fraction and properties of the plus fraction. Different splitting methods, such as Constant Mole Fraction, Whitson and Modified Whitson, were tried to help match PVT data. In this study, simulation experiments showed that the current components through C11+ were adequate for accurate matching.

**Table 3.6—Compositional analysis of recombined well-stream fluid through C11+.**

| Component | Wellstream Mole% |
|---|---|
| N2 | 0.404 |
| CO2 | 0.365 |
| C1 | 34.675 |
| C2 | 6.997 |
| C3 | 5.367 |
| IC4 | 1.174 |
| NC4 | 2.338 |
| IC5 | 0.985 |
| NC5 | 1.282 |
| C6 | 3.763 |
| C7 | 2.333 |
| C8 | 2.670 |
| C9 | 2.193 |
| C10 | 1.791 |
| C11+ | 33.663 |
| C11+ Specific Gravity | 0.887 |
| C11+ Molecular Weight (lb/ln-mole) | 365.600 |

**Table 3.7—Constant composition expansion data at 131 °F.**

| Pressure, (psig) | | Relative Volume | Total Density (g/cc) | Y - Function | Isothermal Oil Compressibility (vol/vol)/psi |
|---|---|---|---|---|---|
| 4000 | | 0.98460 | 0.77310 | N/A | N/A |
| 3750 | | 0.98639 | 0.77170 | N/A | 7.3158 |
| 3500 | | 0.98821 | 0.77027 | N/A | 7.4472 |
| 3250 | | 0.99007 | 0.76883 | N/A | 7.5858 |
| 3000 | | 0.99197 | 0.76736 | N/A | 7.7713 |
| 2750 | | 0.99392 | 0.76585 | N/A | 7.9833 |
| 2500 | | 0.99593 | 0.76430 | N/A | 8.2165 |
| 2250 | | 0.99802 | 0.76271 | N/A | 8.5001 |
| 2020 | Psat | 1.00000 | 0.76119 | N/A | 8.8118 |
| 1750 | | 1.03960 | 0.73220 | 3.8628 | N/A |
| 1506 | Pres | 1.09301 | 0.69642 | 3.6332 | N/A |
| 1250 | | 1.18069 | 0.64470 | 3.3686 | N/A |
| 1000 | | 1.32349 | 0.57514 | 3.1064 | N/A |
| 750 | | 1.58124 | 0.48139 | 2.8561 | N/A |
| 500 | | 2.13215 | 0.35701 | 2.6068 | N/A |
| 400 | | 2.55667 | 0.29773 | 2.5075 | N/A |

**Table 3.8—Differential liberation data at 131 °F.**

| Pressure, (psig) | | Oil Density (g/cc) | Solution Gas/Oil Ratio, $R_{sD}$ (scf/stb) | Relative Total Volume, $B_{tD}$ (rb/stb) | Relative Oil Volume, $B_{oD}$ (rb/stb) | Gas Formation Volume, Factor, $B_g$ (rb/mscf) | Gas Deviation Factor, Z | Incremental Gas Specific Gravity (Air=1.000) | Cumulative Gas Specific Gravity (Air=1.000) |
|---|---|---|---|---|---|---|---|---|---|
| 4000 | | 0.7731 | 408 | 1.2059 | 1.2059 | N/A | N/A | N/A | N/A |
| 3750 | | 0.7717 | 408 | 1.2081 | 1.2081 | N/A | N/A | N/A | N/A |
| 3500 | | 0.7703 | 408 | 1.2104 | 1.2104 | N/A | N/A | N/A | N/A |
| 3250 | | 0.7688 | 408 | 1.2126 | 1.2126 | N/A | N/A | N/A | N/A |
| 3000 | | 0.7674 | 408 | 1.2150 | 1.2150 | N/A | N/A | N/A | N/A |
| 2750 | | 0.7659 | 408 | 1.2174 | 1.2174 | N/A | N/A | N/A | N/A |
| 2500 | | 0.7643 | 408 | 1.2198 | 1.2198 | N/A | N/A | N/A | N/A |
| 2250 | | 0.7627 | 408 | 1.2224 | 1.2224 | N/A | N/A | N/A | N/A |
| 2020 | Psat | 0.7612 | 408 | 1.2248 | 1.2248 | N/A | N/A | N/A | N/A |
| 1700 | | 0.7659 | 357 | 1.2844 | 1.2071 | 1.510 | 0.8330 | 0.6825 | 0.6825 |
| 1400 | | 0.7712 | 308 | 1.3768 | 1.1893 | 1.867 | 0.8520 | 0.6657 | 0.6742 |
| 1100 | | 0.7761 | 256 | 1.5378 | 1.1719 | 2.411 | 0.8740 | 0.6637 | 0.6707 |
| 800 | | 0.7808 | 204 | 1.8516 | 1.1549 | 3.411 | 0.9010 | 0.6713 | 0.6708 |
| 500 | | 0.7860 | 148 | 2.6036 | 1.1360 | 5.642 | 0.9270 | 0.7015 | 0.6774 |
| 200 | | 0.7920 | 84 | 5.6961 | 1.1130 | 14.143 | 0.9550 | 0.7987 | 0.7014 |
| 100 | | 0.7946 | 61 | 10.4445 | 1.1036 | 26.899 | 0.9660 | 0.9021 | 0.7148 |
| 0 | | 0.8172 | 0 | N/A | 1.0481 | N/A | 0.9980 | 1.4980 | 0.8315 |

**Table 3.9—Measured oil viscosity and calculated gas viscosity data at 131 °F.**

| Pressure psig | Measured Oil Viscosity (cp) | Calculated Gas Viscosity (cp) | Oil / Gas Viscosity Ratio |
|---|---|---|---|
| 4000 | 2.812 | N/A | N/A |
| 3500 | 2.690 | N/A | N/A |
| 3000 | 2.567 | N/A | N/A |
| 2500 | 2.445 | N/A | N/A |
| 2020 | 2.322 | N/A | N/A |
| 1700 | 2.430 | 0.0161 | 150.932 |
| 1400 | 2.713 | 0.0150 | 180.867 |
| 1100 | 3.100 | 0.0141 | 219.858 |
| 800 | 3.630 | 0.0134 | 270.896 |
| 500 | 4.400 | 0.0128 | 343.750 |
| 200 | 5.512 | 0.0123 | 448.130 |
| 100 | 6.060 | 0.0120 | 505.000 |
| 0 | 7.108 | 0.0111 | 640.360 |

The second step in PVT matching involved grouping components to speed up compositional simulation. For large numbers of components, the computing time needed to solve the flash equations may be as great as the time needed to solve the flow equations. Running a simulation with more than nine components (for example) may result in impractically long computing times (Schlumberger, 2007), especially for fully implicit solutions. The number of grouped 'pseudo-components' needed in a compositional simulation depends on the process that is modeled. For depletion, 2 pseudo-components may sufficient (black-oil model). For miscible flow, more than 10 components may sometimes be needed. In general, 4 to 10 components should be sufficient to describe the phase behavior.

The primary basis for grouping is to combine components with similar molecular weights. Obvious candidates to group are IC4 with NC4, and IC5 with NC5. An

exception to this rule is that $N_2$ is usually added to C1 and $CO_2$ is usually added to C2. Their molecular weights would suggest that I should group $N_2$ (molecular weight =28) with C2 (molecular weight =20) and not with C1 (MW=16). The main criterion for a successful grouping is whether the new grouped components can predict observed experimental results as well as the original ungrouped components. If a compositional simulation model is run, the results of the simulation should be independent of whether the new grouped components or the original ungrouped components are used. Considering possible $N_2$ and $CO_2$ injection, after several experiments I grouped C2, C3, IC4 and NC5 together and IC5, NC5, and C6 together (**Table 3.10**). **Table 3.11** shows the regrouped components and their properties. After grouping, I compared the shape of the phase diagram with the ungrouped phase diagram (**Fig. 3.45**). The phase plot does not change markedly after grouping, indicating that a good grouping has been achieved.

**Table 3.10—Grouping method.**

| Row | Component | New Index | Group |
|---|---|---|---|
| 1 | N2 | 1 | N2 |
| 2 | CO2 | 2 | CO2 |
| 3 | C1 | 3 | C1 |
| 4 | C2 | 4 | C2+ |
| 5 | C3 | 4 | C2+ |
| 6 | IC4 | 4 | C2+ |
| 7 | NC4 | 4 | C2+ |
| 8 | IC5 | 5 | C5+ |
| 9 | NC5 | 5 | C5+ |
| 10 | C6 | 5 | C5+ |
| 11 | C7 | 6 | C7 |
| 12 | C8 | 7 | C8 |
| 13 | C9 | 8 | C9 |
| 14 | C10 | 9 | C10 |
| 15 | C11+ | 10 | C11+ |

**Table 3.11—Regrouped components and their properties.**

| Components | ZI (percent) | Weight fraction (percent) | Mol Weight | Spec Gravity |
|---|---|---|---|---|
| N2 | 0.404 | 0.075264 | | |
| CO2 | 0.365 | 0.10683 | | |
| C1 | 34.675 | 3.6995 | | |
| C2+ | 15.876 | 4.3307 | 41.018 | 0.56472 |
| C5+ | 6.03 | 3.1899 | 79.545 | 0.66184 |
| C7 | 2.333 | 1.4895 | | |
| C8 | 2.67 | 1.8999 | | |
| C9 | 2.193 | 1.7647 | | |
| C10 | 1.791 | 1.5961 | | |
| C11+ | 33.663 | 81.848 | 365.6 | 0.8866 |

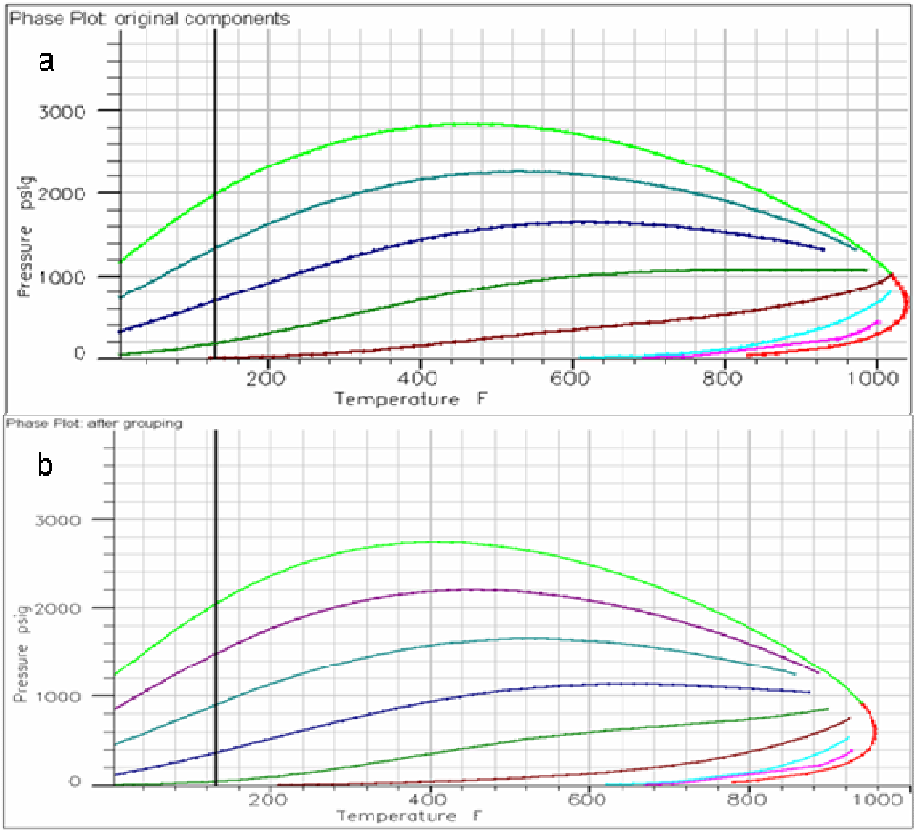


**Fig. 3.45—Shapes of the phase diagrams (a) before and (b) after grouping.**

The next step was to tune an EOS to match PVT data observations. I used the 3-parameter, Peng-Robinson EOS. In PVT analysis, the saturation pressure should be matched first. The saturation pressure is usually very sensitive to the Omega_A, Omega_B, $P_{crit}$ and $T_{crit}$ of the plus component. I used Omega_A and Omega_B of the C11+ component as variables to conduct regression to match saturation pressure first, and then I used $P_{crit}$, $T_{crit}$, and volume shift of C7, C8, C9, C10, and C11+ components to match oil and gas densities, gas Z-factor, and oil and gas formation volume factors. **Figs. 3.46** to **3.52** show the PVT matching results for relative volume (CCE), liquid density (DL), oil and gas formation volume factors (DL), GOR (DL), gas gravity (DL), and vapor Z-factor (DL) matches before and after regression of the variables defined above. After regression, the matching results were greatly improved. Viscosity was matched last because viscosity is a flow property. The EOS will predict static equilibrium properties, but not flowing properties. The Lohrenz-Bray-Clark (LBC) method was used for viscosity correlations. **Figs. 3.53** and **3.54** show the oil and gas viscosity matching results before and after regression. Oil viscosities were matched accurately, and the gas viscosities match was fair. I concluded that all of the matches are adequate for compositional simulation.

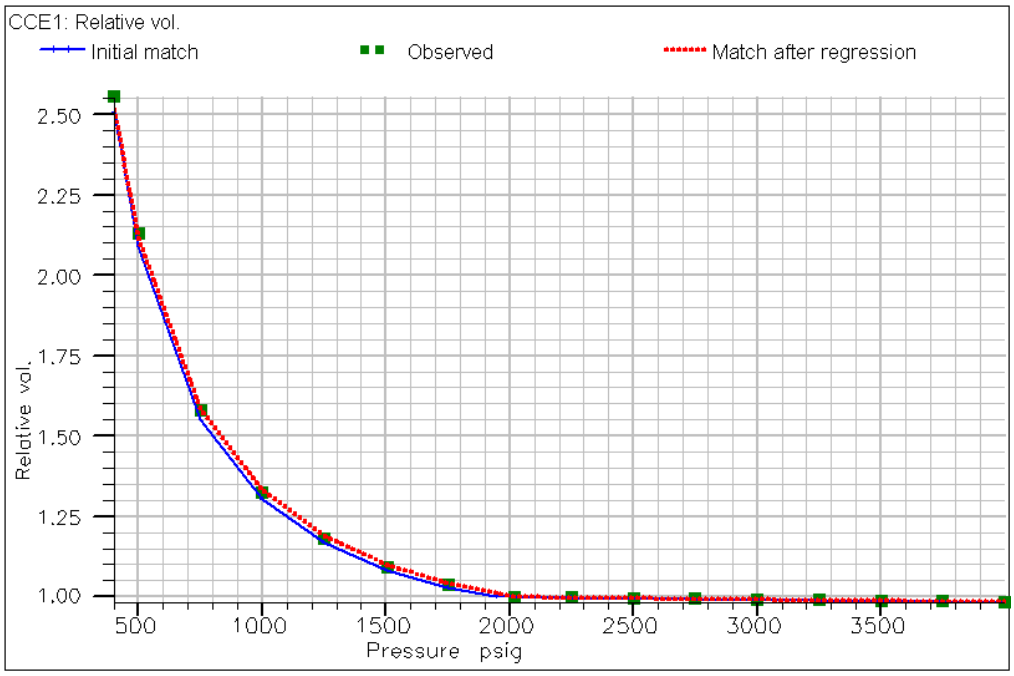


**Fig. 3.46—Relative volume (CCE) match before and after regression.**

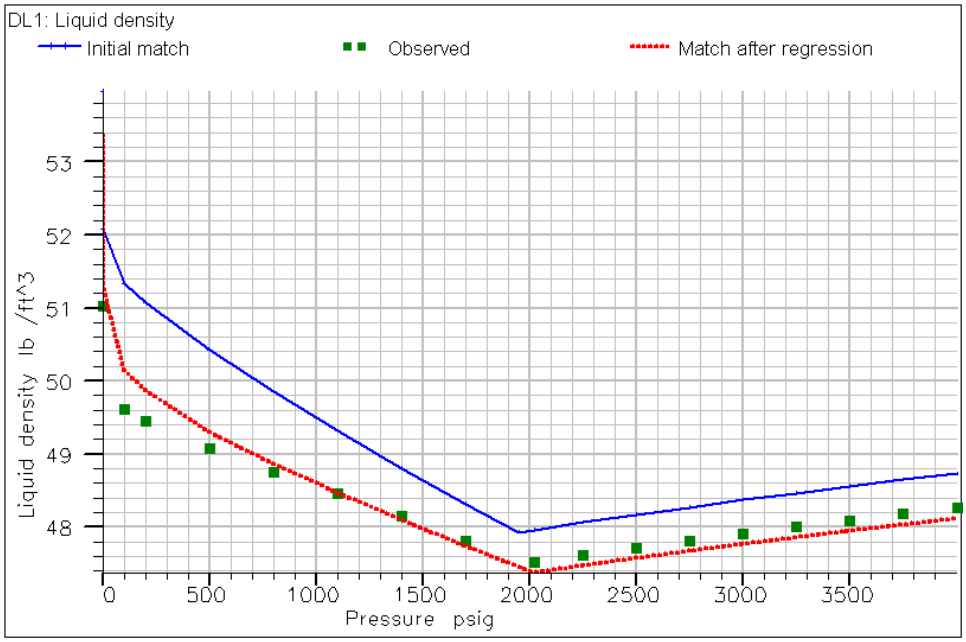


**Fig. 3.47—Liquid density (DL) match before and after regression.**

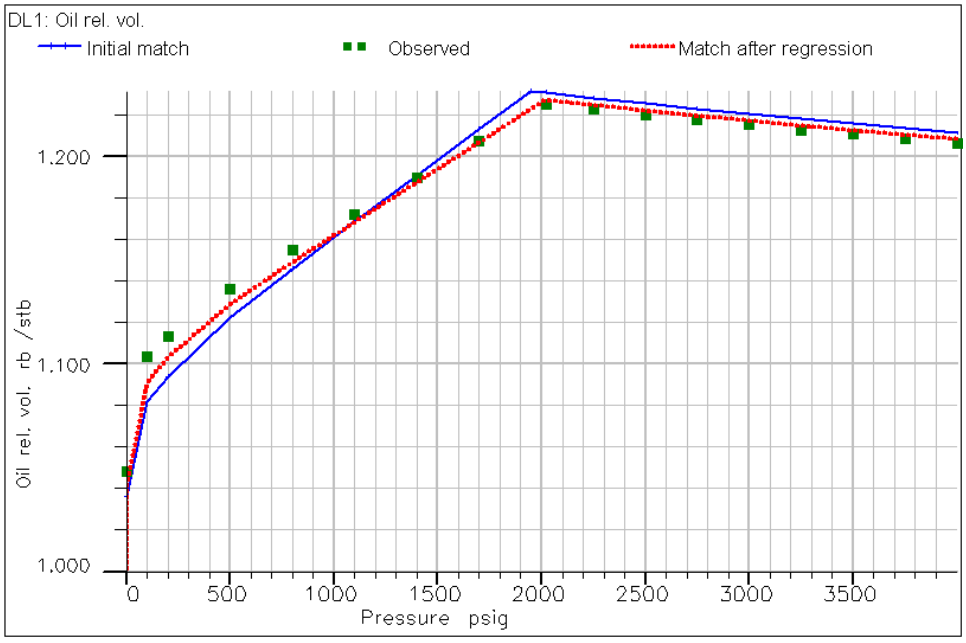


**Fig. 3.48—Oil formation volume factor match before and after regression.**

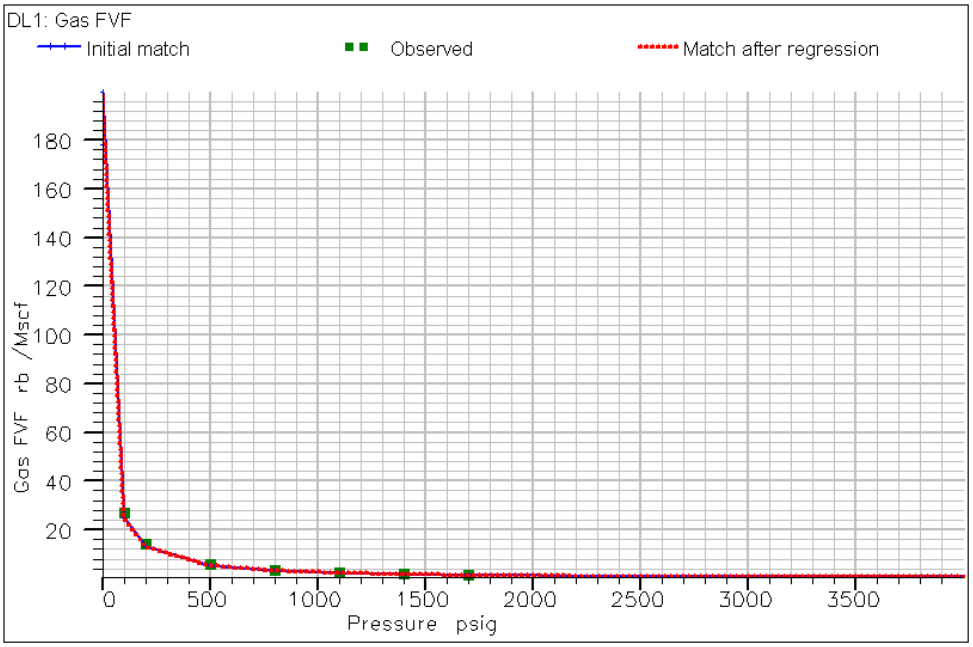


**Fig. 3.49—Gas formation volume factor (DL) match before and after regression.**

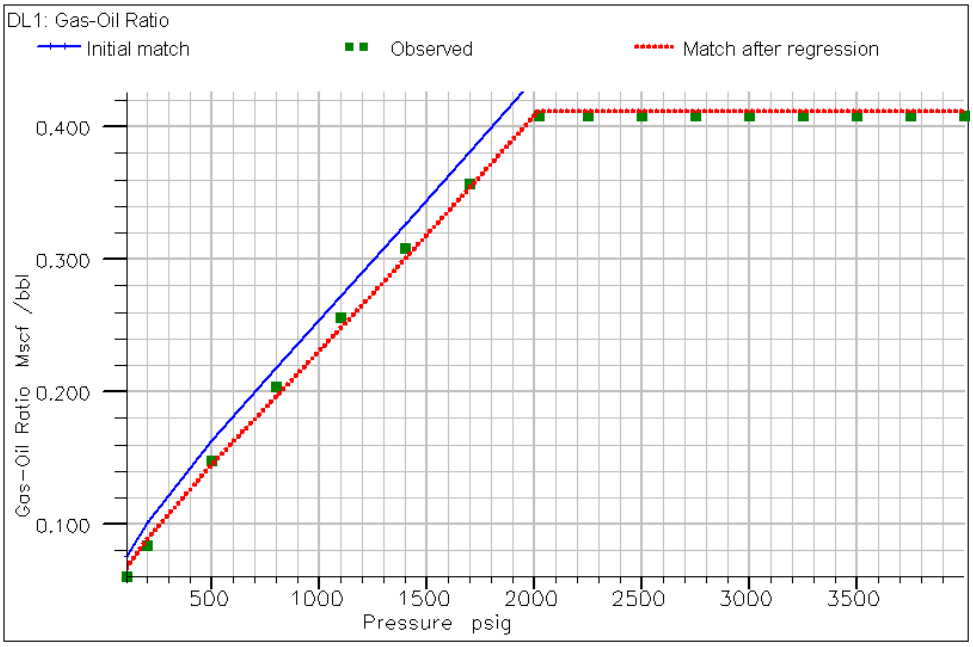


**Fig. 3.50—GOR (DL) match before and after regression.**

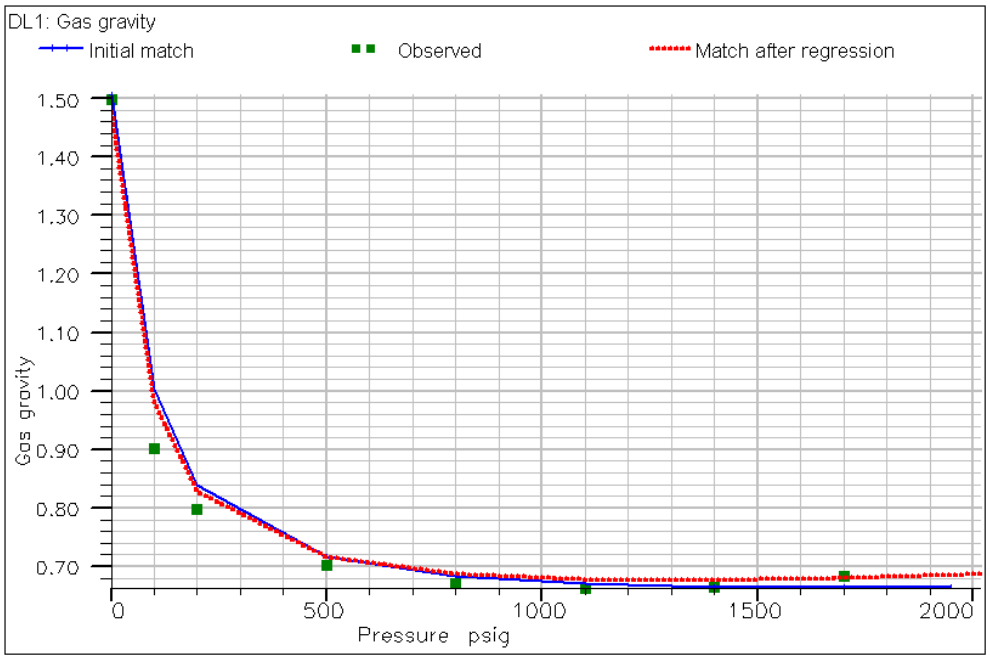


**Fig. 3.51—Gas gravity (DL) match before and after regression.**

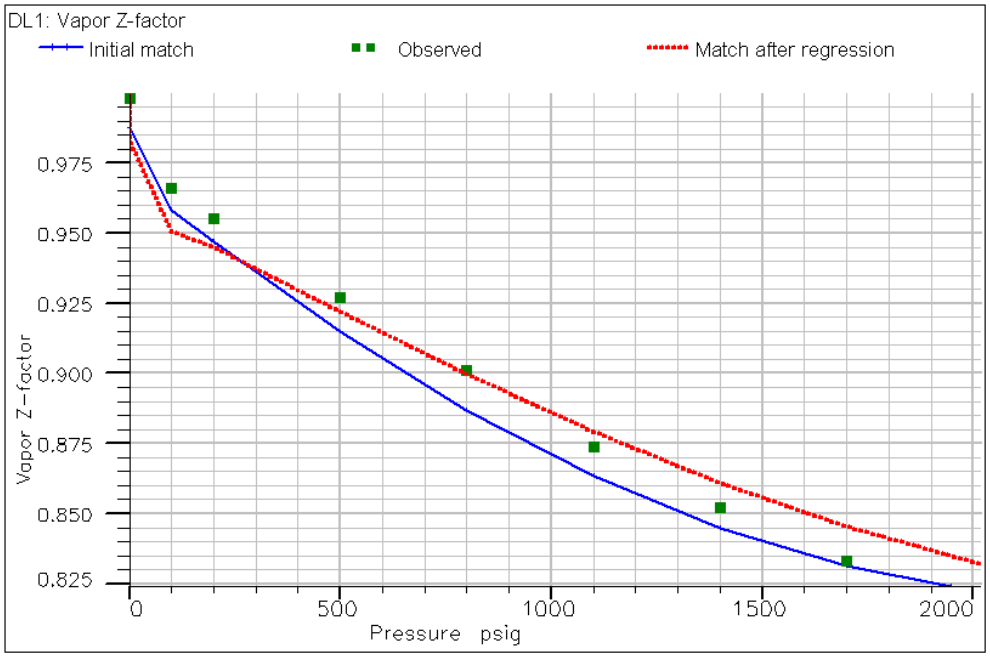


**Fig. 3.52—Vapor Z-factor (DL) match before and after regression.**

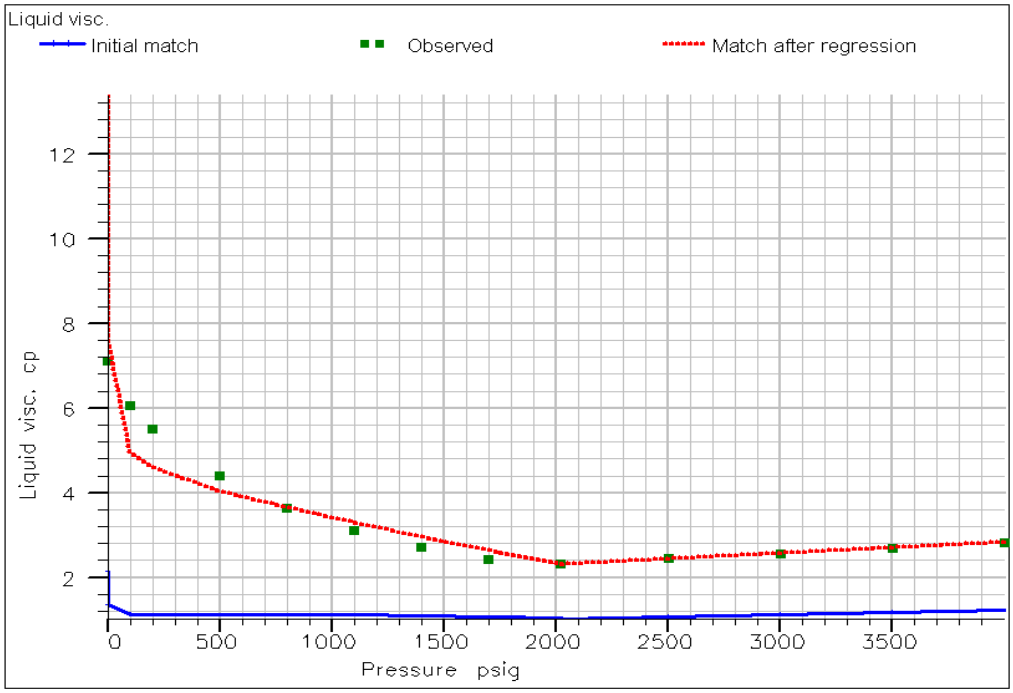


**Fig. 3.53—Oil viscosity match before and after regression.**

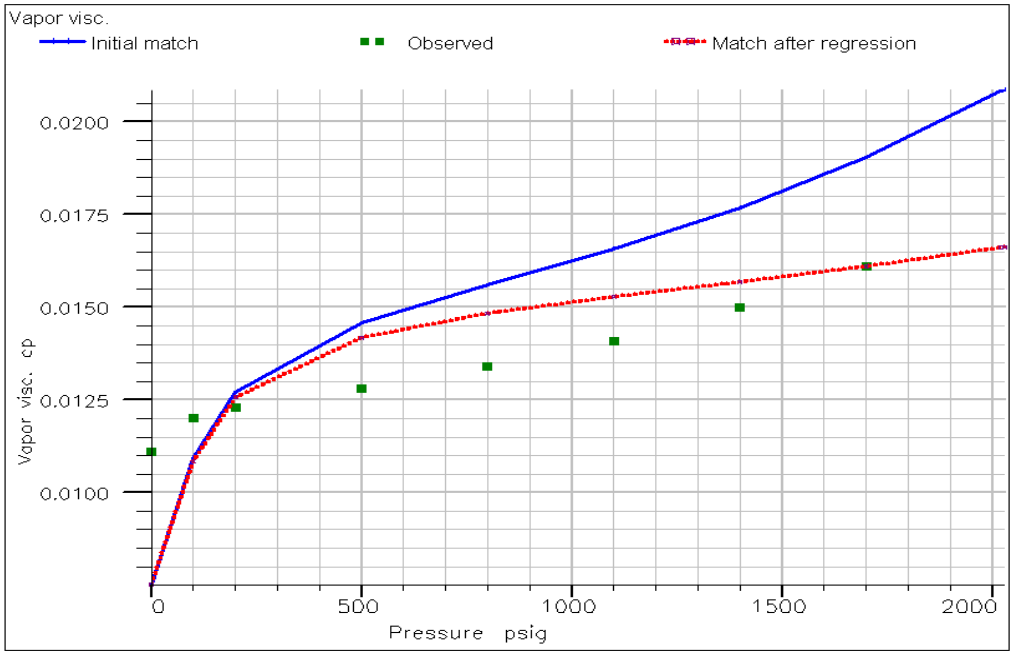


**Fig. 3.54—Gas viscosity match before and after regression.**

## 3.10 EVALUATION OF DEVELOPMENT STRATEGIES

The history-matched reservoir model was used to evaluate reservoir development and recovery strategies. Primary depletion, secondary recovery (water flooding), and tertiary recovery ($CO_2$, $N_2$, and gas flooding) were evaluated to demonstrate how the study area would have been best developed. In addition, I investigated whether it is better to produce under primary for a period of time prior to water flooding or to water flood immediately after development.

### Evaluation of Water-Flood Strategies

Water flooding is dominant among fluid injection methods. Its popularity is due to (1) the general availability of water, (2) the relatively low cost, (3) the relative ease with which water is injected and its ability to spread through an oil-bearing formation, and (4) water's efficiency in displacing oil. Especially for economically marginal oil fields, water flooding is usually the primary recovery method for maintaining reservoir pressure and improving oil recovery. Several simulation cases were run to compare primary-then-water-flood and water-flood-only strategies and to evaluate water-flood timing for existing and new development areas.

#### *Evaluation of Water-Flood Strategies for an Existing Area*

Two cases were designed and modeled to compare primary-then-water-flood and water-flood-only strategies, mimicking actual field development history (drilling and perforation activities, production and injection history data) in the study area. These two cases were designed to determine, in real field development situations for an individual

injector, if converting a producer to an injector (current strategy) is better than drilling an injector directly. These cases allowed us to compare the simulation results with historical production data and, thus, they provide insights to evaluation of water-flood strategies for existing areas.

Case 1

All wells follow production history to December 1994, and then producers are constrained with constant oil rates and converted injectors are constrained with real injection rates. The bottom-hole pressure constraints (secondary constraints) for producers and injectors are 650 psia and 7000 psia, respectively. This essentially is a primary-then-water-flood strategy.

Case 2

All wells follow production history to December 1994. For each injector there was a production period before it was converted to an injector. Instead of predicting the production period for that well, Case 2 will predict this period as injection period, using an estimated constant injection rate constraint, and then predict the injector with the actual injection rate constraint for the injection period. The bottomhole pressure constraints are same as Case 1. Case 2 also predicts all producers using constant oil rate constraint. This essentially is a water-flood-only strategy.

**Fig. 3.55** shows the oil production rates and cumulative oil production for historical data and Cases 1 and 2. Case 2 (water flooding at beginning) gives slightly less oil production than Case 1 in the early time of water flooding, but in the late time of

water flooding (after 5 years), Case 2 provides much higher oil rates than Case 1 and the historical observed rates. The recovery factors of Cases 1 and 2 are 2.7% and 3.5%, respectively, after 25 years. These simulation results indicate water-flood only strategy provides more oil recovery than primary-then-water-flood strategy over the life of the field.

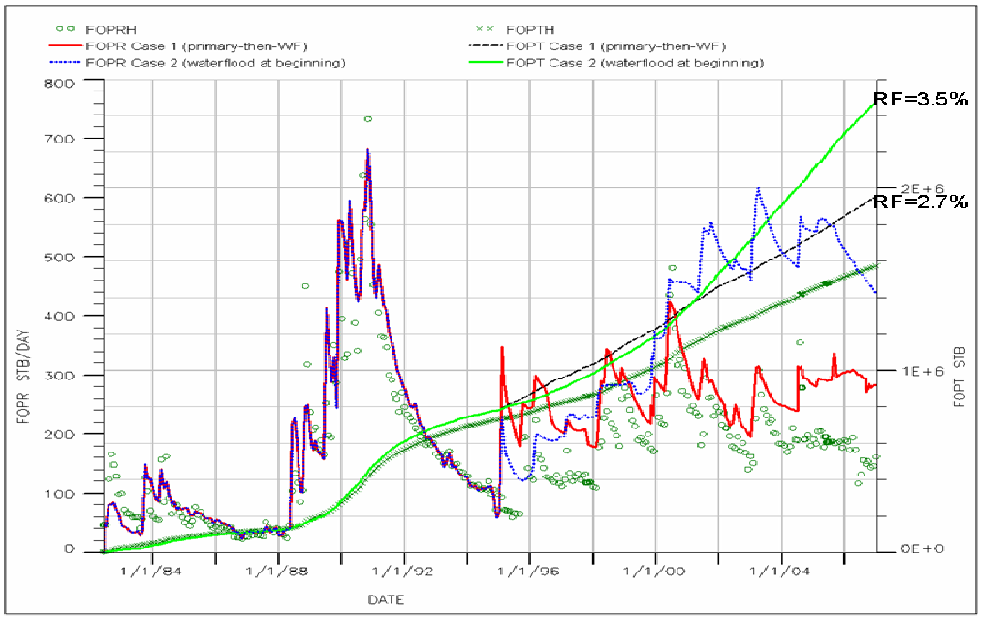


**Fig. 3.55—Oil production rates and cumulative oil production for historical data and Cases 1 and 2.**

To assess the economic implication of the two cases, I considered the time value of production, because Case 1 has higher oil production in the early time period. Instead of calculating net present value (NPV), I determined net present production (NPP), which is the production discounted to time zero (**Eq. 3.16**),

$$NPP = \sum_{j=1}^{j=n} (Q_t)/(1+i)^j \qquad \text{..... (3.16)}$$

where $Q_t$ is the total production in year j and i is the discount rate, which is 8% in this study.

The discounted oil production values at the end of simulation were 0.7 and 0.79 MMSTB for Cases 1 and 2, respectively. Case 2 still yields a higher recovery factor than Case 1 even when discounted. Case 1 produces much more gas than Case 2 (**Fig. 3.56**), resulting in low oil recovery. These results also support that water flooding should be started as early as possible.

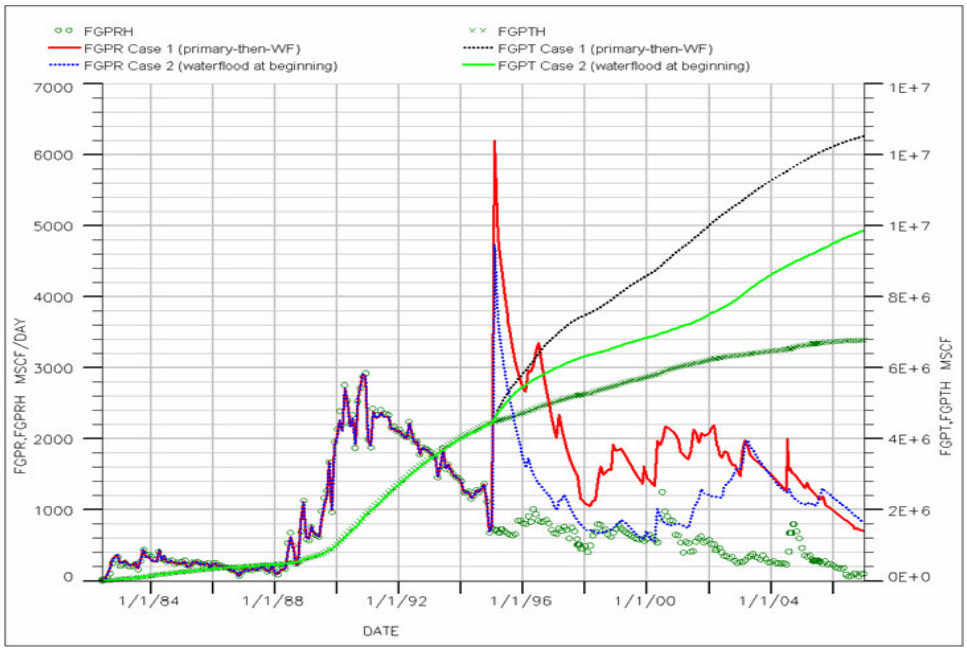


**Fig. 3.56—Gas production rates and cumulative gas production for historical data and Cases 1 and 2.**

*Evaluation of Water-Flood Strategies for New Development Areas*

Instead of mimicking actual field development and production history, in this section I assume I are at the beginning of development of a new area. I investigated whether it is better to initially produce oil for a period of time prior to water flooding, or to water flood immediately upon development. The predictions are based on the study

area (using the same 40-ac, 5-spot pattern) but start from time zero, so they could be used to guide development of new areas in the field.

Different cases were designed as follows:

Case 3 - primary depletion using the current 40-ac, 5-spot pattern well locations;

Case 4 - water flooding at beginning of the simulation using the current 40-ac, 5-spot pattern; and

Case 5 – first, primary depletion as Case 1, then after 2 years starting water flooding.

A 2-year period of primary depletion was selected in Case 5 based on the actual field history. According to the field operator, the average period for converting a producer to an injector is 2 to 2.5 years. In the study area, the average duration is 33 months. **Fig. 3.57** shows typical actual GOR profiles during this period (from the first day as a producer to the first day as an injector) for wells W1499, W1973, and W2102, as well as GOR for the whole study area. The GOR profile (Fig. 3.57) of the primary depletion period of Case 5 is close to those actual GOR profiles of the individual wells in the field. Thus, Case 5 with a 24-month primary depletion is consistent with the field operator's operation policy and can be used to evaluate the primary-then-water-flood strategy.

The general guidelines and physical constraints imposed on the prediction cases are:

(1) minimum flowing bottom-hole pressure is 650 psia;

(2) maximum oil rate constraint for each well is based on actual maximum oil rate for that well;

(3) maximum injection rate constraint for each well is based on the actual average injection rate for that well;

(4) maximum injection bottom-hole pressure is 7000 psia; and

(5) prediction time is from 06/01/1982 to 02/01/2008.

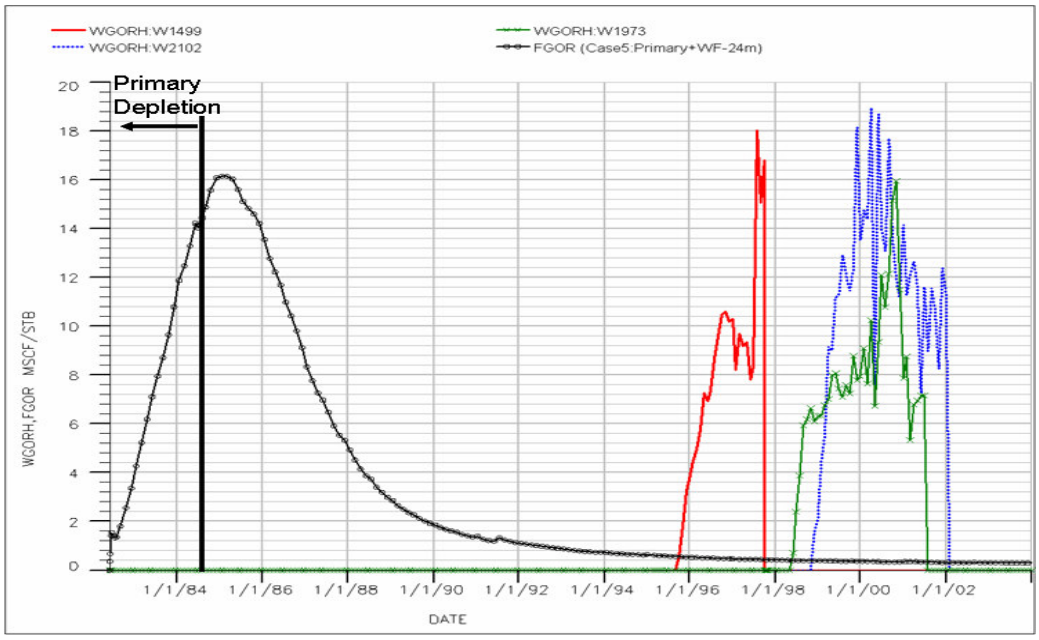


**Fig. 3.57—Typical GOR profiles from the first day as a producer to the first day as an injector for wells W1499, W1973, and W2102, and GOR for the whole study area.**

**Fig. 3.58** shows the study area oil production rates and cumulative oil production of Cases 3 through 5. Primary depletion (Case 3) produces very high initial oil production rates, but it results in very low production rates (less than 100 bbl/day) for the study area after 5 years (January 1988). After 10 years (January 1992), the study area is not economically producible (< 50 bbl/day) for Case 3. Primary depletion only yields 2.0% oil recovery at the end of prediction (Feb. 2008). Case 4 (water flooding at beginning) gives medium oil production rates in early time, but the rate decline is slow. Even at the end of simulation, the oil production rate is approximately 400 bbl/day.

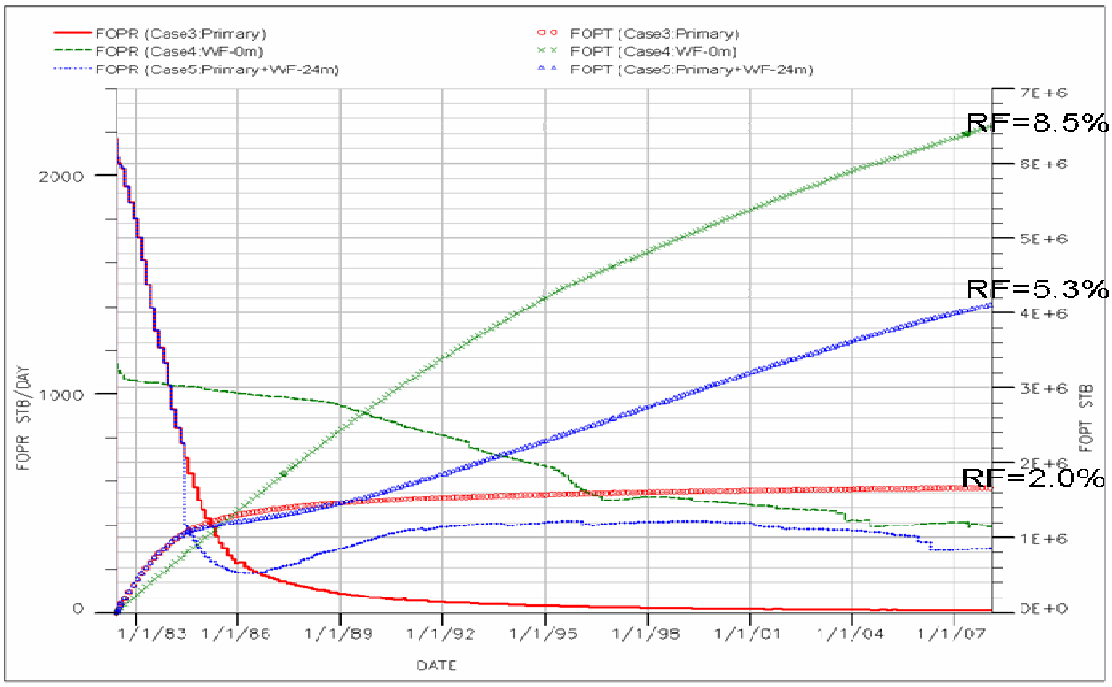


**Fig. 3.58—Study area oil production rates and cumulative oil production of Cases 3 to 5.**

The overall recovery of Case 4 at the end of simulation is 8.5%. Case 5 yields 5.3% oil recovery at the end of simulation. There is a big difference in oil recoveries between Case 4 and Case 5, although the water flood for Case 5 is only delayed 2 years. One possible reason is that Case 5 produces more gas than Case 4 in the first 2 years (primary depletion), (**Fig. 3.59**), resulting in an increase in oil viscosity due to large loss of solution gas from the oil. From the PVT data, I know that oil viscosity in Monument Butte field is relatively high (7.1 cp at surface conditions). High content of solution gas in the oil can greatly decrease oil viscosity (Fig. 3.53). Because reservoir pressure has been maintained above the bubble point pressure for Case 4 (**Fig. 3.60**), the oil is still gas-saturated, resulting in greater oil mobility. For Case 5, even when water is injected after 2 years and the reservoir is re-pressured above the bubble point pressure, oil

production cannot be increased significantly because of high oil viscosity and unfavorable oil-water mobility ratio.

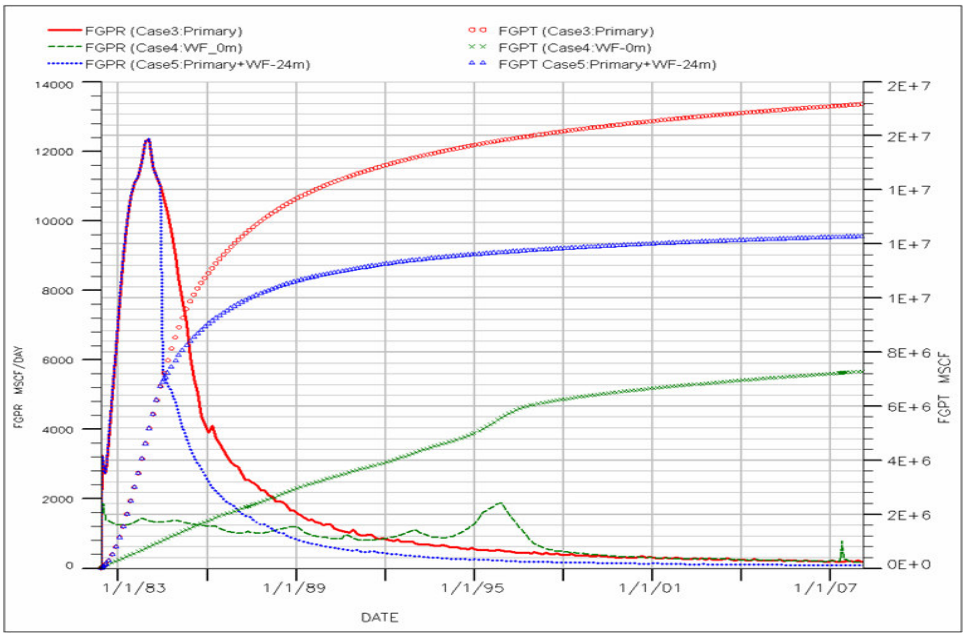


**Fig. 3.59—Study area gas production and cumulative gas production for Cases 3 to 5.**

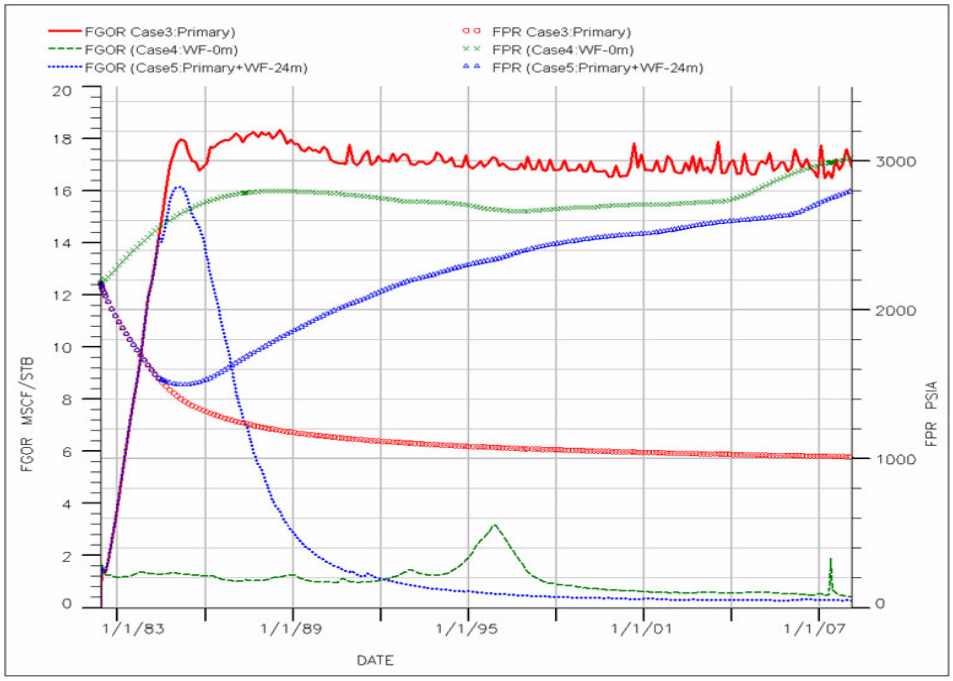


**Fig. 3.60—Study area reservoir pressure and GOR profiles for Cases 3 to 5.**

To verify the above conclusions, average oil viscosity and bubble point pressure in the study area were calculated for Cases 4 and 5 (**Figs. 3.61 and 3.62**). As expected, the average oil viscosities for Case 5 are higher than those of Case 4. The period of big increase of average oil viscosities for Case 5 corresponds to the period of very high GORs (Fig. 3.61). The average bubble point pressure for Case 5 is lower than that of Case 4, resulting in higher oil viscosities (Fig. 3.62). The increase in oil viscosities also leads to earlier water breakthrough (**Fig. 3.63**). Case 5 has a sharp increase in water cut immediately after water flooding starts, whereas the water cut of Case 4 increases slower.

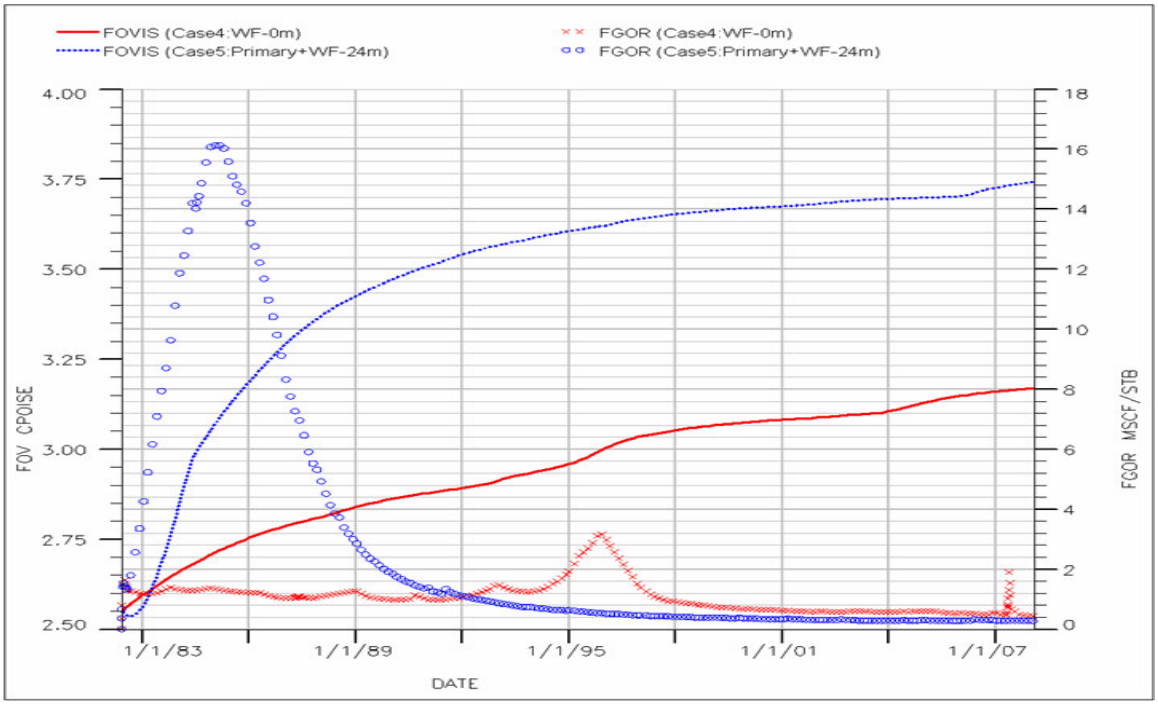


**Fig. 3.61—Study area average oil viscosity and GOR profiles for Cases 4 and 5.**

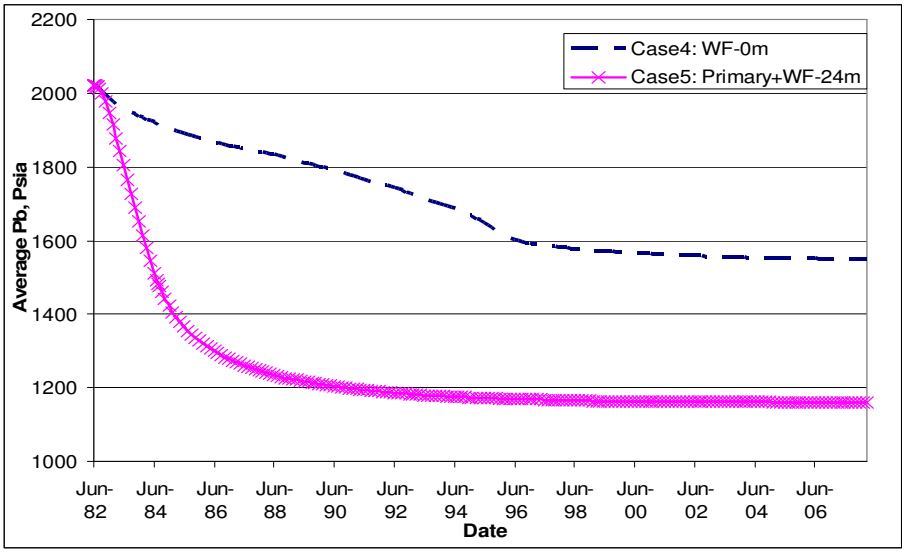


**Fig. 3.62—Study area average bubble point pressure profiles for Cases 4 and 5.**

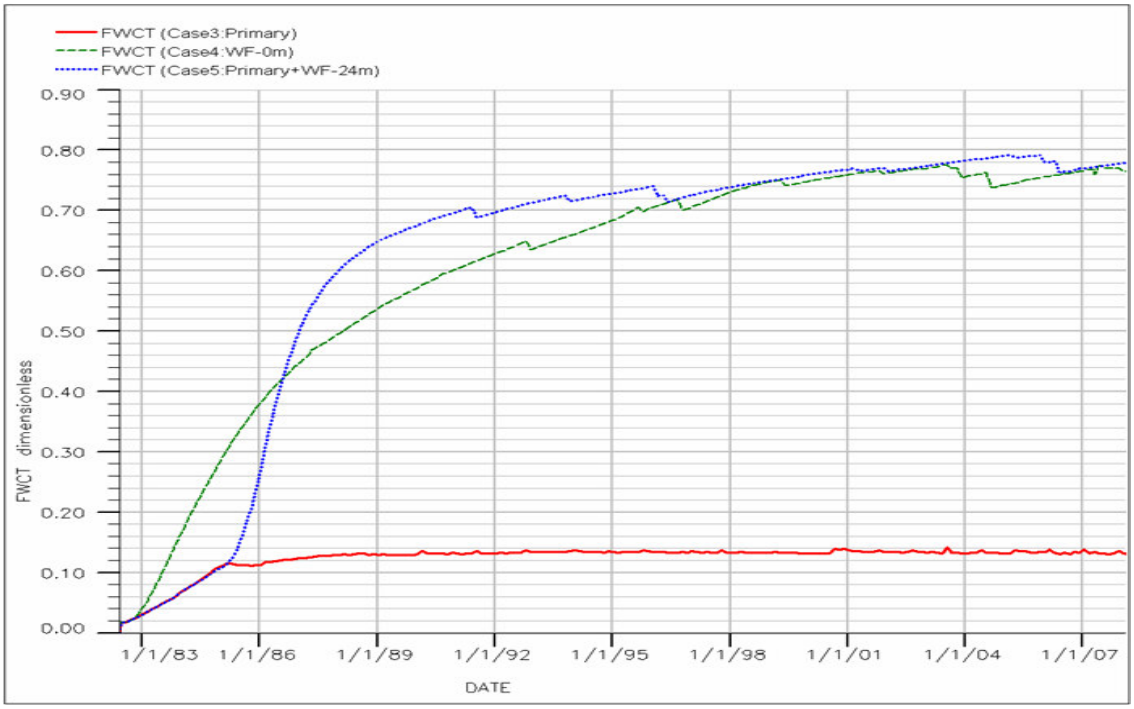


**Fig. 3.63—Study area water cut profiles for Case 3 to 5.**

To find the best timing for water flooding, I designed additional simulation Cases 6 – 11, as described below:

Case 6 - first primary depletion as Case 1, then after 3 months starting water flooding;

Case 7 - first primary depletion as Case 1, then after 6 months starting water flooding;

Case 8 - first primary depletion as Case 1, then after 12 months starting water flooding;

Case 9 - first primary depletion as Case 1, then after 43 months (1/1/1986) starting water flooding;

Case 10 - first primary depletion as Case 1, then after 96 months (6/1/1990) starting water flooding; and

Case 11 - first primary depletion as Case 1, then after 156 months (6/1/1995) starting water flooding.

Seventeen injectors were converted from 17 producers when water flooding started for Cases 5 to 11. **Figs. 3.64** and **3.65** show the oil production rates and cumulative oil production, respectively, for Cases 4 to 11. **Fig. 3.66** shows oil recoveries for Cases 4 to 11 at the end of simulation. Cases 4, 6, and 7 give medium field oil rates at the beginning, but the decline rate decreases with time. For Cases 4, 6, and 7 (starting water flooding within 6 months), there is only a small difference in oil recovery (Figs. 3.64, 3.65, and 3.66), but there is a significant difference (about 1 MMbbls) in oil recovery between Cases 7 and 8 (starting water flooding after 12 months). The oil production rates and cumulative oil production for Case 8 are quite low compared with Case 7. These results indicate water flooding should be started no later than 6 months

after first production to maximize oil recovery. Water cut profiles for Cases 4 to 11 also indicate that water flooding should start as early as possible **(Fig. 3.67)**.

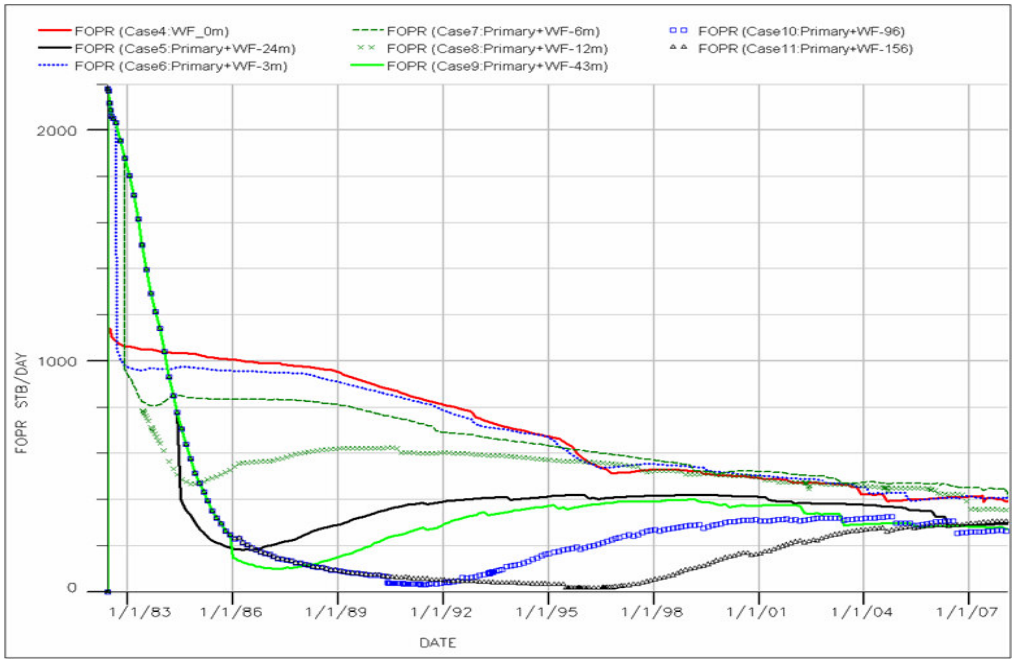


**Fig. 3.64—Oil production rates for Cases 4 to 11.**

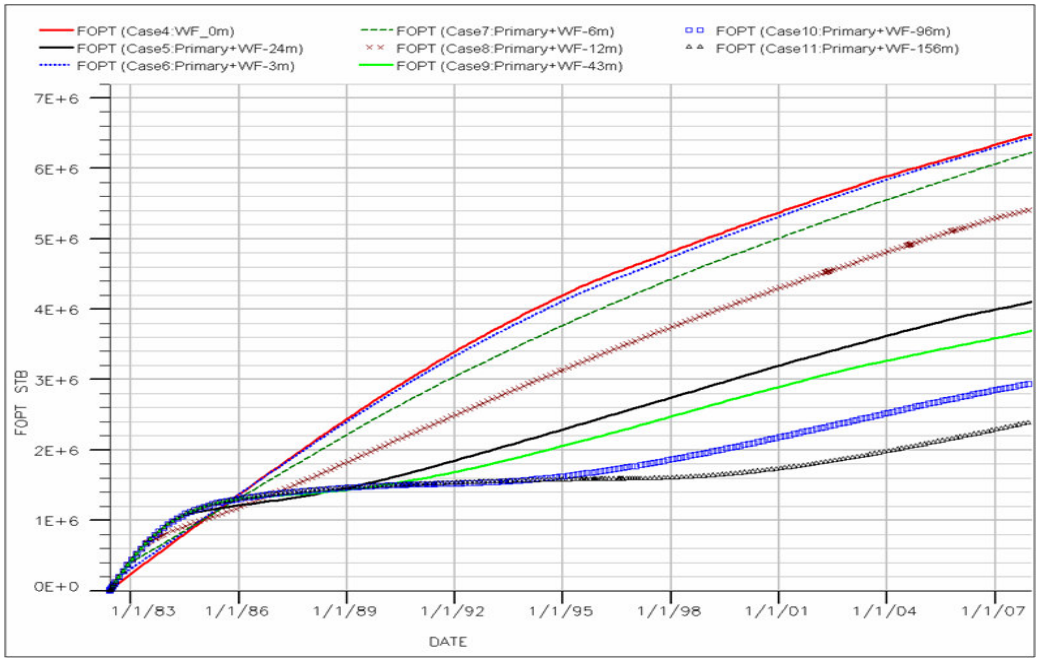


**Fig. 3.65—Cumulative oil production profiles for Cases 4 to 11.**

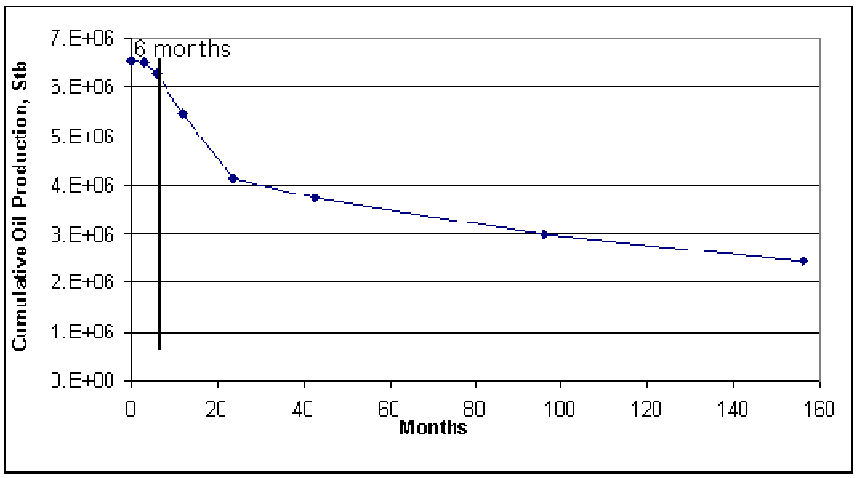


**Fig. 3.66—Oil recoveries for Cases 4 to 11 at end of simulation. X axis is the duration before water flooding started.**

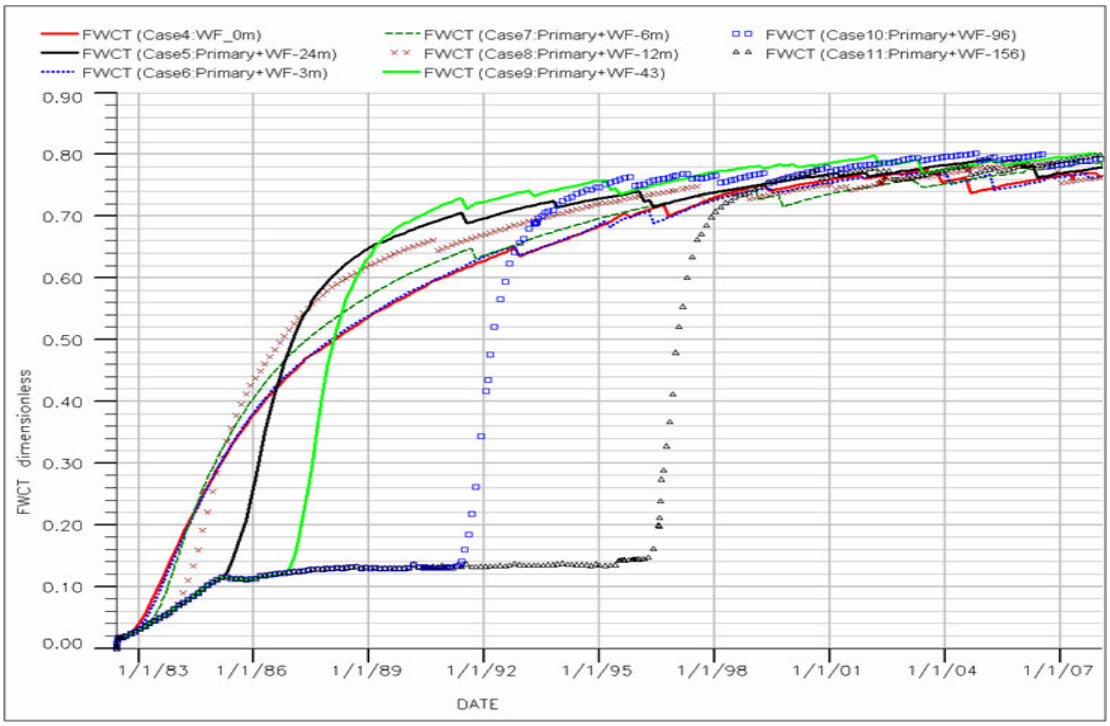


**Fig. 3.67 Water cut profiles for Cases 4 to 11.**

Although Case 4, water flood only, has the highest cumulative oil production at the end of simulation (Fig. 3.65), the choice between a water-flood-only strategy vs. a primary-then-water-flood strategy should be based on economics. **Fig. 3.68** shows the

discounted oil production at the end of simulation (2/01/2008) for Cases 4 to 11. Cases 4 and 6 still yield the highest recoveries, even on a discounted basis. This result supports the conclusion that water flooding should be started as early as possible.

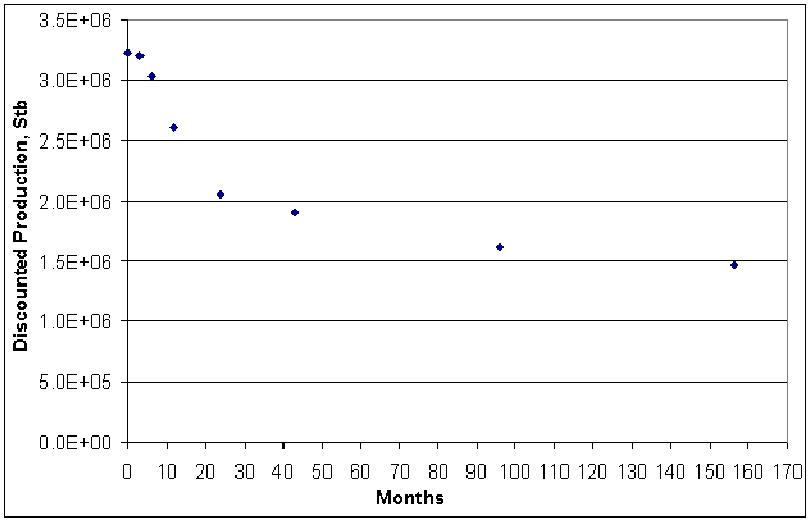


**Fig. 3.68—Discounted oil production at the end of simulation (2/1/208) for Cases 4 to 11.**

## Evaluation of Tertiary Recovery Strategies

With a combined recovery of less than 2% by primary and secondary recovery methods, the oil recovery in the greater Monument Butte area may be improved using tertiary recovery methods that feature miscible displacement. Candidate tertiary methods are water alternating with gas (WAG), $CO_2$ flooding, nitrogen injection, or methane injection. These tertiary methods, which involve miscible displacement processes, were investigated using compositional simulation.

The main advantage of miscibility is that there is no residual oil to gas displacement. Achieving miscibility means increasing displacement efficiency and, thus, recovery. For a given temperature, miscibility depends on the fluid composition

(Shtepani, 2007) and the pressure. The minimum pressure to achieve miscibility is called the minimum miscibility pressure (MMP). Successful design and implementation of a miscible gas injection project depends upon the minimum miscibility pressure (MMP), as well as other reservoir and fluid characteristics (Farzad and Amani, 2007). To estimate the MMP, laboratory experiments, such as slim-tube experiments, need to be conducted. Since I did not have MMP experimental data available for Monument Butte reservoir fluid, I conducted different reservoir simulation runs, starting injection at different reservoir pressures to estimate MMP. Five cases were designed as follows to evaluate different recovery strategies using compositional simulation:

Case 12 (base case) - water flooding from beginning (6/1/1982) using the current 40-ac, 5-spot pattern;

Case 13 - water flooding from beginning, then starting nitrogen ($N_2$) injection on 1/1/2008;

Case 14 - water flooding from beginning, then starting methane ($C_1$) injection on 1/1/2008;

Case 15 - water flooding from beginning, then starting $CO_2$ flooding on 1/1/2008;

Case 16 - water flooding from beginning, then starting water-alternating-$CO_2$ (WAG-$CO_2$) flooding on 1/1/2008.

Formation damage caused by $CO_2$ flooding (e.g., asphaltene precipitation) was not considered for Cases 15 and 16 because we lacked relevant experimental data. Because I did not know at which reservoir pressure I should start injecting gases, I designed two scenarios to find a suitable reservoir pressure for starting injection. In

scenario 1, I used a reservoir pressure of 1710 psia to start injection. I believe that this pressure is lower than the MMP. To achieve a reservoir pressure of 1710 psia, lower water injection rates (40% of average actual injection rate for each injector) were simulated. Gas injection rates for all cases were the same. **Fig. 3.69** shows oil production rate profiles for Cases 12 to 15 for scenario 1. Injecting nitrogen (Case 13) and methane (Case 14) will provide only minor increases in oil production in the early period (2 years), and then oil production rates decrease faster than the base case (Case 12). Injecting $CO_2$ (Case 15) does not increase oil production, and the oil production rates also decrease faster than with the base case. These simulation results indicate that the miscibility of gases with oil can not be achieved with a low reservoir pressure. Gas-oil immiscible displacement suffers an obvious drawback of its very high mobility when there is not gas-oil miscibility present (Righi, 2004).

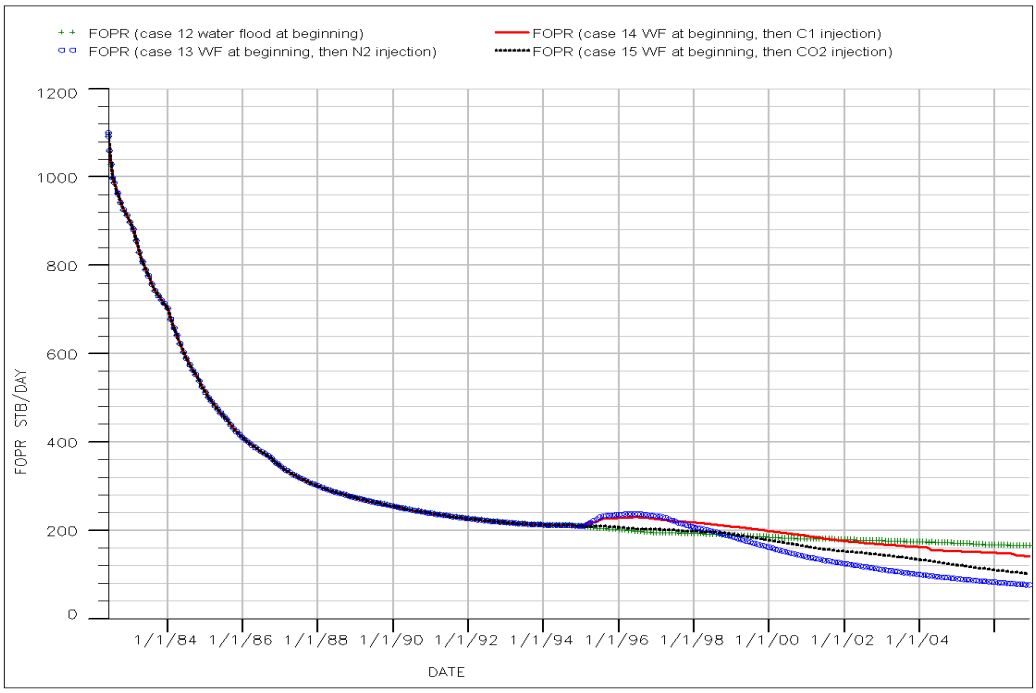


**Fig. 3.69—Oil rate profiles for Cases 12 to 15 in the first scenario.**

In scenario 2, tertiary injection was begun at a reservoir pressure of 3100 psia for all the cases. To achieve the reservoir pressures of 3100 psia, high water injection rates (120% of average actual injection rate for each injector) were used. Each simulation run was from June 1982 to June 2026. **Figs. 3.70** and **3.71** show oil rate and cumulative oil production profiles for Cases 12 to 16, respectively. Injecting nitrogen (Case 13) and methane (Case 14) provided only small increases in oil production in the first two years. After two years of injection, oil production rates were much lower than the base case (Case 12) (Fig. 3.71). If miscible displacement was achieved, oil production rates for Cases 13 and 14 would increase significantly. These results indicate that the miscibility of nitrogen and methane with oil is not achieved with a reservoir pressure of 3100 psia.

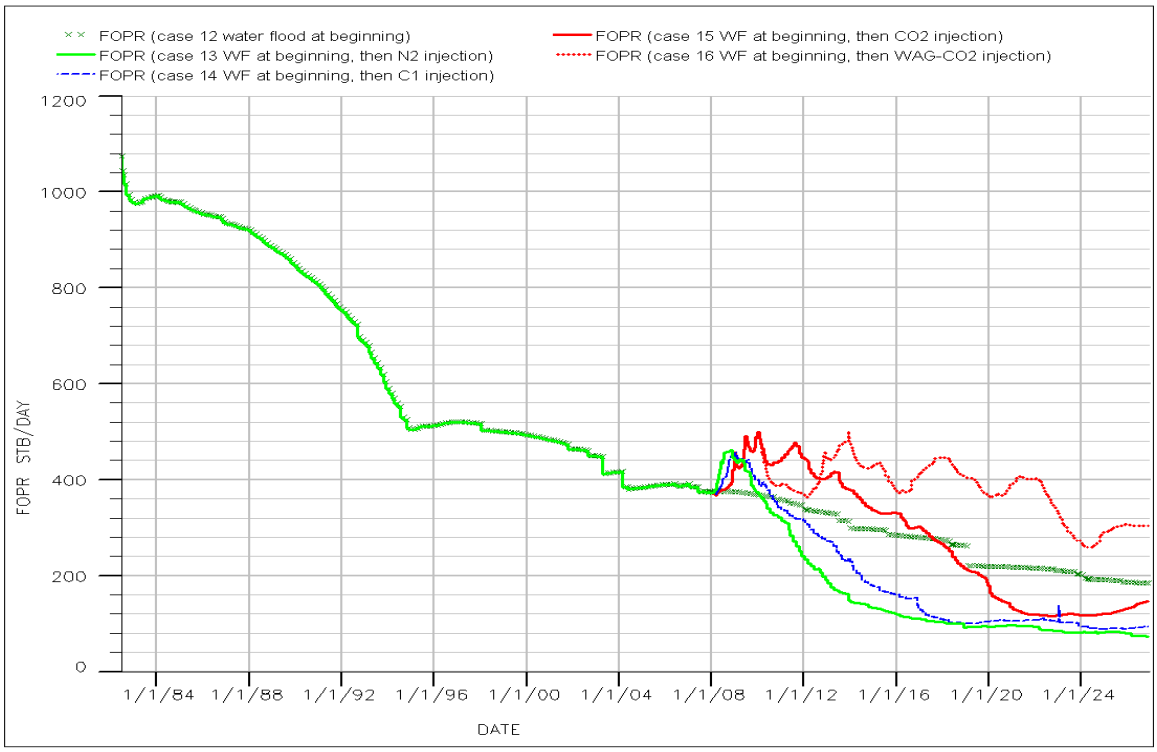


**Fig. 3.70—Oil rate profiles for Cases 12 to 16 in the second scenario.**

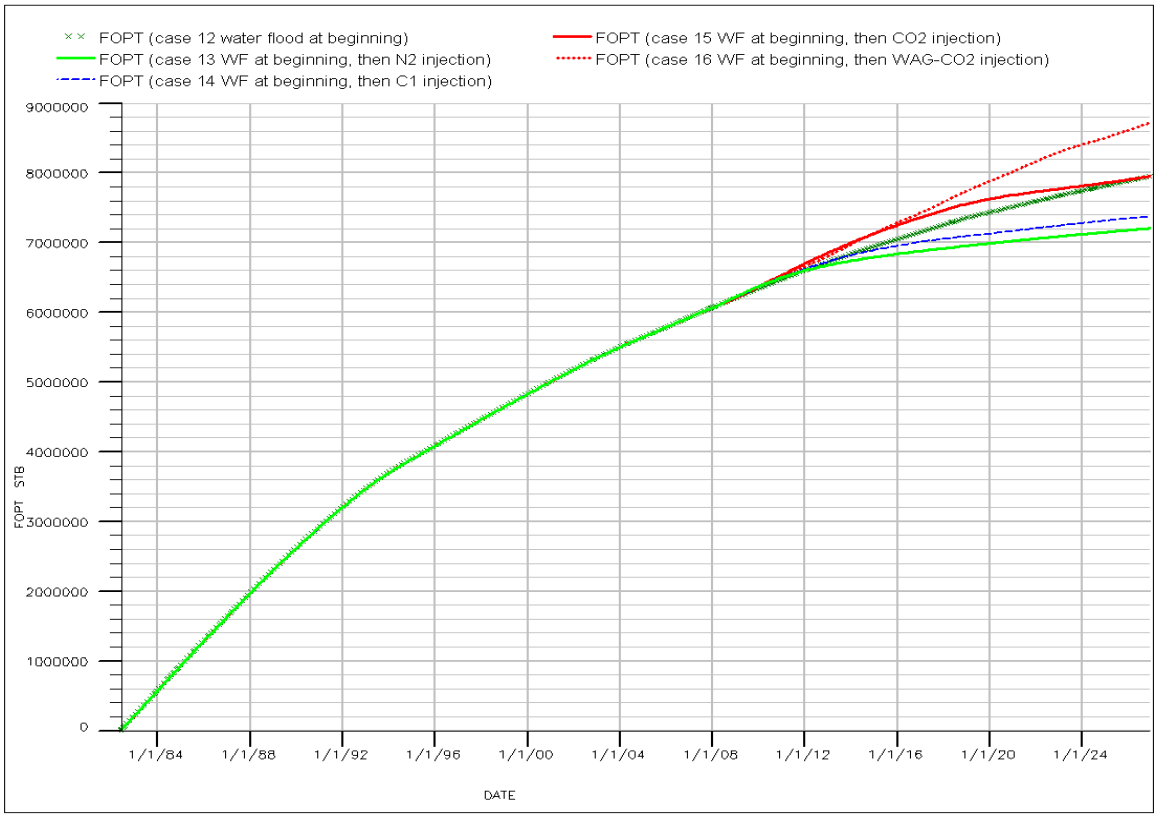


**Fig. 3.71—Cumulative oil production profiles for Cases 12 to 16 in the second scenario.**

Injecting $CO_2$ (Case 15), on the other hand, yielded very high oil production rates and cumulative oil production for a longer period (about 5 years) than did nitrogen and methane (2 years), followed by sharply decreasing oil production rates. These results indicate that miscibility or partial miscibility of $CO_2$ with oil can be achieved with a reservoir pressure of 3100 psia. GOR profiles for Cases 13 to 15 (**Fig. 3.72**) also indicate that for immiscible displacement (Cases 13 and 14) there is early gas breakthrough, whereas for miscible displacement (Case 15), $CO_2$ breakthrough is delayed and the breakthrough time is later than in Cases 13 and 14. Also, I noted that, although miscibility or partial miscibility of $CO_2$ with oil is achieved for Case 15, of oil production decreased sharply (Figs. 3.70 and 3.71) and $CO_2$ breakthrough (Fig. 3.72)

occurred after 5 years of $CO_2$ injection. One possible explanation is that, after $CO_2$ injection, reservoir pressure went below the MMP, causing lower miscibility (**Fig. 3.73**). Another possible explanation is that a higher concentration of $CO_2$ may result in unstable displacement and early breakthrough (Gharbi, 2003). One interesting result is that oil production rates increased after January 2023 for Case 15 (Fig. 3.70), coincident with an increase in reservoir pressure after it had reached its nadir (2490 psia) (Fig. 3.73). This may indicate that the estimated MMP is approximately 2490 psia for $CO_2$ flooding, whereas MMPs for $N_2$ and $C_1$ flooding are much higher than that for $CO_2$ flooding. Thus, $CO_2$ injection was found to be more effective than $N_2$ or $C_1$ flooding under the simulated conditions.

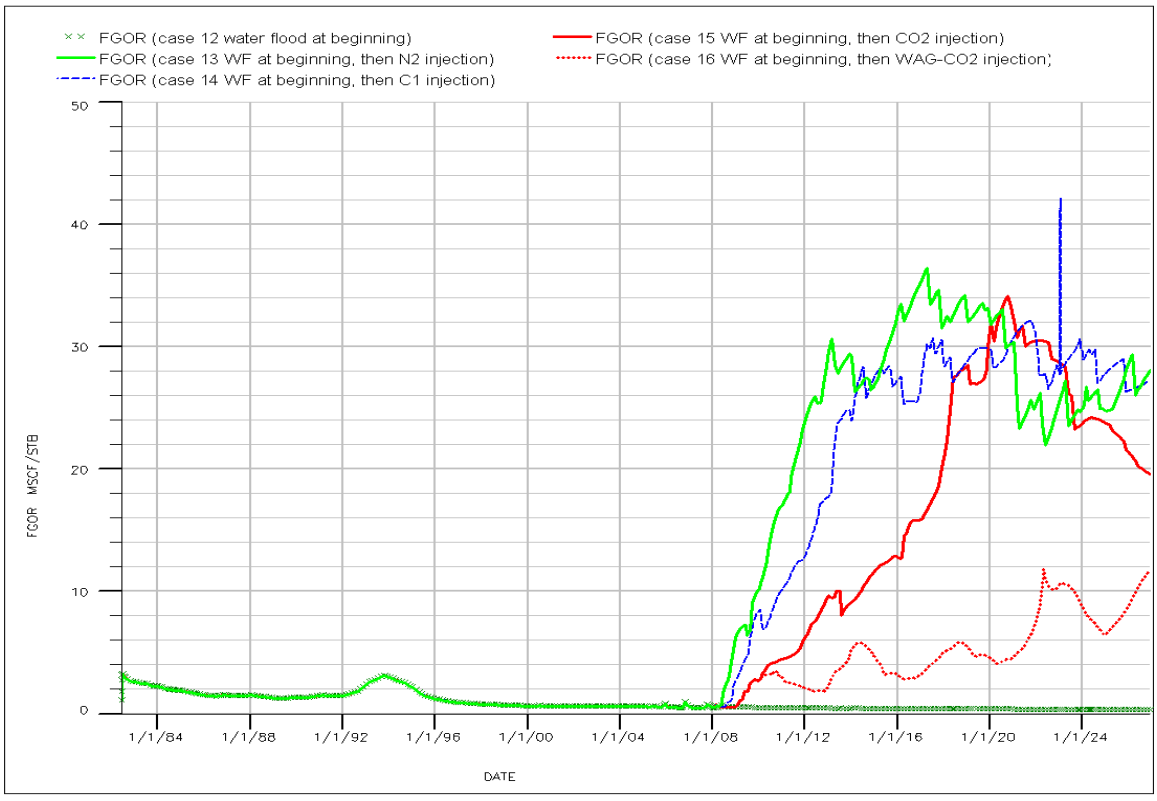


**Fig. 3.72—GOR profiles for Cases 13 to 15 in the second scenario.**

Water-alternating-$CO_2$ injection is commonly used to control early breakthrough of $CO_2$ and unfavorable gas-oil mobility ratio and to maintain reservoir pressure. Case 16 was designed with a WAG half cycle of 2 years (2 years of $CO_2$ injection followed by 2 years of water injection). Simulation results show that WAG-$CO_2$ can maintain very high oil production rates for a longer period than $CO_2$ injection (Figs. 3.70 and 3.71). GORs also are kept at very low values, and gas breakthrough is greatly delayed (Fig. 3.72). Injection of water also maintained the reservoir pressure at approximately 3100 psia fro a long period (Fig. 3.73).

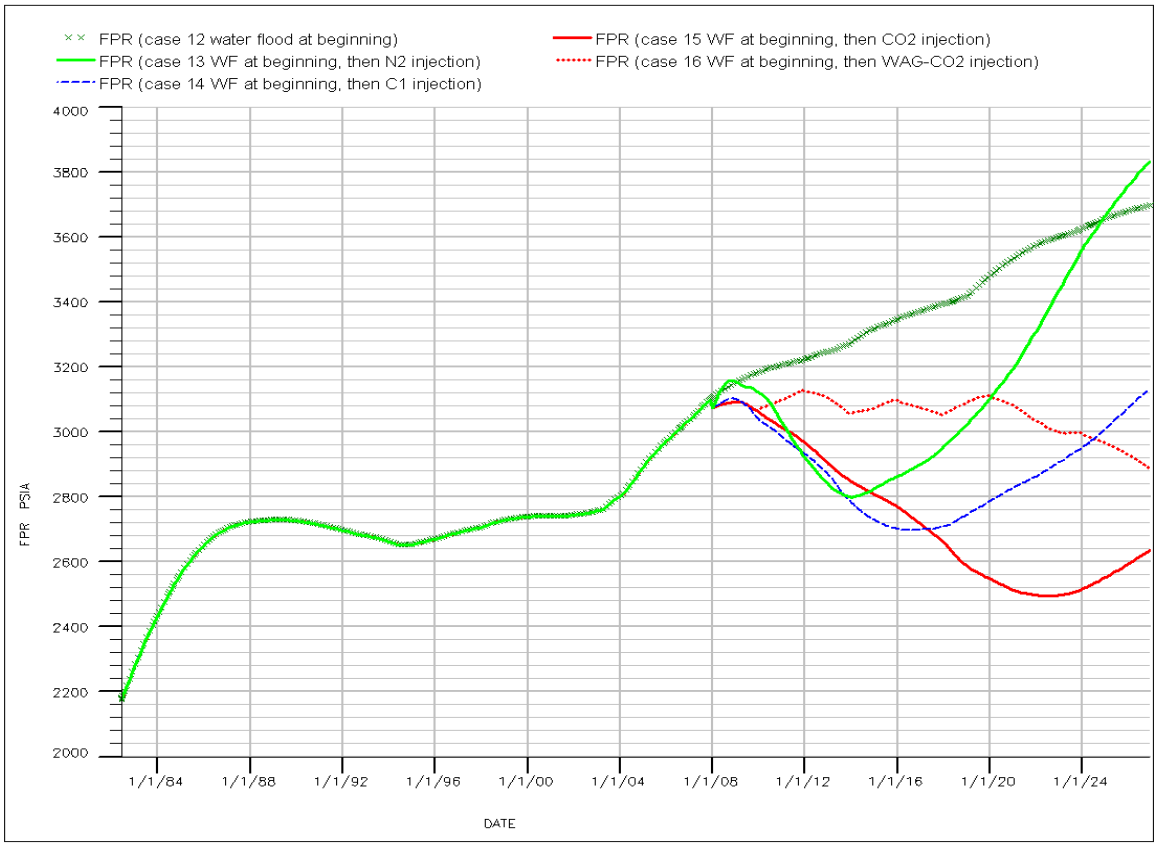


**Fig. 3.73—Reservoir pressure profiles for Cases 12 to 16 in the second scenario.**

**Study Area Future Development**

After I assessed history match results, optimization of water injection strategies, and optimization of tertiary recovery strategies, I designed several prediction cases to guide the future development of the study area. The prediction period was from 1/1/2007 to 12/31/2026.

Case 17 (base case): the base case is constrained by continuing current field operations.

Case 18: $CO_2$ is injected from the beginning of prediction.

Case 19: water-alternating-$CO_2$ is used with a half cycle of 2 years (2 years of $CO_2$ injection followed by 2 years of water injection).

Cumulative oil production profiles for Cases 17 – 19 show that WAG-$CO_2$ gives the highest oil production, with an oil recovery factor of 7.8% (**Fig. 3.74**). $CO_2$ flooding yields 5.7% oil recovery, and the base case has only 4.0% oil recovery.

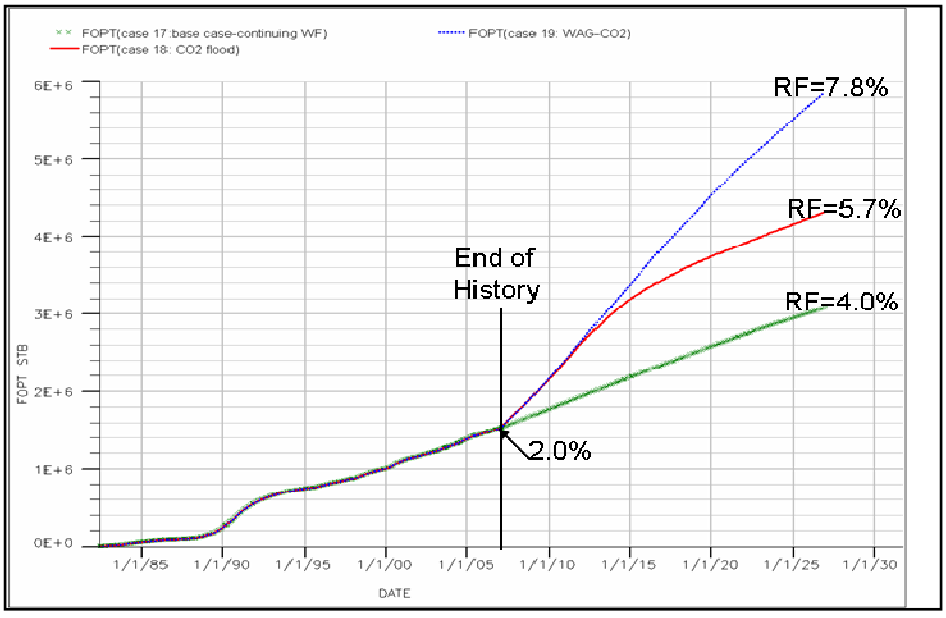


**Fig. 3.74—Cumulative oil production profiles for Cases 17 to 19.**

**Interwell Connectivity vs. Infill Potential**

Since a large volume of oil remains in the reservoir after water flooding, infill drilling may be an effective way to produce this unswept oil. To assess infill potential and the relationship between interwell connectivity and well spacing, two cases were designed:

Case 20: this case was designed to have a 20-ac well spacing. There are 40 producers and 41 injectors, giving a total of 81 wells in the study area.

Case 21: this case was designed to have a 40-ac well spacing. There are 18 producers and 18 injectors, or a total of 36 wells in the study area.

Since I did not know the perforations for the new wells for Case 20 (20-ac well spacing), I perforated all the sand zones for both Cases 20 and 21. This assumption allowed us to compare the two cases directly. Both cases employed a 5-spot well pattern and the same production and injection constraints. The prediction was run from 6/1/1982 to 2/1/2008. Liquid production rate was used to evaluate the relationship between interwell connectivity and well spacing. **Fig. 3.75** shows the study area liquid production rates and liquid production rates per well. The study area liquid production rate for Case 20 is more than twice that of Case 21. The average liquid production rate per well for Case 20 is higher than that of Case 21 in the first 16 years of production, and then two cases have similar average liquid production rates per well. These results indicate that decreasing well spacing will increase both field-wide (study area) and individual well liquid production. If interwell connectivity is not improved, decreasing well spacing to 20 ac/well would not necessarily double field liquid production and also increase

individual well liquid production. Thus, I believe that interwell connectivity is improved by decreasing well spacing based on the 20-acre well spacing model.

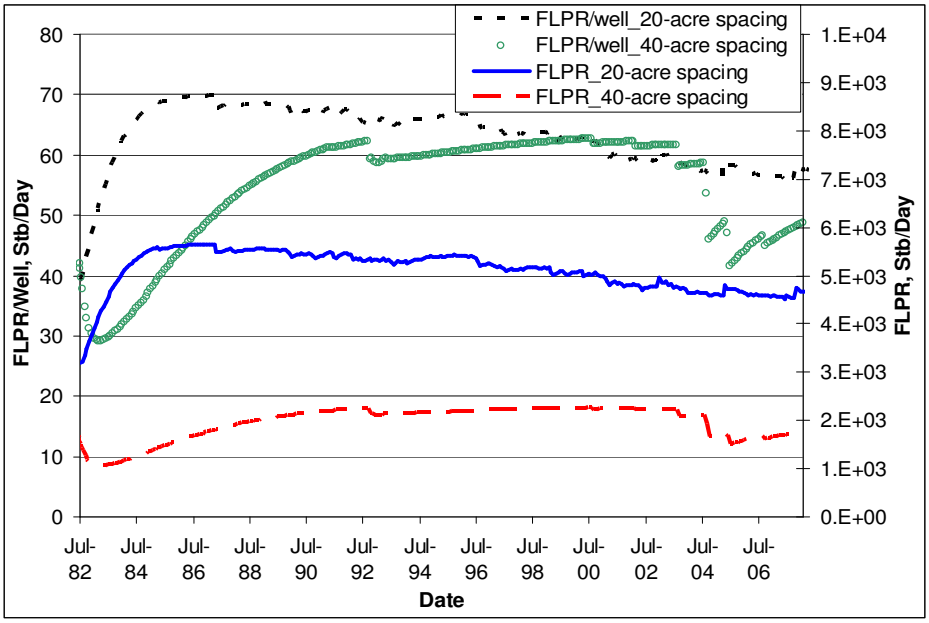


**Fig. 3.75—Study area liquid production and liquid production per well.**

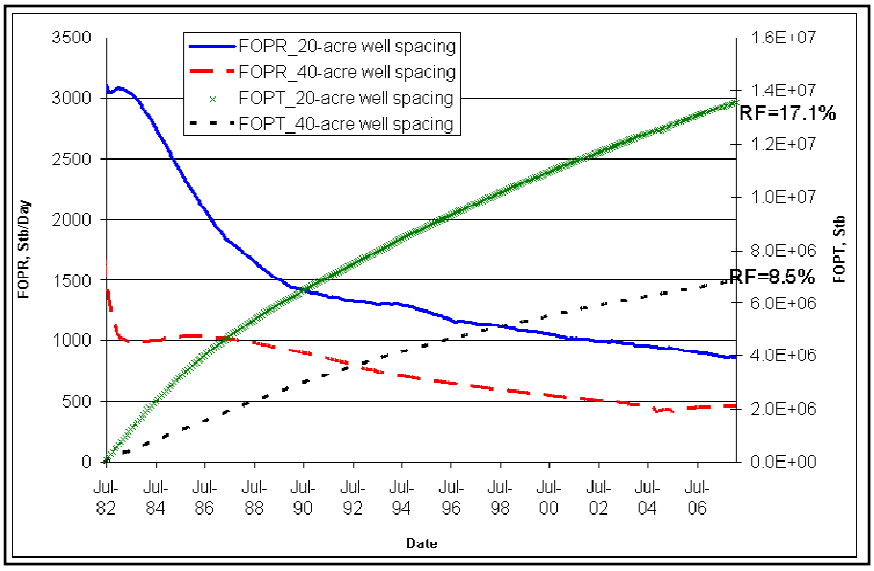


**Fig. 3.76—Study area oil rates and cumulative oil production for Cases 20 and 21.**

Infill drilling potential was evaluated using oil production. **Fig. 3.76** shows study area oil rates and cumulative oil production for Cases 20 and 21. Study area oil production for Case 20 is much higher than that of Case 21. At the end of simulation, Case 20 will recover 17% of OOIP (77.8 MMbbls), whereas Case 21 will produce only 8.5% of OOIP. Oil saturation distribution was mapped (**Fig. 3.77**) to compare Case 20 with Case 21 for the main producing D1 and C sands. At the end of simulation, Case 20 (20-ac well spacing) has much less oil remaining in the reservoir than does Case 21 (40-ac well spacing) for both D1 sand (zone 7) and C sand (zone 11). These results indicate that infill drilling may be an effective way to increase oil recovery in the Monument Butte field. However, if interwell connectivity remains low when well spacing is decreased, oil production will not necessarily increase significantly because interwell connectivity (based on the calibrated 40-acre well spacing model) has a significant impact on the performance of water flooding.

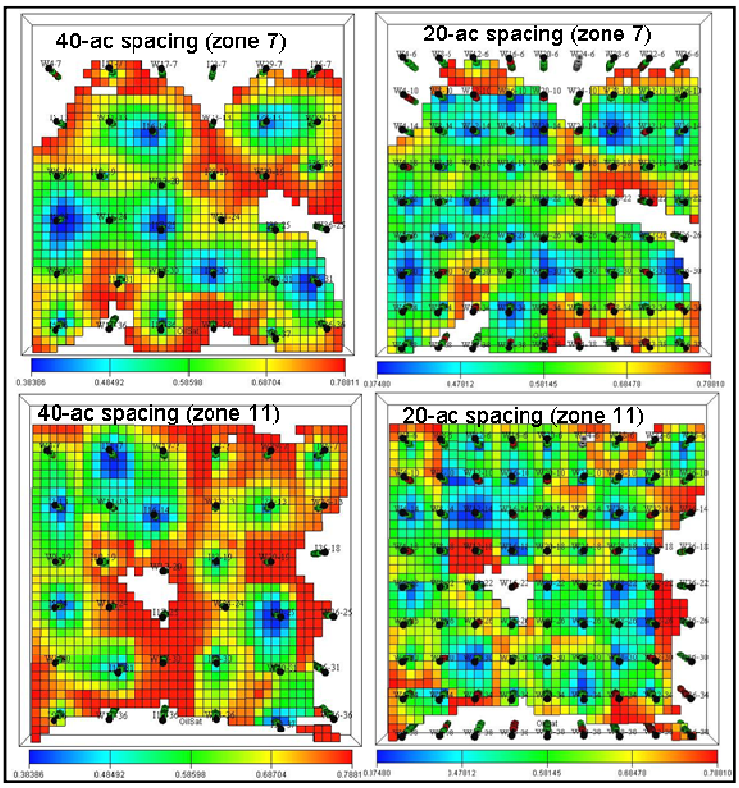


**Fig. 3.77—Oil saturation distribution for 20-ac and 40-ac spacing cases at the end of simulation.**

# 4. CONCLUSIONS

The results of this study can be used to optimize production from Garden Plains and Monument Butte fields. Together, the two studies demonstrate the utility of integrated reservoir studies (from geology to engineering) for characterizing unconventional stripper oil and gas reservoirs and providing optimal oil recovery strategies (primary, secondary, tertiary, and infill drilling) and well spacing for future development. Results of both studies can be applicable to other unconventional stripper gas and oil fields. Specific conclusions for each study are listed as below.

## 4.1 CONCLUSIONS FOR THE STRIPPER GAS FIELD

1. In Garden Plains field, 75% of the SSPK gas wells are stripper wells (production < 60 Mcf/d [1700 $m^3$/d]). During the best year of production, the average daily production wells was 61 Mcf/d per well.
2. Evaluation of SSPK core data demonstrated a good relation between porosity and permeability. Porosity-net-thickness product, and by relation permeability, appear to exert the greatest control on production from SSPK reservoirs in Garden Plains field. Structural position, minor structural features, and spud date (initial reservoir pressure) exercise secondary control on production.
3. The lowermost units (A and B) of the SSPK formation are the primary gas-producing intervals in Garden Plains field. Units A and B were deposited as northeast-trending, very fine-grained, shaly sandstones. Net thickness of Units A+B ranges from 10.5 ft to 22 ft (3.2-6.7 m) and averages 16.5 ft (5 m).

4. Mean porosity and permeability of SSPK Units A and B are 12.4 and 11.8% and 0.54 and 0.35 md, respectively.
5. Net/gross thickness maps and log facies maps indicate complex reservoir facies and reservoir heterogeneity. Porosity and permeability maps corroborate lateral heterogeneity of SSPK reservoirs.
6. The neutron porosity response of SSPK reservoir sandstones in Garden Plains field is greatly affected by high shale content, which necessitated correction of neutron porosity values.
7. Bentonite 1 is a good correlation marker that separates the lower, productive SSPK formation (Units A and B) from the upper SSPK (Units C and D), which have poor reservoir quality and limited production.

## 4.2 CONCLUSIONS FOR THE STRIPPER OIL FIELD

1. Assisted (automatic) history matching process greatly improved both field and individual well performance matching. Geological trends and distribution of permeability were preserved after assisted history matching. Permeability distribution from history matching compared favorably with that from core analyses.
2. Overall connectivity is low for the combined 22 zones in the Wells Draw study area of the Monument Butte field. The numerical value for hydraulic connectivity is 0.056, defined as the number of connected adjacent well pairs divided by the total number of adjacent well pairs. The connectivities evaluated by history matching are 0.65, 0.16, 0.23, and 0.01 for zone 7 (D1 sand), zone 11 (C sands), zone 15 (A

sands), and zone 17 (LODC sands), respectively. The connectivity evaluated by history matching (dynamic evaluation) is generally much lower than the connectivity evaluated using static data (net thickness and perforations).

3. Simulation results indicate interwell connectivity can possibly be increased with decreasing well spacing. Infill drilling can be an effective way to produce unswept oil from the reservoir and increase oil recovery from Monument Butte field. A pilot, 20-acre infill drilling project is needed to verify the viability of infill drilling to increase oil recovery, given the considerable uncertainty remaining in interwell connectivity.
4. Water-flood only strategy provides more oil recovery than primary-then-water-flood strategy over the life of the field. Producing oil below bubble point pressure (in the primary-then-water-flood cases) results in loss of solution gas, increased oil viscosity and less favorable oil-water mobility ratio, and thus causes early water breakthrough and lower oil recovery.
5. For new development areas, water flooding should start as soon as possible (within 6 months). Converting producers to injectors should start within 6 months of production of the producers. If water flooding is initiated after more than 6 months of primary production, oil recovery may be significantly less than if injection is started earlier. The selection of the optimum time to start water flooding should be based upon economics.
6. Tertiary recovery methods may have potential in the Monument Butte field, given the low recovery efficiencies for primary and secondary recovery. However, if poor

primary and water-flood recoveries are due mainly to poor connectivity, then tertiary recovery may result in poor recovery for the same reason.

7. Immiscible gas injection suffers early gas breakthrough and is not an effective way to increase oil recovery. $CO_2$ injection appears to be much more efficient than nitrogen or methane injection in the study area, because $CO_2$ has a lower minimum miscibility pressure (MMP) and results in later gas breakthrough. The MMP for $CO_2$ may be approximately 2500 psia, whereas the MMPs for nitrogen and methane are greater than 3100 psia. Laboratory experiment, such as slim-tube experiments, should be conducted to estimate and verify the MMP for $CO_2$ flooding as well as other injection gases in the Monument Butte field.
8. Water-alternating-$CO_2$ injection appears to be superior to continuous $CO_2$ injection, because it controls early breakthrough of $CO_2$ by making the gas-oil mobility ratio more favorable and maintains reservoir pressure. Laboratory experiments should be conducted to evaluate formation damage (e.g., asphaltene precipitation) caused by $CO_2$ flooding.

# REFERENCES

Abiazie, J. U. 2008. Characterization and Interwell Connectivity Evaluation of Green River Reservoirs, Wells Draw Study Area, Uinta Basin, Utah. M.S. thesis, Texas A&M University, College Station, 108 p.

Ainsworth, R.B. 2005. Sequence Stratigraphic-based Analysis of Reservoir Connectivity: Influence of Depositional Architecture - a Case Study from a Marginal Marine Depositional Setting. *Petroleum Geoscience* **11**, 257-276.

Ates, H., Bahar, A., El-Abd, S., Charfeddine, M., Kelkar, M., and Datta-Gupta, A. 2003. Ranking and Upscaling of Geostatistical Reservoir Models Using Streamline Simulation: a Field Case. Paper SPE 81497 presented at the SPE 13th Middle East Oil Show and Conference, Bahrain, 9-12 June.

Bissel, R. C. 1994. Calculating Optimal Parameter for History Matching. Paper presented at the Fourth European Conference on the Mathematics of Oil Recovery, Roros, Norway, 7-10 June.

Bloch, J., Schroder-Adams, C. J., Leckie, D. A., McIntyre, D. J., Craig, J., and Staniland, M. 1993. Revised Stratigraphy of the Lower Colorado Group (Albian to Turonian), Western Canada. *Bulletin of Canadian Petroleum Geology* **41**(3): 325-348.

Bloch, J., Schroder-Adams, C. J., Leckie, D. A., Craig, J., and McIntyre, D. J. 1999. *Sedimentology, Micropaleontology, Geochemistry, and Hydrocarbon Potential of Shale from the Cretaceous Lower Colorado Group in Western Canada* (Vol. 531): Bulletin of Geological Survey of Canada.

Buckley, L., and Tyson, R. V. 2003. Organic Facies Analysis of the Cretaceous Lower and Basal Upper Colorado Group (Cretaceous), Western Canada Sedimentary Basin - a Preliminary Report. *Summary of Investigations* **1**.

Budding, M.C., Paardekam, A.H.M. and van Rossem, S.J. 1992. 3D Connectivity +9and Architecture in Sandstone Reservoirs. Paper SPE 22342 presented at the SPE International Meeting on Petroleum Engineering, Beijing, China, 24 - 27 March.

Cheng, Y., McVay, D.A., Wang, J., and Ayers, W.B. 2008. Simulation-Based Technology for Rapid Assessment of Redevelopment Potential in Marginal Gas Fields--Technology Advances and Validation in Garden Plains Field, Western Canada Sedimentary Basin. *SPE Reservoir Evaluation & Engineering* **8** (3):521-534. SPE-100583-PA.

Chidsey, T.C., Jr., Morgan, C.D., McClure, K.P., Bon, R.L., Gwynn, J.W. Jarrard, R., and Curtice, R. 2004. Major Oil plays In Utah and Vicinity. Utah Geological Survey, unpublished quarterly technical progress report to the U.S. Department of Energy for the period 01/01/04 – 03/01/04, Contract DE-FC26-02NT15133 (June).

Chopra, A.K., Steverson, C.D., and Carhart, S.R. 1990. Evaluation of Geostatistical Techniques for Reservoir Characterization. Paper SPE 20734 at the SPE Annual Technical Conference and Exhibition, New Orleans, Louisiana, 23 - 26 September.

Christian, L. D., Shirer, J. A., Kimbel, E. L., and Blackwell, R. J. 1981. Planning a Tertiary Oil-Recovery Project for Jay/LEC Fields Units. *JPT* **33**(8), 1535 -1544.

Chu, L., Reynolds, A. C., and Oliver, D. S. 1995. Computation of Sensitivity Coefficients for Conditioning the Permeability Field to Well-Test Pressure Data. *In Situ* **19**, 179.

Coats, K. H. 1982. Reservoir Simulation: State of the Art. *JPT* **34**(8), 1633-1642.

Cosentino, L. 2001. *Integrated Reservoir Studies,* TECHNIP, Paris, France.

Creaney, S., and Allan, J. 1990. Hydrocarbon Generation and Migration in the Western Canada Basin. In J. Brooks (Ed.), *Classic Petroleum Provinces : Special Publication of the Geological Society of London* **50**. London: Blackwell.

Datta-Gupta, A. 2000. Streamline Simulation: A Technology Update. *JPT* **68**(12), 68-73.

Datta-Gupta, A. and King, M. J. 1995. A Semi Analytic Approach to Tracer Flow Modeling in Heterogeneous Permeable Media. *Advances in Water Resources* **18**.

Deo, M.D., Sarkar, A., Nielson, D.L., Lomax, J.D., and Pennington, B.I. 1994. Monument Butte Unit Case Study: Demonstration of a Successful Waterflood in a Fluvial Deltaic Reservoir. *Proc.,* SPE/DOE Ninth Symposium on Improved Oil Recovery, Tulsa, Oklahoma 143.

Deo, M.D., Nielson, D.L., Lomax, J.D., Dyer, J.E., and Lutz, S.J. 1996. Green River Formation Waterflood Demonstration Project. Utah Geological Survey, Unpublished final report to the U.S. Department of Energy for the period 10/01/92 - 12/31/95, Contract DE/BC/14958-15 (November).

Dubrule, O.R.F. ed. 1998. Geostatistics in Petroleum Geology, *AAPG Continuing Education Course Note Series* **38**.

Farzad, I. and Amani, M. 2007. Evaluating Reservoir Production Strategies in Miscible and Immiscible Gas-Injection Projects. Paper SPE 108014 presented at the Latin American and Caribbean Petroleum Engineering Conference, Buenos Aires, Argentina, 15-18 April.

FrontSim, Version 2007.1, 2007, Geoquest Schlumberger, Houston, Texas.

Galloway, W.E. 2002. Paleogeographic Setting and Depositional Architecture of a Sand Dominated Shelf Depositional System, Miocene Utsira Formation, North Sea Basin. *Journal of Sedimentary Research* **72**(4), 76-90.

Gharbi, R. B. C. 2003. Integrated Reservoir Simulation Studies to Optimize Recovery from a Carbonate Reservoir. Paper SPE 80437 presented at the SPE Asia Pacific Oil and Gas Conference and Exhibition, Jakarta, Indonesia, 9-11 September.

Glass, D. J. 1990. Lexicon of Canadian Stratigraphy, Including Eastern British Columbia, Alberta, Saskatchewan, and Southern Manitoba. Calgary, Alberta: Canadian Society of Petroleum Geologists.

Haldorsen, H.H. and MacDonald, C.J. 1987. Stochastic Modeling of Underground Reservoir Facies (SMURF). Paper SPE 16751 at the SPE Annual Technical Conference and Exhibition, Dallas, Texas, 27 - 30 September.

Haldorsen, H.H. and Damsleth, E. 1990. "Stochastic Modeling," *JPT* **42**, 404-412.

Hill, R. E. 2004. Stratigraphic Controls on West African Deepwater Reservoir Connectivity and Production Performance. *AAPG Bulletin* **88**.

Idrobo, E. A., Choudhary, M., and Datta-Gupta, A. 2000. Swept Volume Calculations and Ranking of Geostatistical Reservoir Models Using Streamline Simulation. Paper SPE 62557 presented at the SPE/AAPG Western Regional Meeting, Long Beach, California, 19-23 June.

IOGCC. 2006. Marginal Oil and Gas: Fuel for Economic Growth, Interstate Oil & Gas Compact Commission, Oklahoma City, Oklahoma, U.S.A.

Isaaks, E. H., and Srivastava, R. M. 1989. An Introduction to Applied Geostatistics. New York, USA: Oxford University Press.

Journel, A.G. and Alabert, F.G. 1990. New Method for Reservoir Mapping. *JPT* **42** 212 - 218.

King, P. R. 1990. The Connectivity and Conductivity of Overlapping Sand Bodies. *North Sea Oil and Gas Reservoirs II* **21**, 353-362.

Landa, J. L., and Horne, R. N. 1997. A Procedure to Integrate Well Test Data, Reservoir Performance History and 4-D Seismic Information. Paper SPE 38653 presented at the Annual Technical Conference and Exhibition, San Antonio, Texas, 5-8 October.

Larsen, D. G. and Zellitti, Z. 1997. Three-Year Study in the Green River Formation of the Uintah Basin Optimizes Completion Technology. Paper SPE 38363 presented at the Rocky Mountain Regional Meeting, Casper, Wyoming, 18-21 May.

Leckie, D. A., Bhattacharya, J. P., Bloch, J., Gilboy, C. F., and Norris, B. 1994. Cretaceous Colorado / Alberta Group Strata of the Western Canada Sedimentary Basin. In G. Mossop and I. Shetsin (Eds.), *Geological Atlas of the Western Canada Sedimentary Basin, Calgary* (pp. 335-352): Canadian Society of Petroleum Geologists and Alberta Research Council.

Lee, W. J. and Wattenbarger, R. A. 1996. Gas Reservoir Engineering. Textbook Series, SPE, Richardson, Texas **5**.

Mattax, C.C. and Dalton, R.L. 1990. *Reservoir Simulation.* Monograph Series, SPE, Richardson, Texas.

MGV Energy, Inc., Calgary, Canada, 2004. Unpublished maps and data of Garden Plains field.

Morgan, C.D., McClure, K.P., Bereskin, S.R., Deo, M.D., and Weller, K. 2000. Reservoir Characterization of the Lower Green River Formation, Southwest Uinta Basin, Utah. Utah Geological Survey, Unpublished biannual technical progress report to the U.S. Department of Energy for the period 10/01/99 - 03/31/00, Contract DE-AC26-98BC15103 (June).

Morgan, C.D., McClure, K.P., Bereskin, S.R., Deo, M.D., and Weller, K. 2001. Reservoir Characterization of the Lower Green River Formation, Southwest Uinta Basin, Utah. Utah Geological Survey, Unpublished biannual technical progress report to the U.S. Department of Energy for the period 04/01/00 - 09/30/00, Contract DE-AC26-98BC15103 (February).

Morgan, C.D., McClure, K.P., Bereskin, S.R., and Deo, M.D. 2002. Reservoir Characterization of the Lower Green River Formation, Southwest Uinta Basin, Utah. Utah Geological Survey, Unpublished final report to the U.S. Department of Energy, Contract DE-AC26-98BC15103.

O'Connell, S. 2005. The Second White Specks Medicine Hat and Milk River Formation. A Shallow Gas Core Workshop, Belfield Resources Inc., Calgary.

Oliver, D. S., Reynolds, A. C., Bi, Z., and Abacioglu, Y. 2001. Integration of Production Data into Reservoir Models. *Petroleum Geoscience* 65-73.

Portigal, M. H., Creed, R. M., Hogg, J. R., and Hewitt, M. D. 1989. Oil and Gas Developments in Western Canada in 1987. *Bulletin of Canadian Petroleum Geology* **37**, 334-345.

Pawar, R.J., Deo, M.D., and Dyer, J.E. 1996. Effect of Reservoir Connectivity on Primary and Secondary Recovery. *Proc.*, SPE/DOE Tenth Symposium on Improved Oil Recovery, Tulsa, Oklahoma 147.

Rice, D. D. 1984. Widespread, Shallow Marine, Storm-Generated Sandstone Units in the Upper Cretaceous Mosby Sandstone, Central Montana. *Society of Economic Paleontologists and Mineralogists* **34**, 143.

Rietz, D. and Palke, M. 2001. History Matching Helps Validate Reservoir Simulation Models. *Oil & Gas Journal* (December) 47-54.

Righi, E. F., Royo, J., Gentil, P., Castelo, R., Del Monte, A., and Bosco, S. 2004. Experimental Study of Tertiary Immiscible WAG Injection. Paper SPE 89360 presented at the SPE/DOE Symposium on Improved Oil Recovery, Tulsa, Oklahoma, 17-21 April.

Ryder, R.T., Fouch, T.D., and Elison, J.H. 1976. Early Tertiary Sedimentation in the Western Uinta Basin, Utah. *Geological Society of America Bulletin* **87**, 496-512.

Scheepens, C. C. J. 2003. 3D Modeling Using Multiple Scenarios and Realizations for Pre-Reservoir Simulation Screening. Paper SPE 82022 presented at the Hydrocarbon Economics and Evaluation Symposium, Dallas, Texas, 5-8 April.

Schlumberger. 2007. PVTi and ECLIPSE 300 Course Manual. Schlumberger Information Solution, Houston.

Schroder-Adams, C. J., Leckie, D. A., Bloch, J., Craig, J., McIntyre, D. J., and Adams, P. J. 1996. Paleoenvironmental Changes in the Cretaceous (Albian to Turonian) Colorado Group of Western Canada: Microfossil, Sedimentological and Geochemical Evidence. *Cretaceous Research* **17**, 311-365.

Shier, D. E. 2004. Well Log Normalization: Methods and Guidelines. *Petrophysics* **45**(3), 268-280.

Shurr, G. W. and Ridgley, J. L. 2002. Unconventional Shallow Biogenic Gas Systems. *AAPG Bulletin* **86**(11), 1939-1969.

Shtepani, E. 2007. Experimental and Modeling Requirements for Compositional Simulation of Miscible CO2- EOR Processes. Paper SPE 111290 presented at the SPE/EAGE Reservoir Characterization and Simulation Conference, Abu Dhabi, UAE, 28-31 October.

SimOpt, Version 2005a, 2005, Geoquest Schlumberger, Houston, Texas.

Snowdon, L. R. 1995. Rock-Eval $T_{max}$ Suppression: Documentation and Amelioration. *AAPG Bulletin* **79**(9), 1337-1348.

Stauffer, D. 1985. *Introduction to Percolation Theory*, London: Taylor and Francis Inc.

Stelck, C. R., Moore, W. E., and Pemberton, S. G. 2002. Early Turonian (Late Cretaceous) Age of the Tuskoola Sandstone Pine River Area, Northeastern British Columbia. *Canadian Journal of Earth Sciences* **39**, 1783-1793.

Taylor, A.W. and Ritts, B.D. 2004. Mesoscale Heterogeneity of Fluvial Lacustrine Reservoir Analogues: Examples from the Eocene Green River and Colton Formations, Uinta Basin, Utah, USA JPT (January 2004), 3.

Vasco, D. W. and Datta-Gupta, A. 2001. Asymptotics, Streamlines and Reservoir Modeling: A Pathway to Production Tomography. *The Leading Edge, Special Issue on Reservoir Modeling.*

Weber, K.J and van Geuns, L.C. 1990. Framework for Constructing Clastic Reservoir Simulation Models. *JPT* **42** 1248-1253.

Wen, X. H., Clayton, D. V., and Cullick, A. S. 1998. High Resolution Reservoir Models Integrating Multiple-Well Production Data. Paper SPE 38728 presented at the SPE Annual Technical Conference and Exhibition, San Antonio, Texas, 5-8 October.

Wendschlag, D. D. and Clark, T. J. (1983). Fieldwide Simulation of the Anschutz Ranch East Nitrogen Injection Project with a Generalized Compositional Model. Paper SPE 12257 presented at the Reservoir Simulation Symposium, San Francisco, California, Nov. 15-18.

Williams, G. D. and Stelck, C. R. 1975. Speculations on the Cretaceous Paleography of North America. In W. G. E. Caldwell (Ed.), *The Cretaceous System in the Western Interior of North America: Special Paper* (Vol. 13, pp. 1-20): Geological Association of Canada.

Wolcott, D.S. and Chopra, A.K. 1991. Investigating Infill Drilling Performance and Reservoir Continuity Using Geostatistics. Presented at the Third International Reservoir Characterization Technical Conference, Tulsa, Oklahoma, 3–5 November.

Yousef, A.A., Gentil, P., Jensen, J.L., and Lake, L.W. 2005. A Capacitance Model to Infer Interwell Connectivity from Production and Injection Rate Fluctuations. Paper SPE 95322 presented at the Annual Technical Conference and Exhibition, Dallas, Texas, 9–12 October.

Yuan, L. and Strobl, R. 1991. Variograms and Reservoir Continuity. *Proc.,* Third International Reservoir Characterization Technical Conference, Tulsa, Oklahoma, 3–5 November.

# VITA

Jianwei Wang received his Bachelor of Science degree in Petroleum Exploration Engineering from Petroleum Institute of Xinjiang, China in 1999. He entered the Petroleum Geology program at China University of Petroleum (Beijing) in September 2000 and received his Master of Science degree in July 2003. His research interests include integrated reservoir simulation, history matching methods, reservoir characterization, and petrophysical analysis.

Mr. Wang may be reached at Schlumberger DCS, 1700 Research Parkway, Suite100, College Station, TX 77845. His email is flyjwwang2003@yahoo.com.